POLITECNICO DI MILANO

School of Industrial and Information Engineering
Department of Energy

Master Degree in Energy Engineering

Numerical Assessment of an Innovative POCS Substrate as Electrical Heated Solution for ICE After-Treatment Systems

Supervisor: **Prof. Augusto Della Torre**
Co-Supervisor: **Dr. Loris Barillari**

Master Degree Thesis of:
Giulia Zanetta
ID 944297

Academic Year 2020-2021

To my grandparents.

Acknowledgements

Extended Abstract

Background and Introduction to the Problem

The greater awareness of the effects of pollution on human health and the environment has pushed technology towards the development of increasingly advanced emission reduction systems.

Over the years the transport sector has seen a lot of improvements to reduce the emissions produced, both for the fuels and for the after-treatment systems (ATS) used. However new progress can be developed to further reduce pollutants. This work focuses on the analysis of ATS for gasoline engines. Current ATS technologies have excellent conversion efficiencies of pollutants when they operate at optimal conditions. However, the efficiency decreases when working outside of ideal conditions.

In this thesis work one of the critical points of ATS, the abatement of pollutants at cold start, is analysed.

Development of an innovative POCS solution

In order to obtain the conversion of pollutants, a catalyst is inserted inside the ATS. The catalyst is composed by a porous material covered with the washcoat layer, in which noble metals are present to stimulate the reactions needed for the conversion. This system requires a minimum temperature, the so-called light-off temperature, which is around 600K to activate the conversion of chemical species. In this thesis an innovative pre-catalyst is studied and designed to be inserted

downstream of the engine to reduce the time needed to achieve the light-off temperature.

The main point on which the design of this structure is based is the possibility to introduce electrical heating. In fact, by creating a metallic structure it is possible to apply a potential difference, which allows a current flow and the heating of the structure (via Joule Effect). Starting from the possibility to heat the structure, other factors have to be analysed. The size of the ducts, the new printing technologies, the materials and many other parameters greatly influence the design.
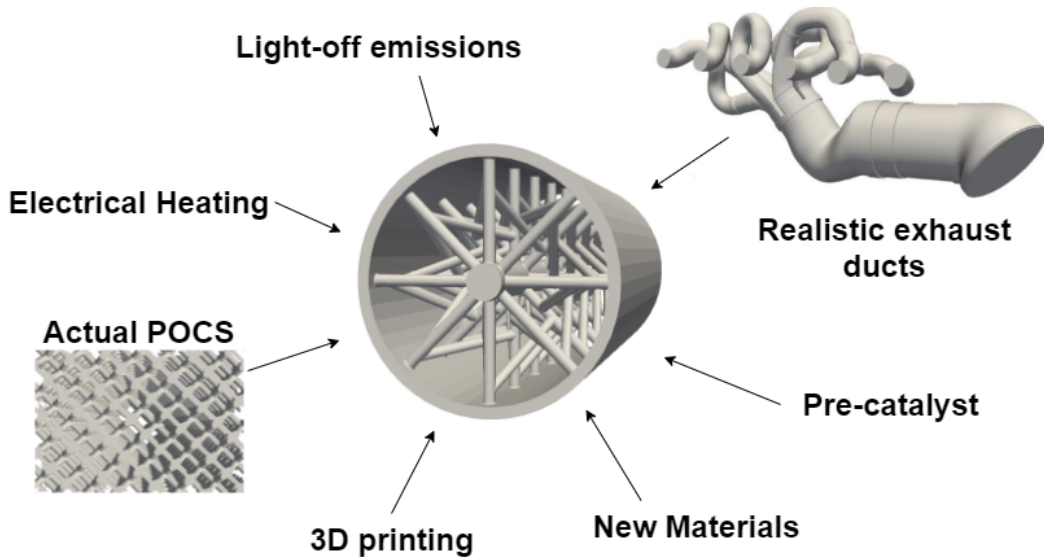

Figure 1: *Development of POCS design.*

New developments in the Additive Layer Manufacturing (ALM) field make the production of complex structures possible. The wide range of printing materials which can be used, linked to the possibility of creating structures with multiple materials, allows the creation of pieces that would not be possible otherwise.

Recently, driven by these developments, the catalysts assist a progressively shifting towards the adoption of Periodic Open Cell Structures (POCS) at the expense of Open Cell Foams. The POCS are structures with morphology and properties similar to Open-Cell Foams but are arbitrarily designed with CAD tools.

The advantage of this structure, in addition to the active heating system that can

be updated, is the possibility to place a washcoat layer on the surfaces. This thin layer, rich in precious metals, can be sprayed on surfaces.

The design phase consists of few steps. First of all a preliminary geometry is designed and analysed, then the geometry is adapted to a realistic duct on the basis of the results of the preliminary analysis. Finally, the abatements of the emissions obtained with the POCS on the entire exhaust line are evaluated.

1) Concept design

A preliminary analysis is carried out on a simplified geometry. A straight pipe of 75mm long with a shape as in the Figure 2 is considered.
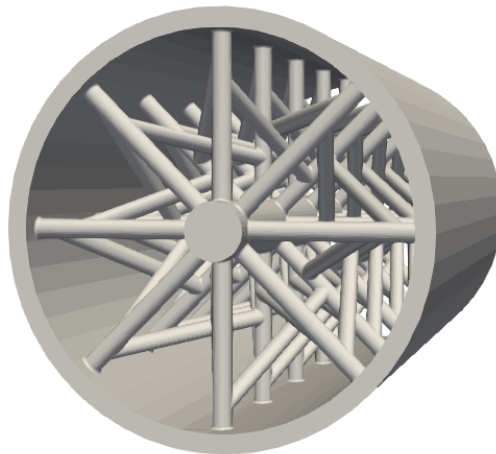

Figure 2: *Preliminary POCS structure.*

The preliminary geometry is composed by a central pipe that is connected to the wall duct thanks to several radial struts and inclined struts that channel the gas flow. The inner pipe is a crucial aspect of the design because it is the region in which positive potential is applied. Here the potential is applied by the introduction of a copper wire inside the pipe, as shown on the left in Figure 3.
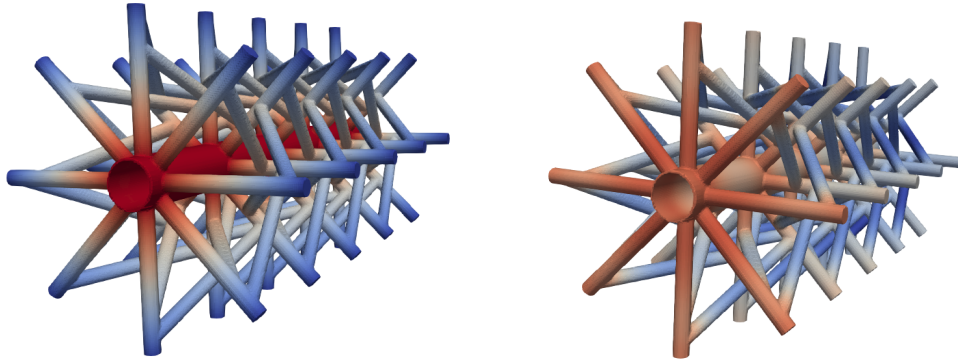
Figure 3: *Potential difference in preliminary POCS geometry and temperature distribution after 10s.*

Despite the good fluid dynamics demonstrated by the reduced pressure losses, the assumptions made on the voltage distribution in the structure cannot be actuated in a realistic piece. Therefore the realistic geometry is designed on the basis of the preliminary geometry but with a different application method of potential difference.

2) Adaptation to a real test case

The preliminary geometry is redesigned to fit into a realistic duct. The realistic geometry follows a twisted duct so the symmetries and parallelism slightly change; in any case, the main geometric characteristics are respected, giving a very similar geometry to the preliminary one.
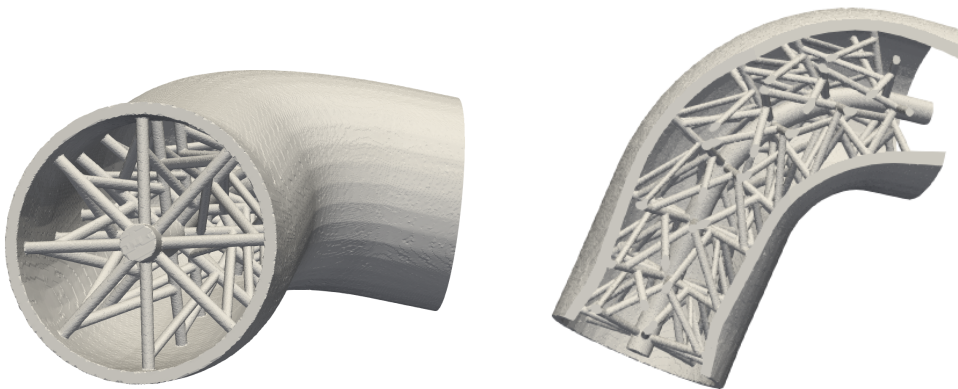

Figure 4: *POCS applied to realistic geometry and its section.*

The copper wire is eliminated and, in order to apply the potential radially as before, the conductivity of the struts is changed from $10^7[\frac{S}{m}]$, typical of steel, to $100[\frac{S}{m}]$, reference value for SiC. In this way the voltage is distributed similarly to the preliminary case allowing to heat all the struts in a more realistic way. The potential is applied to the outside of the duct so the internal pipe is stretched to go beyond the wall, the red surface on the left of Figure 5 is the positive pole. In this case 38V are applied to the positive pole and the potential is distributed as on the right of Figure 5.
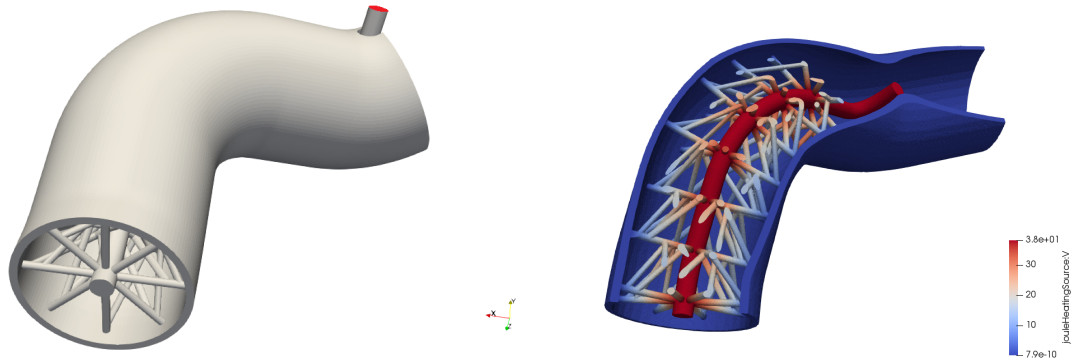

Figure 5: *Position of positive pole (left) and potential distribution inside realistic POCS geometry (right).*

After checking the mesh quality and modifying the application of the potential difference to have a radial distribution, the simulation to evaluate the concentration of pollutants is performed.

For the simulation realistic inlet conditions are applied to the inlet patches. The obtained results are diplayed in Figure 6.
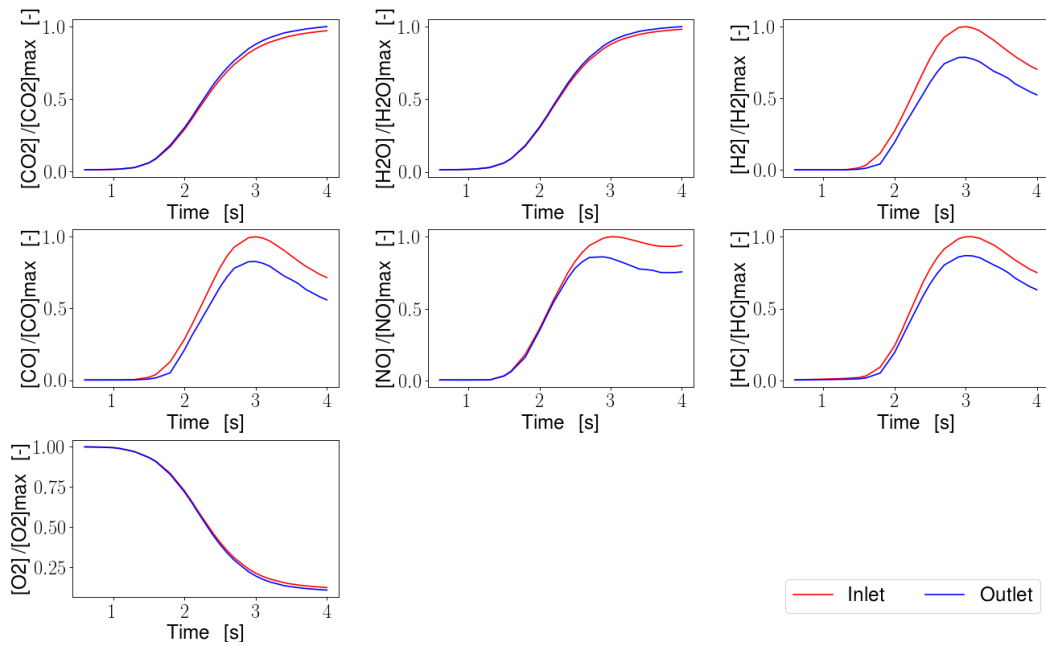
Figure 6: *POCS configuration: diagrams of abatement for different species as function of time.*

A reduction of about 20% is seen 3 seconds after starting. However, in this case it is useful not only to look at the quantities shot down but also at the abatement distribution in the ducts. The higher quantity of pollutants is linked to lower temperature zones.
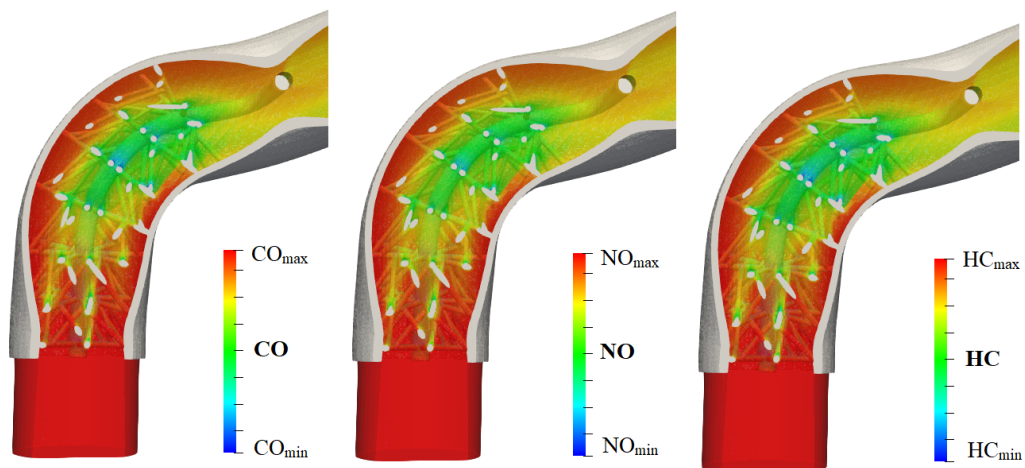

Figure 7: *POCS configuration: diagrams of abatement for the main pollutant species after 4s of simulation.*

3) Analysis of the overall after-treatment system equipped with POCS

After the POCS detailed analysis, the influence that it has over the rest of the exhaust line has to be considered. To do that two simulations, considering the same exhaust geometry, are exploited:

- The realistic engine exit conditions applied to the inlet patches of exhaust ducts.

- The data obtained from the simulation of the previous case study applied to the inlet patches of exhaust ducts.

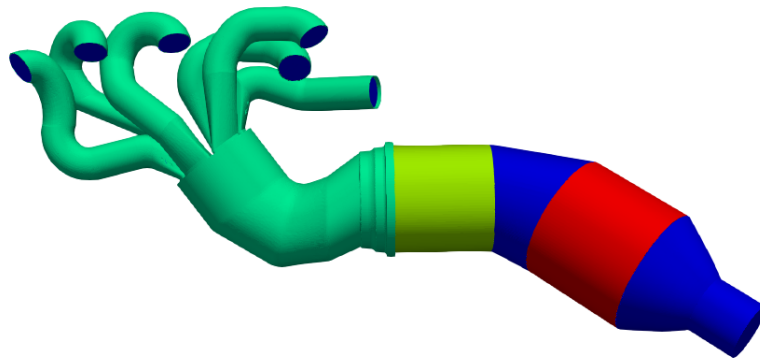The exhaust pipe considered has the following shape, where the red and the green zones are the catalysts.

Figure 8: *Division of the exhaust pipe domain.*

The results obtained by the case without POCS, which is considered the reference case, show the start of abatement around 7 seconds.

Figure 9: *Reference configuration: diagrams of abatement for different species as function of time to evaluate the light-off time. (light-off at 7s)*

Then the analysis is made on the POCS data. In this simulation the higher temperature at the inlet reduces the light-off time, so as reported in the diagrams in Figure 10 after 5 seconds the first changes in abatement are present.

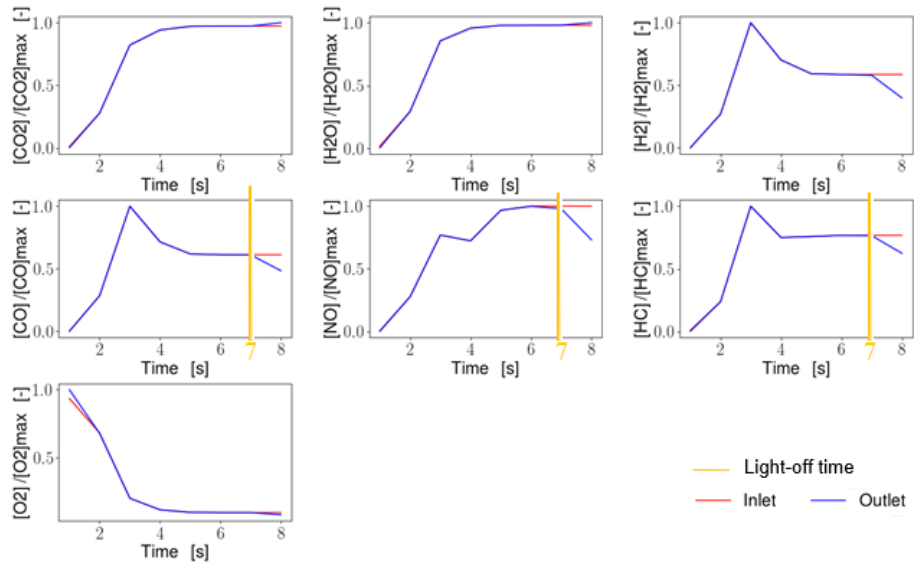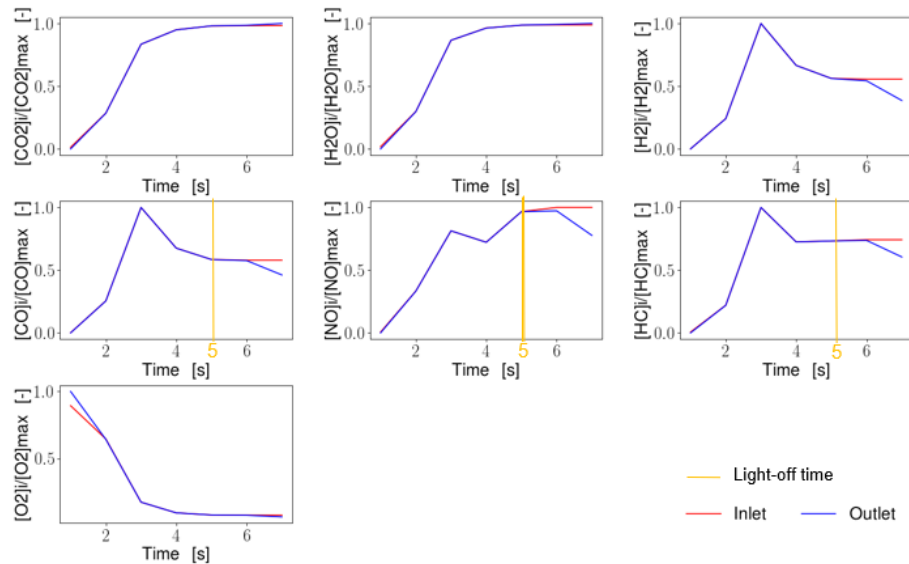**Figure 10:** *Advanced configuration with introduction of POCS: diagrams of abatement for different species as function of time to evaluate the light-off time. (light-off at 5s)*

This phenomenon is evident from the analysis of the average temperatures. As shown in Figure 11, the catalyst exploits very different temperatures between the two cases considered.
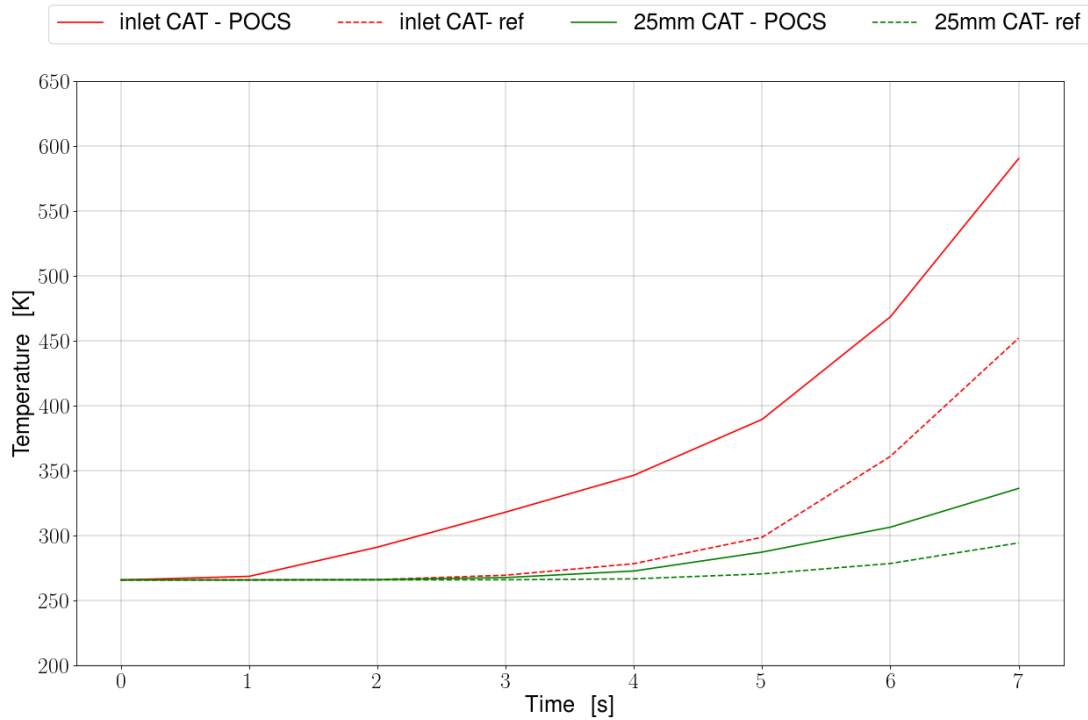
Figure 11: *Comparison of the temperature evolution inside the catalyst for the reference case and for the advanced solution with POCS.*

To better understand the influence of POCS some characteristic parameters, first of all the temperature along the exhaust line, are compared. As can be seen in Figure 12, the presence of POCS greatly increases the inlet temperatures which then decrease due to thermal dispersions.

The Figure 12 and Figure 13 clearly show how the flow cools down before reaching the catalyst but nevertheless reaches the catalyst with a temperature higher than the reference case. In this way the first catalyst light-off time is reduced by two seconds. In addition to the temperature trend, it is useful to compare the abatement capacity. The following diagrams show the cumulative dimensionless pollutant concentrations in the exhaust pipe for the reference case compared to
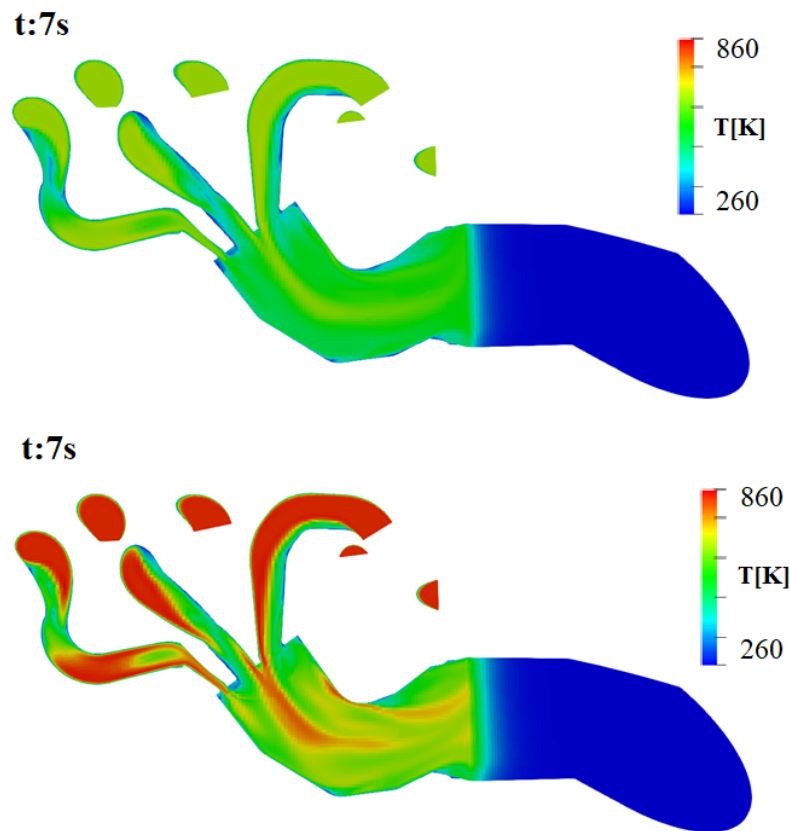
Figure 12: *Comparison of the temperature evolution between base case (above) and POCS case (below) at 7s.*

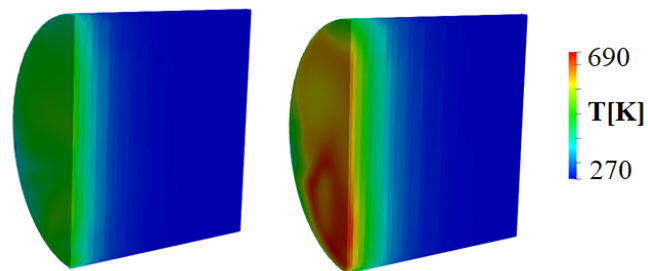**Figure 13:** *Comparison of the first catalyst temperature evolution between base case (left) and POCS case (right) at 7s.*

the exhaust pipe with POCS pre-catalyst.
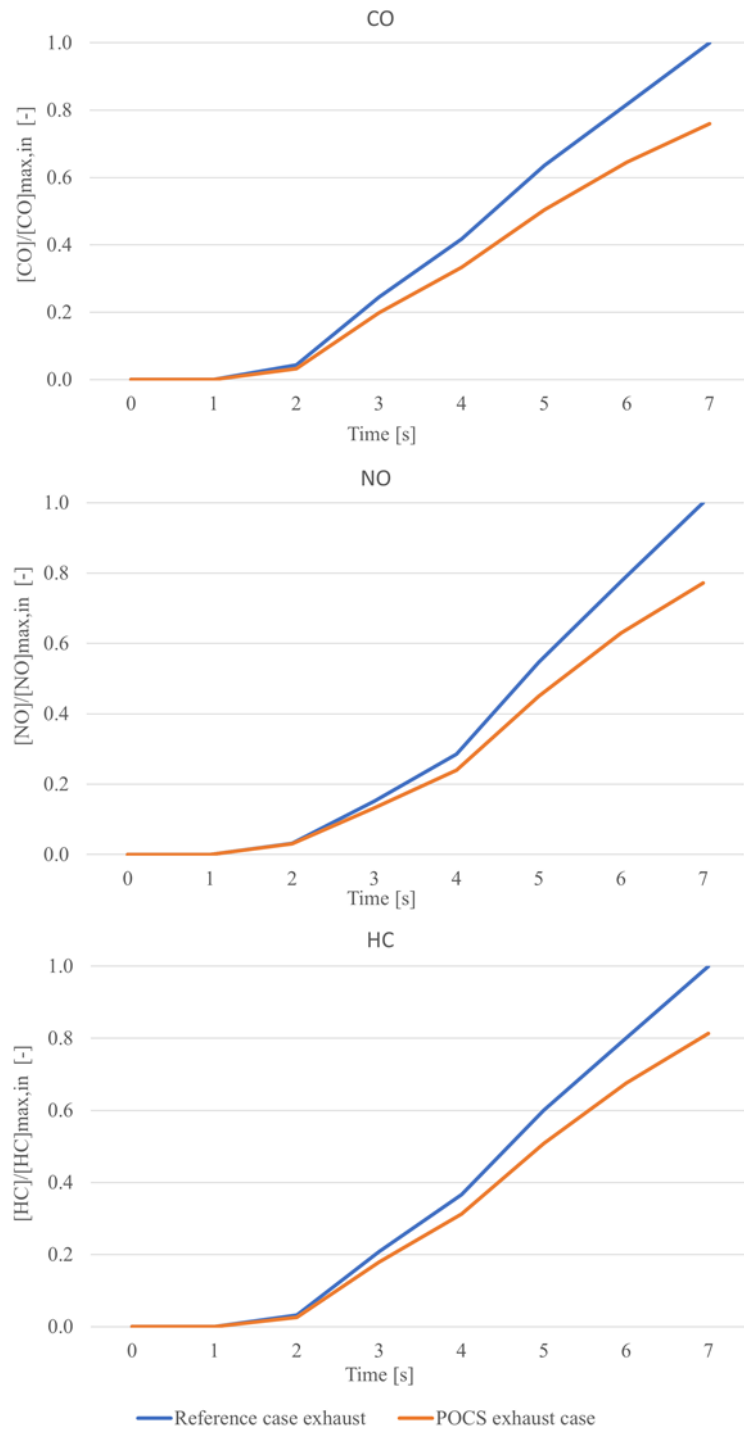
Figure 14: *Comparison of cumulative diagrams for CO, NO and HC.*

Before activating the catalyst in the reference case it is possible to appreciate about 20% reduction of emissions in the POCS case.

Impact on overall engine performances

Finally, to verify the applicability of this structure during the long period, a preliminary analysis is carried out on *gasdyn* code.

Thanks to the pressure drop evaluated through CFD simulation, it is possible to calculate the friction factor.

$$f_w = \frac{\Delta p}{\rho} \frac{2d}{l} \frac{1}{U^2} \tag{1}$$

This value is inserted in the *gasdyn* setup to find out the influence of the POCS structure on a full load engine. In this analysis some performance parameters as the engine rotational speed varies have been compared, considering the base case and the POCS case.

A relevant parameter to be analysed is the brake power.
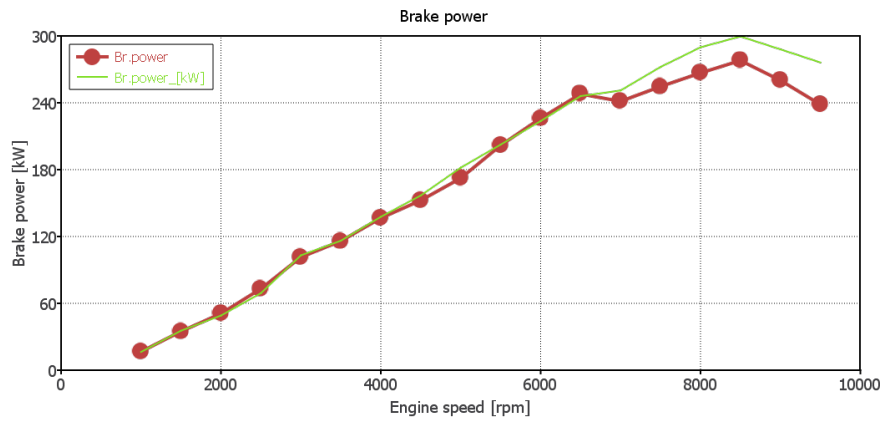
Figure 15: *Comparison of Brake Power between the base configuration and the configuration with POCS.*

As shown in Figure 15, for low rotational speeds there are no sensible variations but for rotational speed higher than 7000 rpm the POCS reduces the power of the engine.

Conclusions

The proposed innovative system can be regarded as a promising solution. The emission abatement results show a very early activation of the reactions, both temporally and spatially, but also a heating of the gas flow that allows to activate in advance also the traditional catalysts. The studied geometry presents good fluid dynamics characteristics as well as great flexibility, this opens up to possible further developments. Although the study is carried out on a gasoline engine, any combustion system could take advantage of this system potential.

Contents

List of Figures

List of Tables

Abstract

In the last twenty years more and more stringent legislations have been adopted to limit pollutant emissions. Even if the impact of transport sector on the air pollution has decreased with the recent after-treatment technologies there are still margins for further improvements. The reduction of the negative effects of transportations is a strategic objective for the EU. In this scenario of abatement of emissions, a fundamental role is played by the after-treatment systems for vehicles. The need to introduce ever more efficient systems for the reduction of pollutants has pushed the research towards innovative solutions. In this framework the present Thesis is developed. The aim of the study is to design and analyze a pre-catalysis system that allows to intervene on the emissions released during the lighting of the vehicle. The pre-catalyst is designed so that it could be heated through the Joule effect, which occurs thanks to the application of a potential difference inside the piece. The pre-catalyst is drawn through CAD tools and analyzed through Computational Fluid Dynamics systems (CFD), specifically through the open-source software called *OpenFOAM*. The analysis is developed by primarily checking the heating of the structure, then the reduction of the pollutants obtained with the introduction of this catalyst. Finally the impact that this component has on the remaining part of the exhaust system is verified. After the fluid dynamics analysis a preliminary 1D simulation at full load is developed, thanks to the software called *gasdyn*, to verify the engine performances. For this study an high performance spark ignition engine is considered, however the study lends to new developments to be applied to vehicles with different fuel system,

fossil an synthetic fuels, and also hybrid vehicles.

Estratto in italiano

Negli ultimi vent'anni, si sono susseguite normative sempre piú stringenti sulle emissioni inquinanti. La riduzione delle emissioni dovute al settore dei trasporti é un obiettivo fondamentale per l'Unione Europea. In questo scenario un ruolo chiave é svolto dai sistemi di post trattamento dei fumi di scarico dei veicoli. Sebbene le recenti tecnologie di post trattamento dei fumi di scarico abbiano ridotto notevolmente la quantitá di inquinanti rilasciati in atmosfera ci sono ulteriori miglioramenti attuabili. La necessitá di introdurre sistemi sempre piú efficienti per ridurre gli inquinanti ha dato una grande spinta alla ricerca portandola verso soluzioni sempre piú innovative. In questo contesto si sviluppa il mio progetto di tesi. L'obiettivo dello studio é quello di progettare un precatalizzatore da inserire all'inizio della linea di scarico del motore e di analizzarne le capacitá di abbattimento delle sostanze inquinanti, in particolare vengono analizzate le emissioni prodotte durante l'accensione del veicolo. Il principale problema di emissioni nei veicoli é legato alla temperatura del catalizzatore, che deve essere sufficiente ad attivare le reazioni chimiche di trasformazione. Per questo il precatalizzatore che vuole essere introdotto nei condotti é pensato per poter essere scaldato attraverso l'effetto Joule, applicando una differenza di potenziale che provoca il passaggio della corrente nel pezzo. Questa struttura é disegnata attraverso l'utilizzo di software CAD e analizzato fluidodinamicamente attraverso simulazioni CFD, eseguite tramite il software open-source *OpenFOAM*. L'analisi si é svolta partendo dalla verifica del riscaldamento della struttura, poi si é verificato l'abbattimento degli inquinanti con il precatalizzatore ed infine si é confrontato l'impatto di questo pezzo

sull'intera linea di scarico. Infine, dopo l'analisi fluidodinamica, é stata svolta un'indagine preliminare per verificare le prestazioni a pieno carico attraverso il software *gasdyn* per simulazioni 1D. Lo studio é svolto considerando un motore ad accensione comandata ad alte prestazioni, tuttavia i risultati ottenuti possono essere estesi a diverse tipologie di motori, considerando sia combustibili differenti, fossili e sintetici, sia veicoli ibridi.

parole chiave: *sistemi di post trattamento, precatalizzatore, CFD, emissioni, OpenFOAM, light-off*

Chapter 1

Introduction

In recent years the strong sensitivity to eco-sustainability has led to a great boost to the research towards systems that reduce emissions in order to minimize the environmental impact.

Air pollution in urban centres depends on several factors, but the main ones are related to traffic, domestic heating, industries, and agriculture. However, these factors have different importance from city to city. In the urban centres of large cities, emissions from vehicles and domestic heating predominate.

New technologies made it possible to carry out more precise analyzes of pollutants, which led to the introduction of more stringent laws.

In the last few years, the range of vehicle types has expanded a lot to meet the new regulations. Electric and hybrid cars appeared on the market leading to a great growth in sales compared to traditional internal combustion engines cars.

At the same time, the research on exhaust gas after-treatment systems has taken a big step forward, mostly because gasoline engines will still be part of the range of car sold for many years, but above all that hybrid cars will still need more efficient exhaust gas treatment systems.

The vehicle hybridization certainly leads to a reduction in CO_2 emissions, however the presence of an electric motor, which partially compensates for the combustion engine, leads to a reduction in the temperature of the exhaust gases. This increases the activation times of the catalyst, which will operate with lower effi-

ciencies for a longer time.

After the emissions scandal involving the discovery of the emissions falsification of cars equipped with a diesel engine, new emissions measurement tests were introduced. However, with the definition of the newer EURO standards, more stringent values are being defined for emissions, as well as even more realistic tests.

To meet the new regulations, the need to study new technologies is evident.

In this context this thesis work takes place.

The use of electrical heating, which is able to reduce light-off times and therefore to have less emissions during the cold start, is the objective of this research. The thesis focuses on the design of a pre-catalyst system capable of realising the mentioned objective.

In this specific case the analysis is carried out on a high-performance spark ignition engine, specifically a V12 naturally aspirated engine. However the system could be used for both spark ignition and compression ignition engines, for different types of fuel, fossil and non-fossil, but also for hybrid vehicles.

This analysis is performed through Computational Fluid Dynamics systems (CFD), specifically *OpenFOAM*, which allows to evaluate the abatement of emissions, and through 1D thermo-fluid dynamic simulation model, *gasdyn*, to evaluate the performances of the entire engine system.

1.1 Reference European Regulations

"The protection of air quality and reduction of greenhouse gas emissions is a priority for the European Commission" [1]. The European Commission opens in this way the chapter about the emission in the automotive sector. This demonstrates the importance given to counteract the pollutants emissions. The European emission standards are the standards for exhaust emissions of new vehicles sold in the European Union and EEA member states and the UK.

Emission standards for passenger cars are summarised in the following table for different regulations, in particular with regards to gasoline engines.

Tier	Date	CO	THC	VOC	NOx	PM	PN
EU1	$1992-1993$	2.72	-	-	-	-	-
EU2	$1996-1997$	2.2	-	-	-	-	-
EU3	$2000-2001$	2.3	0.20	-	0.15	-	-
EU4	$2005-2006$	1.0	0.10	-	0.08	-	-
EU5a	$2009-2011$	1.0	0.10	0.068	0.06	0.005*	-
EU5b	$2011-2013$	1.0	0.10	0.068	0.06	0.0045*	-
EU6b	$2014-2015$	1.0	0.10	0.068	0.06	0.0045*	$6 \cdot 10^{11}$
EU6c	2018	1.0	0.10	0.068	0.06	0.0045*	$6 \cdot 10^{11}$
EU6d-Temp	$2017-2018$	1.0	0.10	0.068	0.06	0.0045*	$6 \cdot 10^{11}$
EU6d	$2020-2021$	1.0	0.10	0.068	0.06	0.0045*	$6 \cdot 10^{11}$

Table 1.1: *European Standard Emissions for Gasoline passenger cars.*
* Applies only to vehicles with direct injection engines

The last standards, from EURO 6b onwards, include the mass and number of emitted particles.

The new standard EURO 7 has not yet been officially defined, but it is likely to require better performance to further reduce both pollutants introduced into the atmosphere and greenhouse gases.

Compared to the first regulations, the species subject to limitations have been expanded. However the regulated pollutants of the exhaust gases is much wider than this. Hence the new regulation will likely include new species, such as am-

monia (NH_3) and N_2O, and ultrafine particulate matter but also aldehydes which originates during cold starts.

The values reported in the table 1.1 are obtained with different tests. The first test adopted by the European Union to evaluate the light vehicle emissions is called New European Driving Cycle (NEDC). The cycle must be performed on a cold vehicle at $20-30$ ℃ (typically run at 25 ℃). The cycles may be performed on a flat road, in the absence of wind. However, to improve repeatability, they are generally performed on a roller test bench. This type of bench is equipped with an electrical machine to emulate the resistance due to aerodynamic drag and vehicle mass (inertia).

As depicted in the Figure 1.1, the test consists of two phases: about 13 minutes of simulated driving in the city and about 7 minutes of simulated driving on a suburban road. Special equipment and air conditioning are not taken into consideration and the highest speed reached is 120 $[\frac{km}{h}]$.
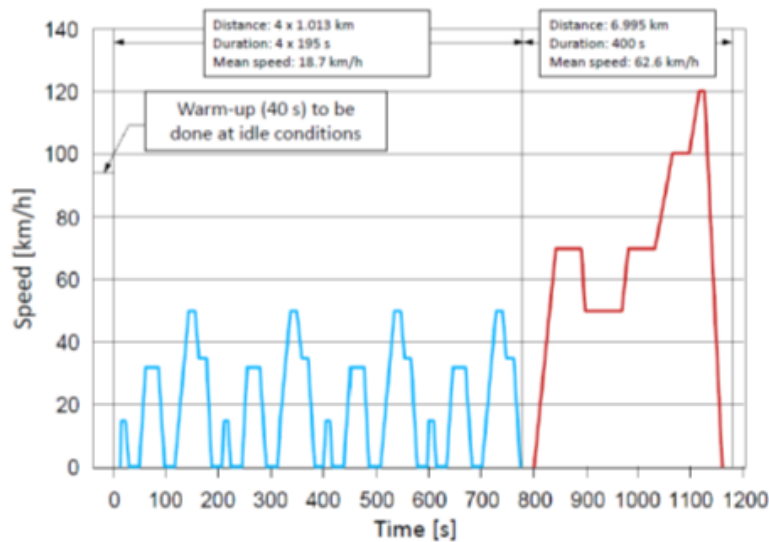
Figure 1.1: *NEDC test procedure: represents vehicle speed as a function of the time [5].*

This test has many critical issues because it differs greatly from the real driving styles on the road. In 2015, thanks to the scandal called "Dieselgate", this methodology was replaced by a more realistic test. The new reference for Eu-

ropean regulation is the Worldwide Harmonized Light Vehicles Test Procedure (WLTP). The WLTP includes more dynamic phases when compared to NEDC, the acceleration rates better reflect real-world driving conditions. The average speed during WLTP testing is 46.5 $\left[\frac{km}{h}\right]$ and the maximum speed is 131.3 $\left[\frac{km}{h}\right]$, compared to 34 $\left[\frac{km}{h}\right]$ and 120 $\left[\frac{km}{h}\right]$ respectively for NEDC testing. The cycle testing time goes up from 20 minutes for NEDC to 30 minutes for WLTP. Vehicles travel a distance of 23.25 km during the WLTP test, compared to 11 km for the NEDC. The WLTP test consists of four parts depending on the maximum speed reached. As reported in Figure 1.2.
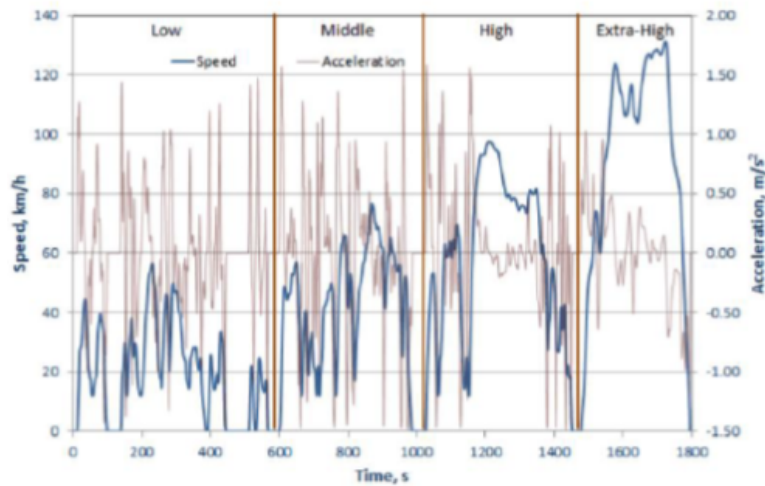
Figure 1.2: *WLTP test procedure: represents vehicle speed as a function of the time [5].*

Since September 1st, 2018, all vehicles registered for the first time are WLTP certified.

Even before the emissions scandal broke, the Commission had proposed to measure emissions in real-world driving conditions. In the RDE (Real Driving Emissions) procedure pollutant emissions are measured by Portable Emission Measuring Systems (PEMS) attached to the car while driving in real conditions on the road. The comparison between the different cycle tests shows the weak points of the laboratory tests at high load and high speed.
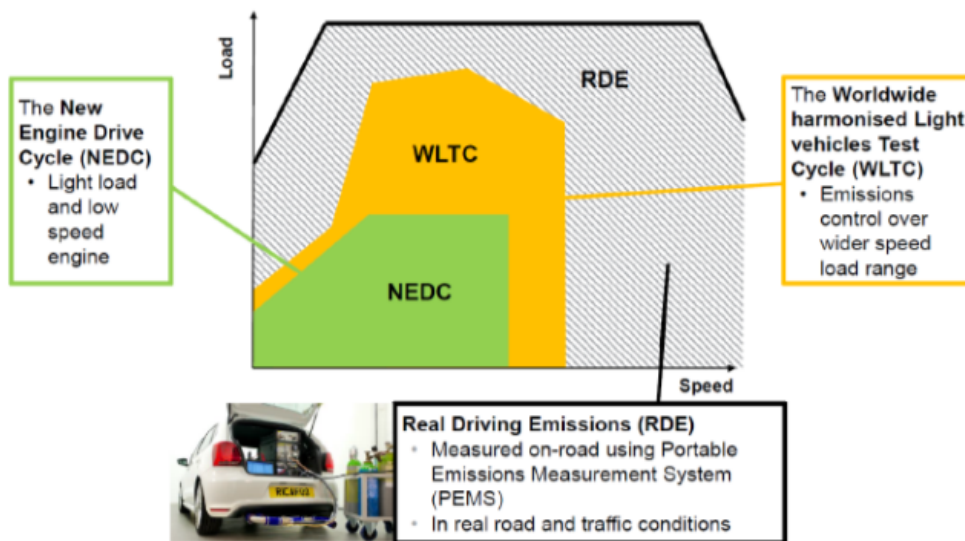
Figure 1.3: *Comparison among test procedures referred to load and speed [5].*

In this context, the development of After-Treatment Systems (ATS) has become fundamental.

1.2 After-Treatment System for Internal Combustion Engines

Internal combustion engines have as their purpose the transformation of chemical energy into mechanical energy through the combustion of fuels.

They can be classified by their combustion characteristics, mainly into spark ignition or compressor ignition engines.

The first type, the spark ignition one, develops the combustion starting from a spark emitted by a plug. Instead, for the second method, the combustion is triggered by the extreme conditions of pressure and temperature produced by piston compression.

In both cases, the burning of fossil fuels produces emissions in the form of nitrogen oxides (NO_x), carbon monoxide (CO), unburned hydrocarbons, and sulphur oxides (SO_x).

1.2.1 Common devices for After-Treatment System

The exhaust gases coming from the combustion chamber require to be cleaned before reaching the environment. The purification step in gasoline engines is realized by a special catalyst structure, called Three-Way Catalysts (TWC), and by a Particulate Filter (GPF). The name TWC refers to the number of pollutants treated, NO_x, CO and hydrocarbons, as well as the use of a catalyst.

The catalyst uses a ceramic or metallic substrate with an active coating incorporating alumina, ceria and other oxides; combinations of precious metals, like platinum, palladium and rhodium, are added to promote the pollutants conversion reactions.

The catalyst is a monolith structure composed of several parallel channels, in which the exhaust gases flow. The whole structure is called honeycomb.

The honeycomb channels are covered by alumina which is a porous material able
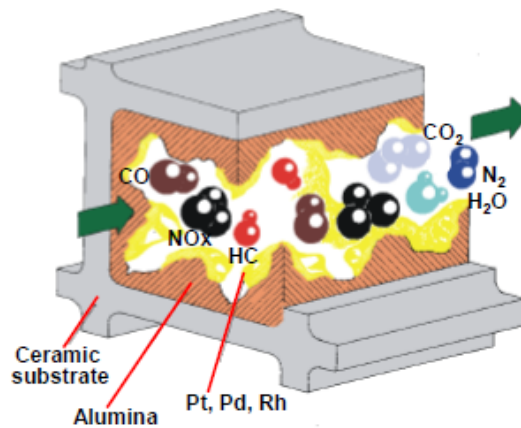
Figure 1.4: *Channel description considering substrate and flow [5].*

to increase the catalytic surface, namely the washcoat. Thanks to this device the residence time of the flux near the active site increases, enhancing the probability to reach the active side, promoting the reaction and so performing the conversion. The catalyst can then simultaneously oxidise carbon monoxide and hydrocarbons to carbon dioxide and water, while reducing NO_x to nitrogen.
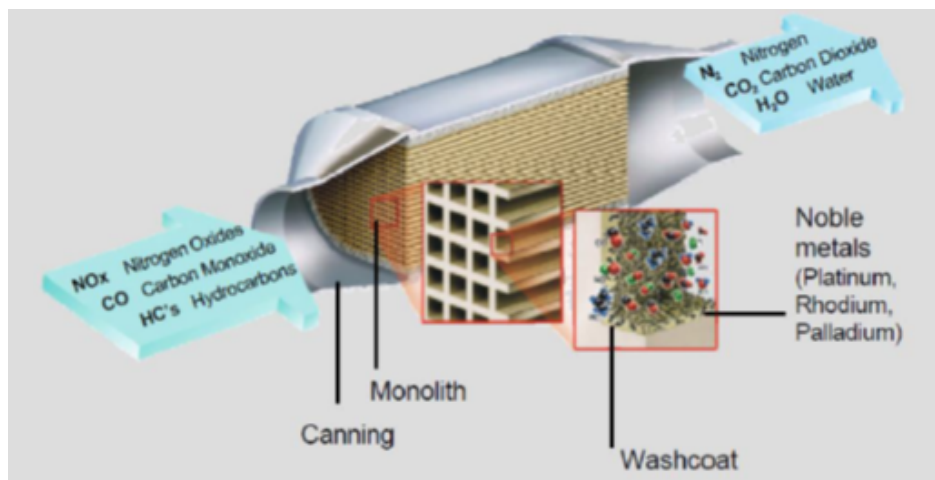
Figure 1.5: *Honeycomb representation [5].*

The basic reactions to schematize the process that takes place in the ATS system are:

Oxidation Reactions
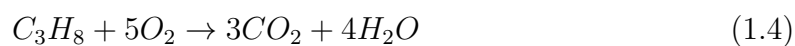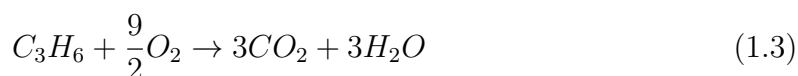
$$CO + \frac{1}{2}O_2 \rightarrow CO_2 \qquad (1.1)$$

$$H_2 + \frac{1}{2}O_2 \rightarrow H_2O \qquad (1.2)$$

$$C_3H_6 + \frac{9}{2}O_2 \rightarrow 3CO_2 + 3H_2O \qquad (1.3)$$

$$C_3H_8 + 5O_2 \rightarrow 3CO_2 + 4H_2O \qquad (1.4)$$

Reduction Reactions

$$NO + CO \rightarrow CO_2 + \frac{1}{2}N_2 \qquad (1.5)$$

HC Steam Reforming

$$C_3H_6 + H_2O \rightarrow CO + 2H_2 \qquad (1.6)$$

$$C_3H_8 + H_2O \rightarrow CO + \frac{7}{3}H_2 \qquad (1.7)$$

Water Gas Shift Reaction

$$CO + H_2O \rightarrow CO_2 + H_2 \qquad (1.8)$$

Oxygen Storage

$$Ce_2O_3 + \frac{1}{2}O_2 \rightarrow CeO_2 \qquad (1.9)$$

$$CO + 2CeO_2 \rightarrow Ce_2O_3 + CO_2 \qquad (1.10)$$

$$C_3H_6 + 12CeO_2 \rightarrow 6Ce_2O_3 + 3CO_2 + 3H_2O \qquad (1.11)$$
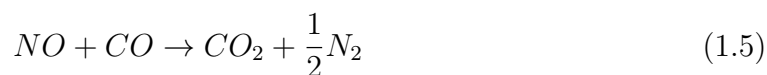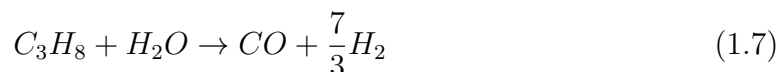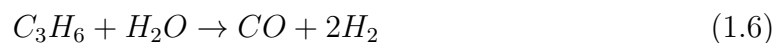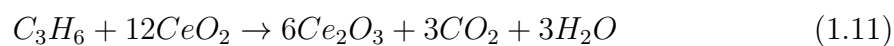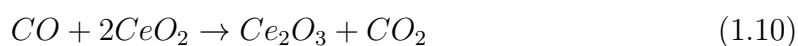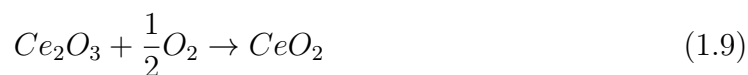
The metals used for the catalyst have different purposes. Palladium and platinum are the active components for CO and HC oxidation and the main role of rhodium is in NO_x reduction. Instead Ceria is able to store oxygen. The actual importance of oxygen storage/release during dynamic operations is determined not only by the oxygen storage capacity of the cerium-based oxide but also by the rates of the cerium oxidation and reduction processes.

Depending on the operating conditions of the engine and the exhaust gas composition, conversion rates upwards of 98% can be achieved at close to stoichiometric (λ) conditions. The weak point is represented by the start-up period, during which the exhaust gas temperature is lower than 250°C, denying the heating of the catalyst itself.

Instead, the Gasoline Particulate Filters (GPF) belong to an emission aftertreatment technology based on Diesel Particulate Filters (DPF), developed to control particulate emissions from Gasoline Direct Injection (GDI) engines. The GPF has been developed and offers an effective route to reduce the number of ultrafine particles under all driving conditions. The GPFs use the same type of wall-flow substrates as diesel particulate filters and can be included in the exhaust system downstream of the TWC or the catalyst coating can be directly applied to the filter substrate to form a four-way catalyst.

The substantial difference between the DPF and the GPF is due to the engine-out particulate emissions, that is 10-30 times lower in gasoline engines.

The exhaust temperature is also different, the higher temperature in gasoline pipe is enough to auto regenerate the device, typically during the vehicle deceleration where oxygen becomes largely available.

The Euro 6 regulations set PN (as well as PM) limits for GDI vehicles that are equivalent to those for diesels. The emission standards set PN limit of $6.0 \cdot 10^{11}$ #/km for NEDC and WLTC test cycle (Euro 6c).

Figure 1.6: *Gasoline Particulate Filter [5].*

1.2.2 Light-off temperature

The catalyst light-off is the minimum temperature necessary to activate the catalytic reaction, which is higher than 300℃.

During the start-up of the engine the temperature of the catalyst is lower, because it exploits the heat transfer of the exhaust gases coming from combustion to warm itself up. This aspect reduces the efficiency of the catalyst conversion.

The introduction of start&stop strategies on vehicles and different forms of hybridization of engines have further made the thermal management of the aftertreatment system an issue of extreme concern. To reduce this deficiency many suggestions have been provided. The change of the position of the catalyst closer to the engine, in order to exploit higher gas temperatures, is one of the most employed strategies. However it is not enough to satisfy the new emission legislations.

Alternative solutions have been proposed for catalyst light-off, for example the electrical heating of the catalyst.

1.2.3 Future Scenarios for After-Treatment System

Hybridization is a promising way to reduce CO_2 emission in transport sector. Nevertheless the internal combustion engine that works intermittently due to the presence of the electric motor decreases the temperature of the exhaust gases, this leads to longer light-off times and therefore to often work with inactive catalyst. The development of synthetic fuels will certainly increase in the transport sector. These fuels can be produced through CO_2 capture methods, so becoming carbon-neutral emitters. However, combustion in an internal combustion vehicle is bound to the use of air as a comburent. For this reason the production of nitrogen dioxide and nitrogen oxide is inevitable [6].

As is evident from the examples given here, the after-treatment systems will play a key role also in the decarbonization scenario.

Chapter 2

Methodology

2.1 Simulation Model

The development of new simulation technologies and the improvement of computing power have led to a different modeling method.

The accurate prediction of the performances of the after-treatment system is a complex problem, which requires a proper modeling of the different physical phenomena occurring in the device, such as heat-transfer, mass-transfer, chemical reactions, flow through porous media, also introducing suitable approximations.

This type of analysis is possible using fluid dynamics software combined with experimental characterization. In this way it is possible to introduce a preliminary analysis of the behaviours avoiding the physical construction of the component, thus reducing the design costs.

This thesis work is developed through the analysis of many different aspects of the engine system. The main part of the work is focused on the three-dimensional analysis of the abatement of a pre-catalyst and the consequent influence on the ATS of the complete exhaust pipe. However the evaluation of the impact on the overall after-treatment system is performed by 1D simulation model.

The 1D modeling is performed through a numerical code implemented by the Energy Department of the Politecnico di Milano, called *gasdyn*. The numerical code used is widely described and detailed in literature [19].

The innovative part of the project is analyzed through fluid dynamics software (CFD) which is the application of numerical methods to solve and analyze problems related to fluid flows. It is a branch of fluid mechanics which is based on the use of discretization methods to provide numerical solutions. In particular the computational model adopted in this case study is an open-source CFD code, *OpenFOAM*, based on finite volume discretization.

As shown in the figure below, the modeling approach considers a multi-region framework. This is used to work on different physical domains, such as: the fluid, which describes the gas flow through the system; the solid, which describes the metallic walls constituting pipes and canings; the substrate, which describes the catalysed porous media (honeycomb or open-cell foam) on which surface reactions take place.
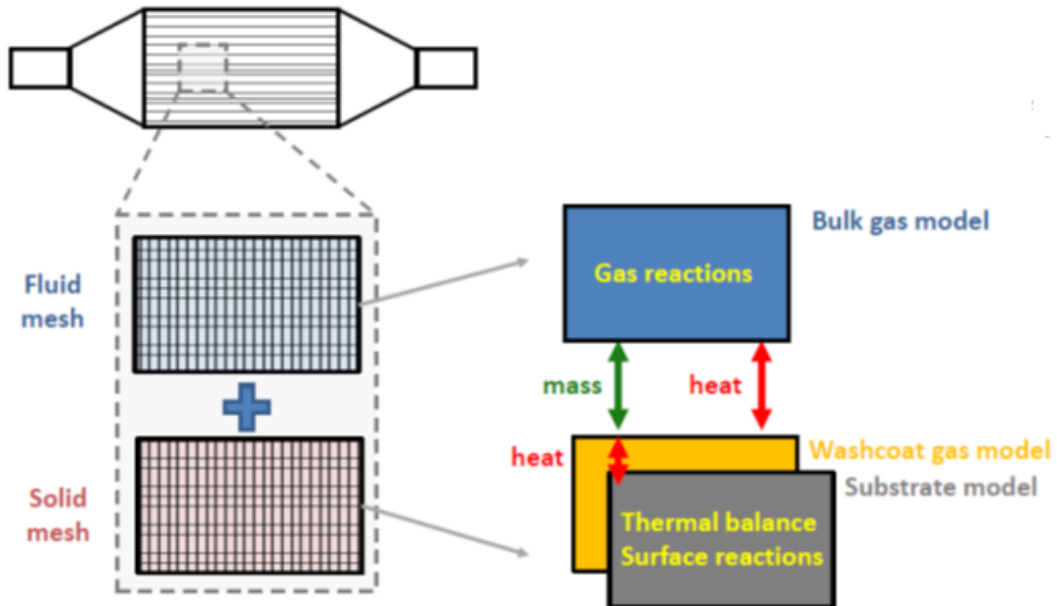
Figure 2.1: *Domain schematization of a multi-region simulation. [10]*

The multi-region model defined in this way allows to meticulously describe the thermal transient, which is essential to know the light-off behaviour.

2.2 Governing Equations for After-treatment System

Considering a multi-region system, it is important to correctly define the interactions between the different domains. The fundamental equations to describe the physical phenomena on the fluid and catalyst mesh are different.
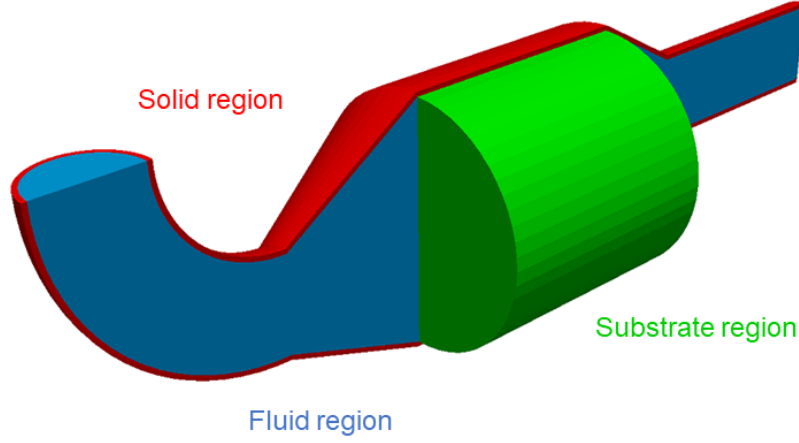
Figure 2.2: *Domain representation.* [16]

The provided governing equations are differential equations of conservation of mass, momentum, and energy, which come out from the balance on a generic control volume. These laws can be written in integral form, applicable to an extended region or volume, or in differential form, applicable to a point which represents a fluid particle.

The two forms are respectively:

$$\frac{\partial}{\partial t} \int_{\Omega} \rho\phi d\Omega + \int_{S=\partial\Omega} \rho\phi\vec{u} \cdot \vec{n} dS = \int_{\Omega} s d\Omega \qquad (2.1)$$

$$\frac{\partial}{\partial t}(\rho\phi) + \vec{\nabla} \cdot (\rho\phi\vec{u}) = s \qquad (2.2)$$

15

Where Ω represent the volume considered, S the boundary surface, ϕ the intensive quantity considered, ρ the density, u the velocity vector.

The two equations are completely equivalent in the mathematical sense but different with regards to discretization.

It is possible to move from one formulation to the another by applying the Gauss theorem.

Conservation of Mass

The governing flow equation which results from the application of the conservation of mass physical principle is called the continuity equation.

This conservation law requires that mass is neither created nor destroyed. This, applied to the finite control volume, imposes the mass flow difference throughout the system between inlet and outlet to be zero. This concept is explicated by:

$$\frac{Dm}{Dt} = 0 \tag{2.3}$$

Where: m is the mass, t is the time.

Expressing the mass as the integral of density over the volume

$$m = \int_V \rho dV \tag{2.4}$$

The conservation law can be rewritten as:

$$\frac{Dm}{Dt} = \frac{D}{Dt} \int_V \rho dV = 0 \tag{2.5}$$

Using the differential form:

$$\frac{\partial \rho_g}{\partial t} + \vec{\nabla} \cdot (\rho_g \vec{U}_g) = 0 \tag{2.6}$$

where the gradient of $(\rho_g \vec{U}_g)$ represents divergence of the velocity times density. The subscript g is used to indicate the gas phase.

Conservation of Momentum

The momentum equation is based on Newton's second law:

$$\vec{F} = m\vec{a} \tag{2.7}$$

That means the net force on the fluid is equal to its mass times the acceleration of the fluid element. This law can be written as:

$$\frac{\partial M}{\partial t} = \sum F \tag{2.8}$$

Where: M is the momentum, t is the time, F the forces.

Considering the momentum equal to:

$$M = \int_V \rho U \, dV \tag{2.9}$$

The Rate of change of momentum of a fluid particle is equal to the sum of forces acting on the particle. The net force acting on the control volume is the integral of the stress tensor, σ, over the surface, plus the integral of mass density multiplied by the accelerations acting on the body, over the volume. The forces described above can be distinguished in two main groups:

Body Forces: in which ρ is the density, g is the acceleration and V is the volume.

$$\vec{F}_{body} = \int_V \rho g \, dV \tag{2.10}$$

Surface Forces: In which σ is the stress tensor, n is the normal vector, S is the surface. These act on fluid elements through direct contact with the surface of the element.

$$\vec{F}_{surf} = \oint_S \bar{\bar{\sigma}} \cdot \vec{n} \, dS \tag{2.11}$$

Combining the equations just described, the conservation of momentum can be written as:

$$\frac{\partial \rho_g \vec{U}_g}{\partial t} + \vec{\nabla} \cdot (\rho_g \vec{U}_g \vec{U}_g) = \rho_g \vec{g} + \vec{\nabla} \cdot \bar{\bar{\sigma}} \tag{2.12}$$

Conservation of Energy

Conservation of Energy is the first law of thermodynamics. The variation of energy over time correspond to the sum of the work and heat.

$$\frac{DE}{Dt} = \frac{DW}{Dt} + \frac{DQ}{Dt} = \dot{W} + \dot{Q} \tag{2.13}$$

Where $\frac{D}{Dt}$ represents the material derivative, E is the energy, Q is the heat and W is the work.

The conserved quantity is the total energy, defined as the sum of fluid internal energy plus its kinetic energy per unit mass:

$$E = u + \frac{1}{2}U^2 \tag{2.14}$$

Summarizing all these concepts, the energy equation becomes:

$$\frac{\partial}{\partial t}(\rho_g(e_g + \frac{1}{2}|\vec{U_g}|^2)) + \vec{\nabla} \cdot (\rho_g(u + \frac{1}{2}|\vec{U_g}|^2)\vec{U_g}) = \vec{g} \cdot \vec{U_g} + \vec{\nabla} \cdot (\overline{\overline{\sigma}} \cdot \vec{U_g}) + \\ -\vec{\nabla} \cdot \vec{q} + Q \tag{2.15}$$

It is possible to recognize a convective term, a diffusive term and the volume and surface terms.

Conservation of Chemical Species

Starting from the validity of continuity equation, it is feasible to analyze the mass as made of nuclei. It is well known that the identity of the atomic nuclei does not change, when, in the occurrence of a chemical reaction, they form new bonds with other atoms forming new molecules. Due to this last fact, the conservation law of mass can be expressed as algebraic conservation equations of the numbers of nuclei of each chemical element.

Equations describing chemically reactive flows considering an arbitrary specie (k) can be expressed as follow:

$$\frac{\partial \rho Y_k}{\partial t} + \vec{\nabla} \cdot (\rho Y_k \vec{U}) = -\vec{\nabla} \cdot \vec{J_k} + R_k \tag{2.16}$$

Where Y is the mass fraction referred to the $k-th$ specie, the gradient of J represents the diffusive flux and the term R takes into account the generation and destruction of the $k-th$ specie due to the chemical reactions.

The equation, to respect the mass conservation, requires:

$$\sum Y_k = 1 \tag{2.17}$$

Starting from the general conservation equations described above, we can characterize the system of equations for the fluid domain and later for the solid domain.

2.2.1 Constitutive law

To solve a non-linear system of equations different assumptions are required to grind the equations to a possible solution.

The characterization of the flow field of the fluid regions involves some additional constitutive relations to describe the properties of the fluid, the initial and boundary conditions.

The thermal properties of the multi-component mixture are determined based on the JANAF tables. A Sutherland model is applied for the calculation of the transport properties, in order to take into account the dependency of viscosity on the gas temperature. The mass diffusivity is modeled under the assumption of Schmidt number equal to 1 in order to reduce the computational burden. With regard to the gas phase chemistry modeling, an Arrhenius-type expression is adopted to determine the reaction rates.

Equation of State

It is necessary to define a relation between density and thermodynamic conditions.

$$\rho = \rho(p, T) \tag{2.18}$$

A first necessary hypothesis is that the fluid analyzed in this work could be approximated by a perfect gas. Under this condition it is possible to write:

$$\rho = \frac{p}{R^*T} \tag{2.19}$$

$$R^* = \frac{R}{MM} \tag{2.20}$$

Where R is the universal gas constant and its value is 8.314 $[\frac{J}{molK}]$ and MM is the molar mass.

This is the easiest model for EoS but more complex models exist.

Stress Tensor

The characterisation of the stress tensor is derived from the solid mechanic theory, where the stress tensor is split into two tensors: hydrostatic and deviatoric.

$$\bar{\bar{\sigma}} = -p\bar{\bar{I}} + \bar{\bar{\tau}} \tag{2.21}$$

The deviatoric tensor is defined by:

$$\tau_{i,j} = \mu[(\frac{\partial U_j}{\partial x_i} + \frac{\partial U_i}{\partial x_j}) - \frac{2}{3}(\vec{\nabla} \cdot \vec{U})\delta_{i,j}] \tag{2.22}$$

Energy Flux

The energy flux can be expressed using the Fourier Law, that returns the thermal flux as a function of the temperature T and the thermal conductivity k:

$$\vec{q} = -k\nabla T \tag{2.23}$$

Diffusive Flux

It is well modelled by the Fick's law:

$$\vec{J}_k = -\rho D_{k,mix} \vec{\nabla} Y_k \tag{2.24}$$

That is based on diffusion coefficient D, also called diffusivity.

2.2.2 Governing equation for fluid domain

The introduction of the constitutive laws into the general conservation equations produces the following equations which are the specific conservation laws for fluid domain.

Conservation of Mass

$$\frac{\partial \rho_g}{\partial t} + \vec{\nabla} \cdot (\rho_g \vec{U}_g) = 0 \tag{2.25}$$

Conservation of Momentum

$$\frac{\partial \rho \vec{U}_g}{\partial t} + \vec{\nabla} \cdot (\rho \vec{U}_g \vec{U}_g) = \rho_g \vec{g} - \vec{\nabla}(p + \frac{2}{3}\mu_g \vec{\nabla} \cdot \vec{U}_g) + \vec{\nabla}[\mu(\vec{\nabla}\vec{U}_g + \vec{\nabla}\vec{U}_g{}^T)] + \mathcal{R} \tag{2.26}$$

The $\mathcal{R}$ represents the permeability, which depends on the geometrical properties of the substrate and the instantaneous fluid dynamics conditions, and can be determined on the basis of the Reynolds number Re.

Conservation of Energy

$$\frac{\partial \rho_g e_g}{\partial t} + \vec{\nabla} \cdot l \rho_g e_g \vec{U}_g = \rho_g \vec{g} \vec{U}_g - \vec{\nabla} \cdot ([(p + \frac{2}{3}\mu_g \vec{\nabla} \cdot \vec{U}_g) - \mu(\vec{\nabla}\vec{U}_g + \vec{\nabla}\vec{U}_g{}^T)]U_g)$$
$$+ \vec{\nabla} \cdot (\lambda_g \vec{\nabla} T_g) + \rho_g Q_g + \rho_g Q_g{}^R + Q^{w \to g}$$

$$\tag{2.27}$$

Where λ_g represents the thermal conductivity, specifically referred to the gas flow. Q_g represents the generic heat source of the gas, instead $Q_g{}^R$ is the reaction heat for the homogeneous gas reactions and $Q^{w \to g}$ describes the heat transfer occurring between the gas flow (g) and the washcoat (w).

Conservation of Species

$$\frac{\partial \rho_g Y_{g,i}}{\partial t} + \vec{\nabla} \cdot (\rho_g Y_{g,i} \vec{U}_g) = \vec{\nabla} \cdot (\rho_g D_{g,i} \vec{\nabla} Y_{g,i}) + \rho_g R_{g,i} + J_i{}^{wg \to g}. \tag{2.28}$$

Where $D_{g,i}$ is the mass diffusivity, $J_i{}^{wg \to g}$ describes the species transfer occurring between the gas flow (g) and the near wall gas (wg) zone.

2.2.3 Governing equation of solid domains

Considering the solid domain, the governing equations needed are conservation of chemical species near the wall and conservation of energy. The equation for chemical reactions is required because the solid domain includes the substrate where the reaction occur.

Conservation of Species for the near wall gas

$$\frac{\partial \beta_{wg} \rho_{wg} Y_{wg,i}}{\partial t} = \beta_{wg} \rho_{wg} R_{wg,i} - J_i^{wg \to g} \qquad (2.29)$$

Where $J_i^{wg \to g}$ is the mass transfer, β_{wg} is the volumetric fraction coefficient, $R_{wg,i}$ is the reaction source term, and $Y_{wg,i}$ is the chemical species mass fraction.

Conservation of Energy for the near wall gas

$$\frac{\partial \beta_{wg} \rho_{wg} c_{wg} T_{wg}}{\partial t} = Q^{w \to wg} \qquad (2.30)$$

Where $Q^{w \to wg}$ is the heat transfer .

Conservation of Energy for the substrate

$$\frac{\partial \beta_s \rho_s c_s T_s}{\partial t} = \beta_s \rho_s Q_s + \nabla \cdot (\lambda_s \nabla T_s) + Q^{w \to s} \qquad (2.31)$$

This equation describes the substrate interaction, where λ_s is the conductivity, $Q^{w \to s}$ the heat transfer.

The term Q_s is very important in this work because it gives the possibility to introduce the heating of the substrate by an external source (e.g. electrical heating). Comparing the equations of fluid and solid regions the relationship between adjacent regions is evident.

The coupling of the different models is described by the scheme reported in Figure 2.3.
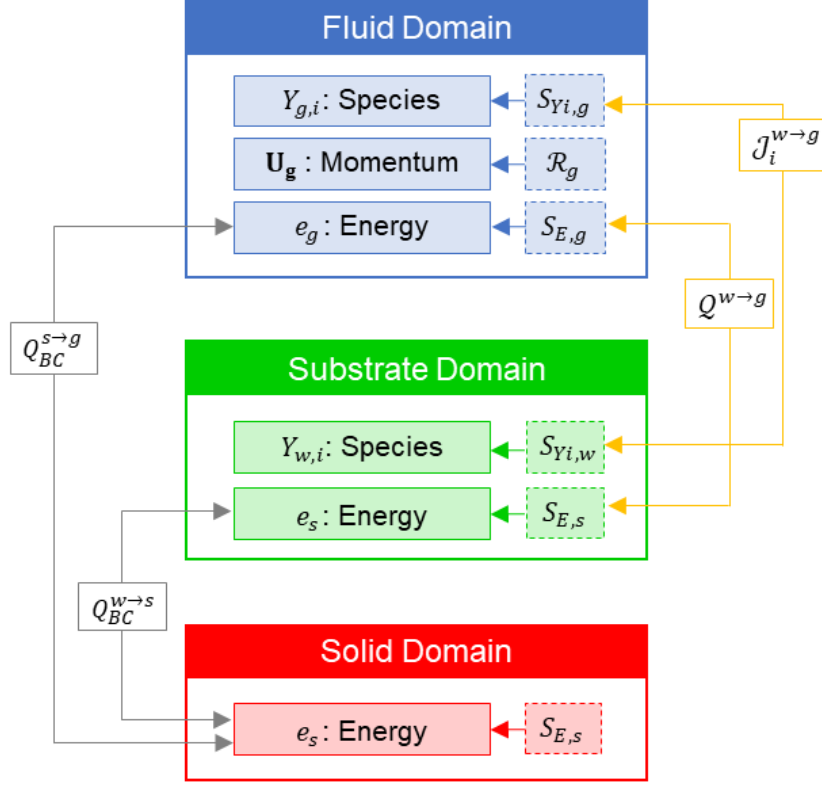
Figure 2.3: *Overview of the governing equations solved for each domain and of the coupling terms for describing their interaction. [16]*

The fluid domain exchanges with both solid domain, though heat transfer, and substrate domain, through heat and mass transfer.

The catalyst sub-model

The model described requires sub-models to specify each component of the setup. The boundary conditions are typically used for coupling the regions. The temperature, for example, is imposed over the interface boundary.

According to the following relations, λ is the conductivity, T is the temperature, i and j represent the two adjacent regions, L is the distance.

$$T_w = T_i - \frac{\lambda_j L_i}{\lambda_i L_i + \lambda_j L_j}(T_i - T_j) \tag{2.32}$$

$$T_w = T_j + \frac{\lambda_i L_j}{\lambda_i L_i + \lambda_j L_j}(T_i - T_j) \tag{2.33}$$

The permeability model defines the fluid-dynamic resistance encountered by the gas flowing through the porous medium. The flow resistance source term $\mathcal{R}_g$ is defined as:

$$\mathcal{R}_g = f(Re)\frac{4}{d_c}\frac{1}{2}\rho U_g{}^2 \tag{2.34}$$

Where f is the friction factor that can be evaluated according to different models, as the Churchill correlation.

Instead, the heat transfer is:

$$Q^{w \to s} = Nu(Re, Pr)\frac{\lambda}{d_c}S_V V(T_g - T_w) \tag{2.35}$$

Similarly, the mass transfer:

$$J_i{}^{w \to s} = Sh(Re, Sc)\frac{D}{d_c}S_V V(C_g - C_w) \tag{2.36}$$

In the last formulations the use of adimentional numbers is evident. $\mathcal{R}_g$ refers to the Reynolds number, instead $Q^{w \to s}$ contains the Nusselt number, that is a function of Reynolds and Prandtl, and $J_i{}^{w \to s}$ is proportional to Sherwood, that is a function of Reynolds and Schmidt.

Catalyst reactions

The surface reaction model also considers the conversion occurring on the catalytic washcoat. The Langmuir-Hinshelwood model is adopted.

Considering a generic reaction

$$\alpha A + \beta B \to \gamma C + \delta D \tag{2.37}$$

The reaction rate can be evaluated as:

$$r_i = k_{r,i}\frac{p_A p_B}{TG_i}Eq_{f,i} \tag{2.38}$$

Where k is computed thanks to Arrhenius law, p is the partial pressure of reactants divided by the reference pressure, T is the substrate temperature, G is the inhibition term which takes into account the species competition to occupy the active site and Eq is the equilibrium term.

The terms $k_{r,i}$ and $k_{a,i}$ are Arrhenius type kinetic constants, which regulate the reaction and the adsorption mechanisms:

$$k_{r,i} = A_{r,i} e^{\frac{-E_{r,i}}{RT_w}} \tag{2.39}$$

Most of the reactions taking place in catalytic devices are usually non-reversible, therefore the equilibrium term $E_{r,i}$ is equal to 1. However, some reactions can exhibit a reversible behaviour: in order to account for the chemical equilibrium limitation the equilibrium term can be introduced for the forward reaction.

$$Eq_f = 1 - \frac{C_{s,C}{}^\gamma C_{s,D}{}^\delta}{C_{s,A}{}^\alpha C_{s,B}{}^\beta K_p(T)} \tag{2.40}$$

A key role in chemical reactions of the catalyst is played by Cerium, which has the capacity to store and release oxygen passing from two different stage of oxidation: CeO_2 and Ce_2O_3.

During the lean period oxygen is stored and then, during the rich period, it's released and contributes to oxidize carbon monoxide and unburned hydrocarbons.

$$R_{storage} = k p_i \psi_{Ce_2O_3} \Psi_{Ce} \tag{2.41}$$

$$R_{release} = k p_i (1 - \psi_{Ce_2O_3}) \Psi_{Ce} \tag{2.42}$$

Where k is the Arrhenius term, p the partial pressure, Ψ the total cerium capacity. The evolution of the oxidation state is given by the balance between the activity of the store and release reactions:

$$\Psi_{Ce} \frac{\partial \psi_{Ce_2O_3}}{\partial t} = \sum R_{storage} - \sum R_{release} \tag{2.43}$$

The computational model defined by the equations, meticulously described in this chapter, requires a proper solution procedure to determine the result within an

acceptable time.

The procedure used to solve the governing equations is schematized in Figure 2.4.
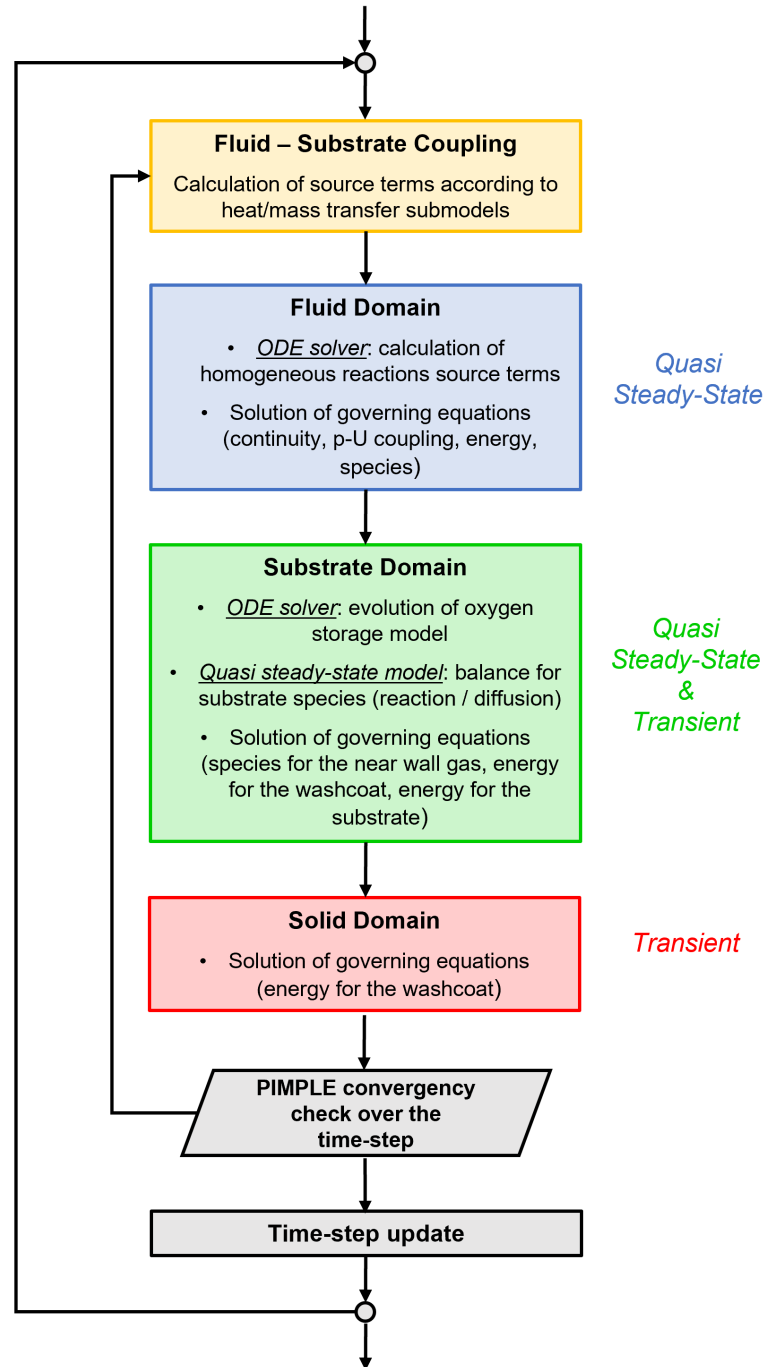
Figure 2.4: *Overview of the iterative numerical procedure. [16]*

Due to the size of the domain, the complexity of the physics, and the time interval to be simulate, the simulation procedure must be appropriately advanced, for this reason it continues to be optimized even now.

The methodology employed in this thesis work is based on the use of a stationary model for the fluid domain, a quasi-stationary and transient model for the substrate domain, and a transient model for the solid domain.

The transient simulation needs a flexible algorithm which combines the high time resolutions of PISO algorithm in the *OpenFOAM* definition and the constraint on the Courant specific of SIMPLE one, allowing for bigger time steps and therefore lower computational time. The compromise found between the two is called PIMPLE that is able to dynamically choose between standard PISO and transient SIMPLE procedure.

For the fluid region, the unsteady operations of the engine are not relevant for the description of ATS behaviour. So it is acceptable to use the timestep proper of the thermal analysis.

The substrate domain has more complex characteristics because it combines aspects that are approximate to quasi-stationary models, such as chemical reactions, with accumulation states that must be described by transient models.

When the accumulation of products/reactants in the washcoat is negligible, the stationary equilibrium between diffusion process and chemistry reactions is considered true, i.e. there is an equal rate of diffusion of the species and the rate of chemical reaction to convert reactants into products.

However, for some reactions this hypothesis is not appropriate. Some species present in the washcoat have the ability to trap the oxygen. This storage process is intrinsically unsteady, because the period of absorption and release cycle is in the order of seconds. In this context ODE solver is required, as it works with sub-cycles able to describe chemical reactions.

The solver works through an iterative procedure in which it searches for the con-

vergence that couples the different domains.

For each iteration, the first operation consists of the coupling between the different overlapping regions, namely fluid and catalyst(s), in order to evaluate substrate permeability and heat- and mass-transfer coefficients. Once the coupling source terms are computed, the equations for the different domains are solved sequentially. When all the operations for the considered iteration are completed, the convergency of the solution over the time-step is checked and, if convergency condition is verified, the time-step is advanced.

Chapter 3

Development of innovative POCS for precatalysis

As previously described, the new after-treatment systems have a great efficiency except for low temperature operating conditions of the catalyst.

An effective solution to promote the catalyst light-off, especially at the start-up and during the low load operation of the engine typical of the urban drive, is the adoption of electrical heating, that is based on the Joule phenomenon.

3.1   Pre-catalyst

The earlier activation of the catalytic converters in internal combustion engines is becoming more challenging.

As said above, the critical issue of the catalyst come out on urban roads, where it is difficult to maintain the correct temperature of the washcoat due to the frequent start and stop, in addition to the starting period itself. To achieve that goal a promising strategy is the introduction of a smaller catalyst immediately downstream of the engine. In this way it is possible to exploit warmer gases but the real challenge is to introduce a method of heating the structure of the catalyst itself to reach the optimal temperature in a short time.

Creating a metallic structure it is possible to introduce a potential difference on the catalyst that provokes the heating of the component.

Starting from these assumptions, the research for geometries and materials suitable for this purpose begins.

3.2 Potential difference - Joule heating

Joule heating is the physical effect in which the flow of current through an electrical conductor is converted into heat.

In particular, when the electric current flows through a solid or liquid with finite conductivity, electric energy is converted to heat through resistive losses in the material. The heat is generated on the microscale when the conduction electrons transfer energy to the conductor's atoms by way of collisions. Typically, this effect is undesired because represents an energy dispersion. The flow of electrons, that generates electric current, is caused by the so-called electromotive force (emf) that is produced by the potential difference between two points in a structure.

This effect is summarized in Ohm's law:

$$I = \frac{V}{R} \tag{3.1}$$

It states that the electric current I, which is the amount of moving electric charge per unit of time, flowing through the conductor is proportional to the difference in electric potential at its ends V and inversely proportional to the resistance of the conductor material R.

The resistance depends not only on the material of the conductor, characterized by its resistivity ρ, but also on its geometry, in particular regarding the length and the cross-section area.

$$R = \frac{\rho l}{A} \tag{3.2}$$

Knowing that, it is easy to evaluate the power and consequently the heat produced, as follow:

$$P = \frac{V^2}{R} \tag{3.3}$$

The simplest modeling approach consists in considering that the overall electrical power is dissipated into heat, and it is uniformly distributed in the heating section:

$$Q_s = P_{el} \tag{3.4}$$

However, this simple model can result too simplified, especially if the actual temperature distribution is considered. As a matter of the fact, the heat generation is not uniform across the heater section. Generally the thermal conduction is defined by the equation:

$$\frac{\rho c_p dT}{dt} = \nabla(k\nabla T) \tag{3.5}$$

Where ρ is the density, c_p the specific heat, k the thermal conductivity and T the temperature.

Introducing the Joule heating term and the heat transfer in solid regions the equation becomes:

$$\frac{\rho c_p dT}{dt} = \nabla(k\nabla T) + \sigma|\nabla V|^2 - \rho c_p U \nabla T \tag{3.6}$$

Where σ is the electrical conductivity, V is the electric potential and U is the velocity vector.

The electrical conduction can be considered a quasi-stationary process in the time scale of heat transfer and convection. Thus, it is described by the simple Lagrangian equation.

$$\nabla(\sigma\nabla V) = 0 \tag{3.7}$$

Note that the electric current density vector $\sigma\nabla$V does not have to be explicitly stored as it can easily be calculated during post-processing. Further, equation is only valid for stationary DC current. In the case of AC or pulsed current, it is necessary to also include the magnetic field and the full set of Maxwell equations. So the Joule heating contribution is defined according to differential form as:

$$\frac{dP}{dV} = JE \tag{3.8}$$

Where the electric field E is evaluated as $E = \nabla V$, the current density J is equal to σE, so the equation becomes:

$$\frac{dP}{dV} = JE = (\sigma E)E = (\sigma \nabla V)\nabla V \tag{3.9}$$

3.3 Periodic Open Cell Structures - POCS

In the last years different types of structures for catalytic applications have been studied. Among these one of the most studied are the open-cell foams, which are cellular materials consisting of interconnected solid struts which form multiple pseudo-spherical void spaces. A great advantage of these structures is the possibility of being produced with both metallic and ceramic materials, moreover these are characterized by light-weight, high specific surfaces and high permeability to the fluid flow. The adoption of open-cell foams seems to be particularly convenient, since the tortuous flow path induced by their micro-structural geometry results in high activity per unit volume [11].

This technology shows high performances in terms of heat/mass-transfer but at high flow rates the foams penalize the system, due to the dense structure.
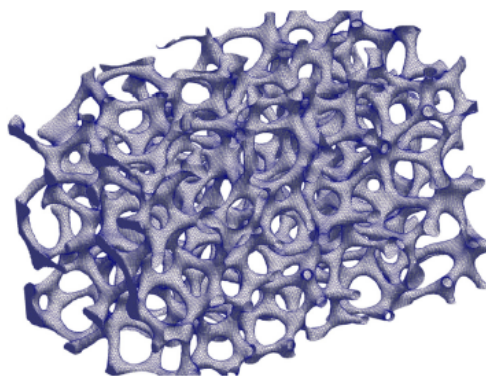
Figure 3.1: *Open-cell foams. [13]*

The recent development of technologies grants a progressively shifting towards the adoption of Periodic Open Cell Structures (POCS). These structures retain

all the advantageous features associated with open cell foams such as high surface area, permeability in all directions and an interconnected solid structure. In addition, their ordered design combined with Computer Aided Design techniques and modern additive manufacturing methods (3D printing) allows for optimizing their geometry towards the selected application needs [17].
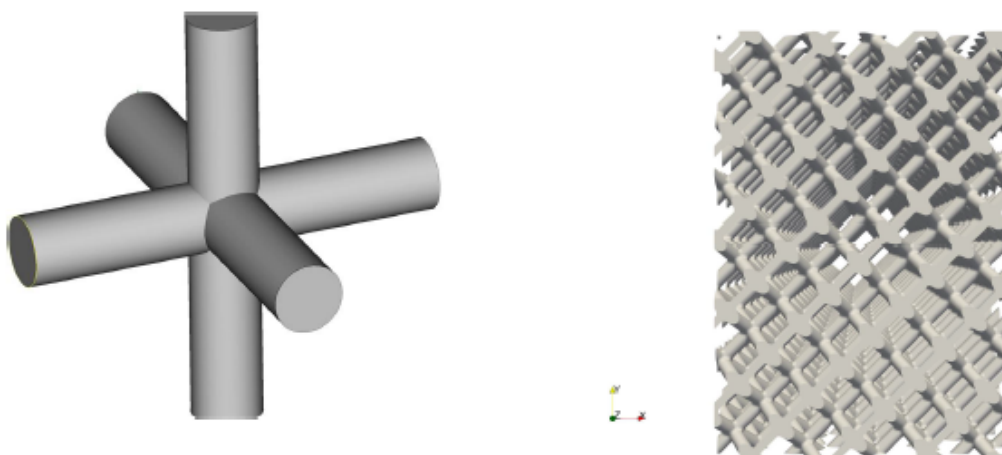
Figure 3.2: *Exempla of actual POCS. [17]*

The idea is to design a POCS made of electrical conductive material. The POCS are structures with morphology and properties similar to open-cell foams but are arbitrarily designed with CAD tools.

The advantage of this structure, in addition to the active heating system that can be updated, is the possibility to place a washcoat layer on the surfaces. This thin layer, rich in precious metals as described in the introduction chapter, can be sprayed on surfaces.

3.4 Additive Layer Manufacturing - ALM

The geometric flexibility introduced by the POCS is possible thanks to recent developments in the field of Additive Layer Manufacturing (ALM). This technique allows to recreate objects on the bases of CAD structure. A very important feature of the Additive Layer Manufacturing is versatility. A wide range of printing

materials can be used, even creating structures with multiple materials.

3.5 Innovative POCS Geometry

All the components previously described in this chapter, were analysed to provide a suitable geometry for advanced emission control.
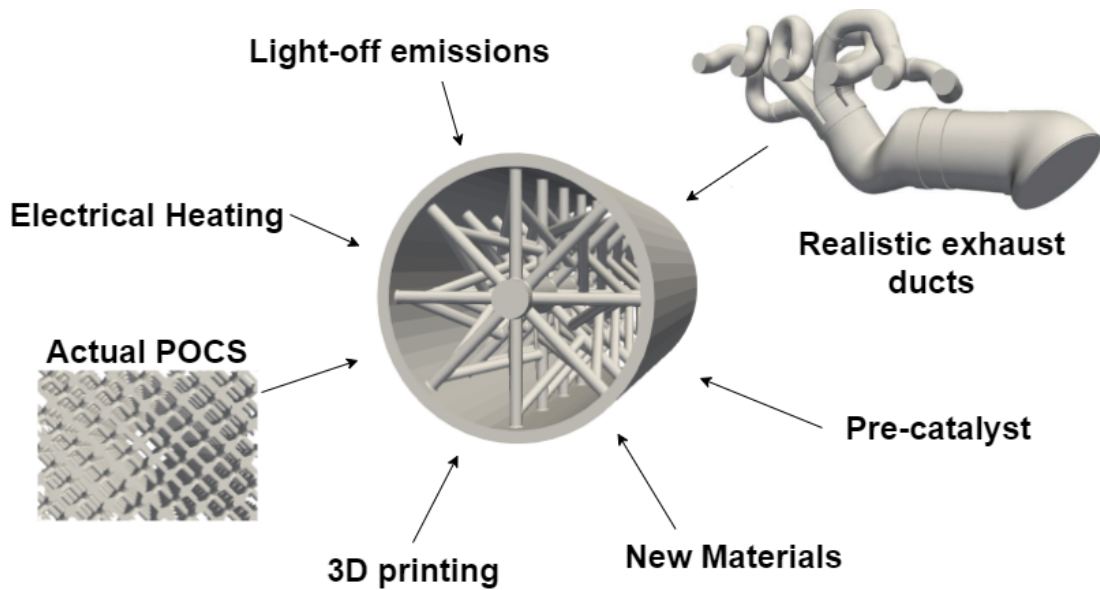
Figure 3.3: *Development of POCS design.*

The focal point on which the design of the piece is based is the heating of the flow, without neglecting the aerodynamics.

Before defining the geometry on a realistic duct, a basic geometry is designed on a straight duct.

To have the best distribution of the heat inside a cylinder heat source must come from its axis, so a central pipe is designed. From this the rest of the structure is defined. To connect the inner pipe to the wall duct eight struts, equally distributed around the central pipe, are defined and then periodically repeated along the pipe at a fixed distance. Finally, inclined struts are introduced to better distribute the heat.
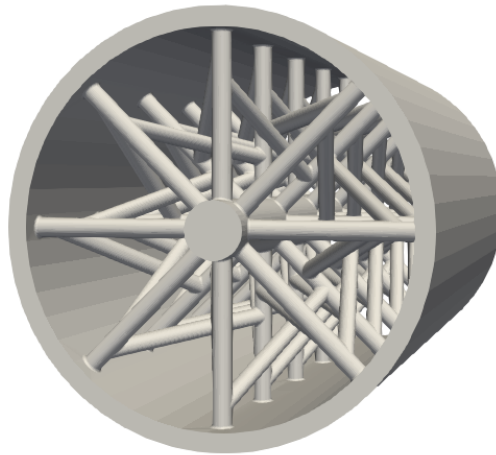
Figure 3.4: *Preliminary POCS structure.*

After the preliminary analysis on this geometry, that will be meticulously describe in the next chapter, the geometry is adapted to a realistic duct.

The realistic duct considered is not linear anymore, so some characteristics have to be modified. The radial struts are not parallel everywhere, also the inclined struts have different lengths. Although some changes have taken place, overall the new geometry reflects well the preliminary one.
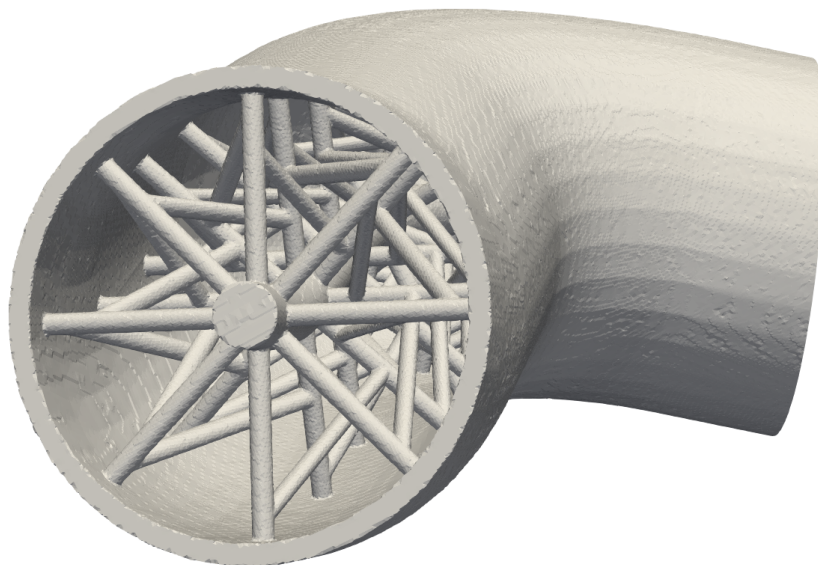
Figure 3.5: *POCS applied to realistic geometry.*
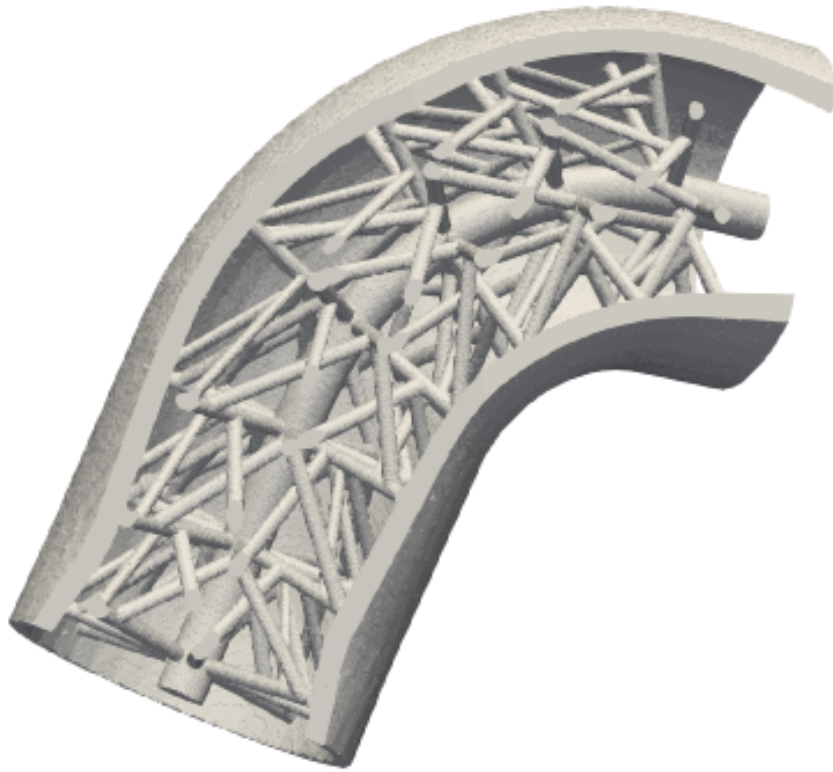
Figure 3.6: *Section of realistic POCS.*

Chapter 4

CFD analysis of ATS equipped with POCS pre-catalyst

OpenFOAM is a highly customizable program, which allows the fluid dynamics analysis of complex objects.

In *OpenFOAM*, there is no generic solver that applies to all types of flow conditions, it allows the development of solvers for fluid and continuum mechanical problems. Anyway, a variety of these solvers and libraries for different applications has been developed over the years and are already present in *OpenFOAM*, categorized on the base of the type of continuum mechanics such as incompressible flow, heat transfer, combustion etc.

The minimum set of files required to run the simulation is contained in the base folders present in the case:

- The *system* folder, which contains the files that control the definition of solution management parameters.

- The *constant* folder, in which the information regarding the grid and all files that characterize the physical properties of the case are placed.

- The initialization folder, called *0*, which contains all the initial values required for the simulation.

The *system* folder contains at least the following three files: the *controlDict* where

run control parameters are set including start/end time, time step and parameters for data output, the *fvSchemes*, where discretisation schemes used in the solution may be selected at run-time, and the *fvSolution* where the equation solvers, tolerances and other algorithm controls are set for the run.

The type of mathematical model for the physical schematization of the problem is defined in the *controlDict*, in this case is *chtcfsMultiRegionPsiReactingQSSCatalystFoam*, one of the solvers developed by the Internal Combustion Engine group of Politecnico di Milano.

In all the cases analyzed, the *system* folder contains, in addition to the above-mentioned files, also the dictionaries concerning the Mesh, such as *BlockMeshDict, snappyHexMeshDict, surfaceFeaturesDict*, and *snappyHexMeshDict* for layers and washcoat.

OpenFOAM allows ample freedom on the choice of schemes applicable to the discretization of the mathematical operators present in the equations of the problem.

4.1   Mesh

As described in a previous chapter, CFD is based on the use of a finite volume discretization. This means that it will be necessary to divide the volume into pieces small enough to accurately describe each geometric feature of the structure. This division is called meshing, or mesh generation. It is the process of generating a two-dimensional and three-dimensional grid, in which complex geometries are divided into elements that can be used to discretize a domain. This step is fundamental to translate the geometrical and mathematical model into the numerical one.

Due to the iterative nature of these calculations, obtaining a solution to the governing equations are not practical by hand and so computational methods such as Computational Fluid Dynamics (CFD) are used. Computers resolution algorithms require the continuous geometry of the object split into millions of fragments, to

which properly apply the equations on the basis of the finite volume discretization.

Creating a high-quality mesh is one of the most critical factors that should be considered to ensure simulation accuracy.

The grid has a considerable impact on the solution accuracy, the convergence speed (or even lack of convergence) and the calculation time.

The mesh generation is typically produced following a few consecutive steps.

First a background mesh is defined through the indications defined in the blockMesh file. This file contains eight coordinates capable of defining a polygon, typically with a rectangular base, then the characteristics on which to build the mesh, the type of block and the number of cells for each coordinate, are defined. Other informations in the same script line, such as the mesh grading in each direction and boundaries specification, are present.

The next step, the castellated mesh, requires the definition of the edgeMesh to be applied. So, through the use of *surfaceFeatures* utility, edgeMesh is extracted from the *trisurface* file.

After the definition of the background mesh, the so-called "cellsplitting"starts. The splitting occurs according to the settings chosen by the user in the castellatedMeshControls sub-dictionary within the file. At first the geometries are defined through a *trisurface* or bounding geometry entities. The splitting process begins with cells being selected according to specified edge features, that are obtained in the previous step. This process is meticulously described in the *SnappyHexMeshDict*, where the refinement is set. The next stage of the meshing process involves moving cell vertex points onto surface geometry to remove the jagged castellated surface from the mesh. Here the number of patch smoothing, tolerance, number of mesh displacement relaxation and maximum number of snapping relaxation are defined.

The mesh output from the snapping stage may be suitable for the purpose, al-

though it can produce some irregular cells along boundary surfaces. In this step additional layers are introduced at boundary layer. In this way better resolution is achieved.

4.2 Preliminary Analysis - POCS structure

Before carrying out an analysis on realistic geometries, a preliminary study to evaluate the basic characteristics is performed. The preliminary geometry of the POCS is designed on a 75 mm long straight duct with a diameter of 40 mm. The geometry consists of a series of perpendicular and inclined struts with a diameter of 2 mm that channel the flow, as shown in the Figure 3.4.

To analyze the fluid dynamics of the geometry the mesh process described above is required. To define the validity of the mesh results, different meshes are compared. This sensitivity analysis is realized on three meshes characterized by different number and size of the cells.

type of mesh	millions of cells	base cell dimensions (x y z) [m]
Mesh1	1.25	(0.000837 0.000837 0.0011)
Mesh2	2.7	(0.00055 0.00055 0.00073)
Mesh3	5	(0.00037 0.00037 0.00057)

Table 4.1: *Properties of different meshes for sensitivity analysis.*

To better compare the employed meshes and visualize their structure, these are reported in Figure 4.3.
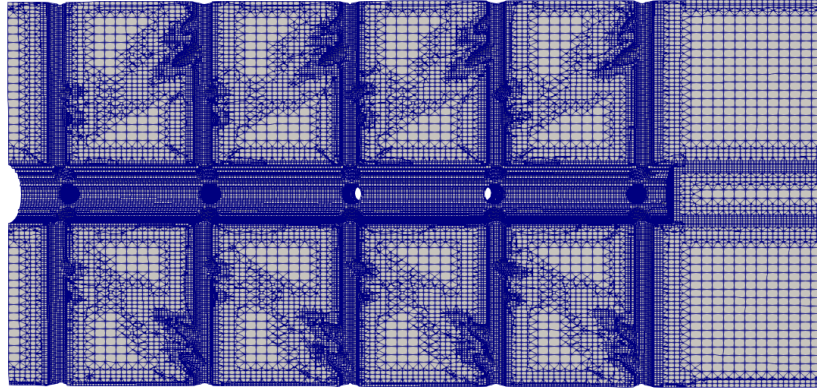
Figure 4.1: *Mesh 1 considering only the fluid part.*
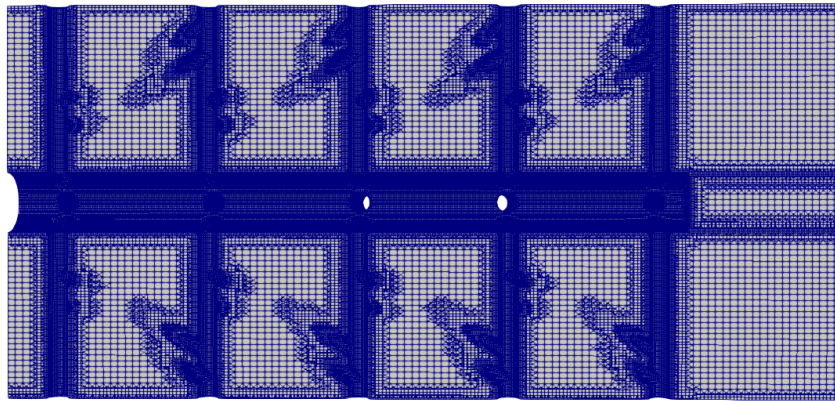
Figure 4.2: *Mesh 2 considering only the fluid part.*
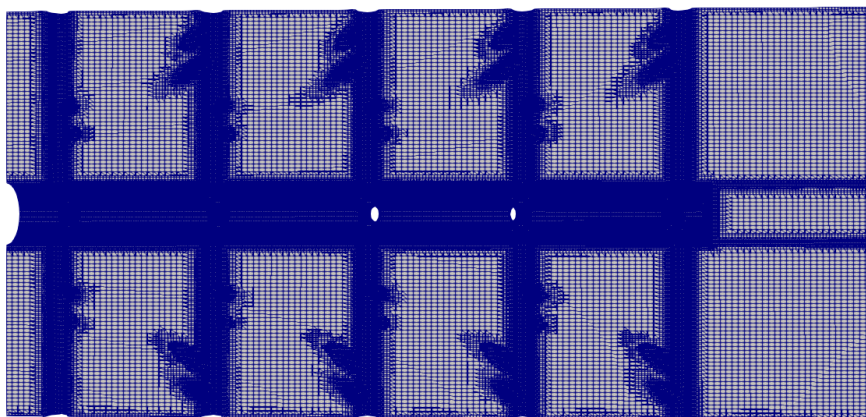
Figure 4.3: *Mesh 3 considering only the fluid part.*

To evaluate the goodness of the model, the *Motorbike* tutorial is used as base structure for the pressure variation analysis. The tutorial is based on *simpleFoam* solver that is a steady-state solver for incompressible, turbulent flows. In this way, the aerodynamics of the model is analyzed through the evaluation of pressure losses.

The tutorial post processing allows to extract the pressure loss data for a fixed speed, for this reason the losses for different speeds are calculated.

With the data obtained by the simulation is possible to define the diagram which considers the pressure loss in $[mbar]$ on the y-axis while the velocity in $\left[\frac{m}{s}\right]$ on the x-axis. The diagram obtained is reported in Figure 4.4.
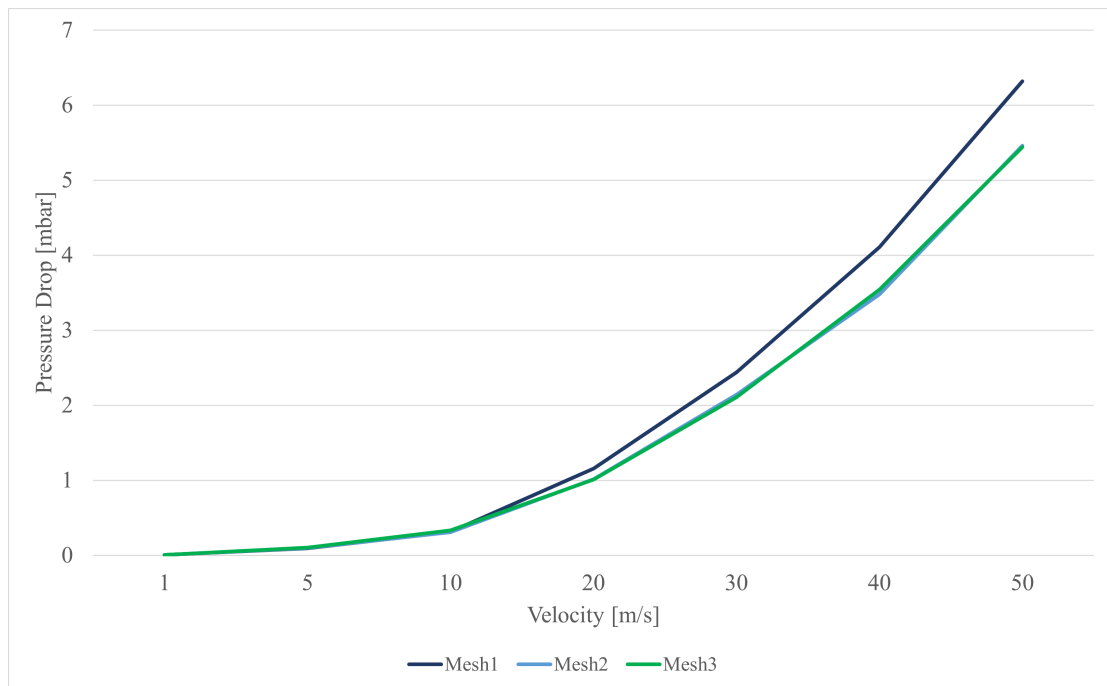
Figure 4.4: *Preliminary POCS structure: sensitivity analysis.*

The difference between the meshes is very low, less than 1 mbar. So the first mesh is set as the reference one to limit the time of simulation, keeping in mind it is only a preliminary analysis.

4.2.1 Potential difference with copper as conductor

The preliminary study aims to evaluate the pressure losses, which are shown previously, and to verify the applicability of the model of the potential difference. The potential difference is then analyzed as follows.

In this case a copper wire is inserted into the central pipe in order to have a better electrical conductivity compared to stainless steel. The position of the copper is strategical to have radial heating around it.

The voltage applied to the copper strut is equal to 1V, while the rest of the POCS can be considered as having zero potential. Hence the potential appears to be distributed as shown in the Figure 4.5.
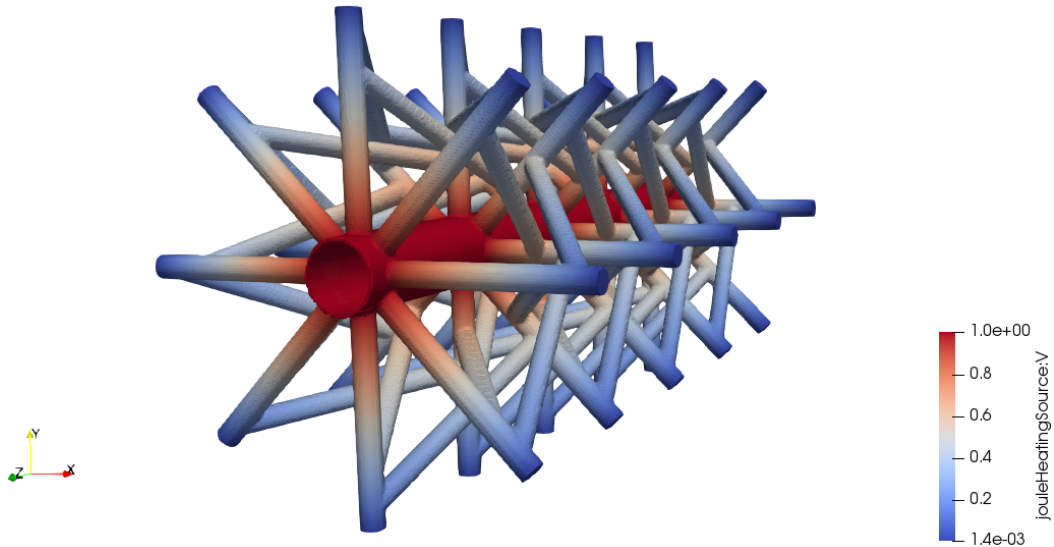
Figure 4.5: *Preliminary POCS structure: potential difference distribution.*

The analysis is made with a flow at 300K and with uniform velocity parallel to the duct.

As shown in the Figure 4.5 the potential is well distributed along the strut, anyway the temperature rises very quickly but not uniformly. In 10 seconds part of the structure achieves a temperature of 2000K, beyond its melting temperature.

For this simulation the potential is assumed as uniformly distributed along the
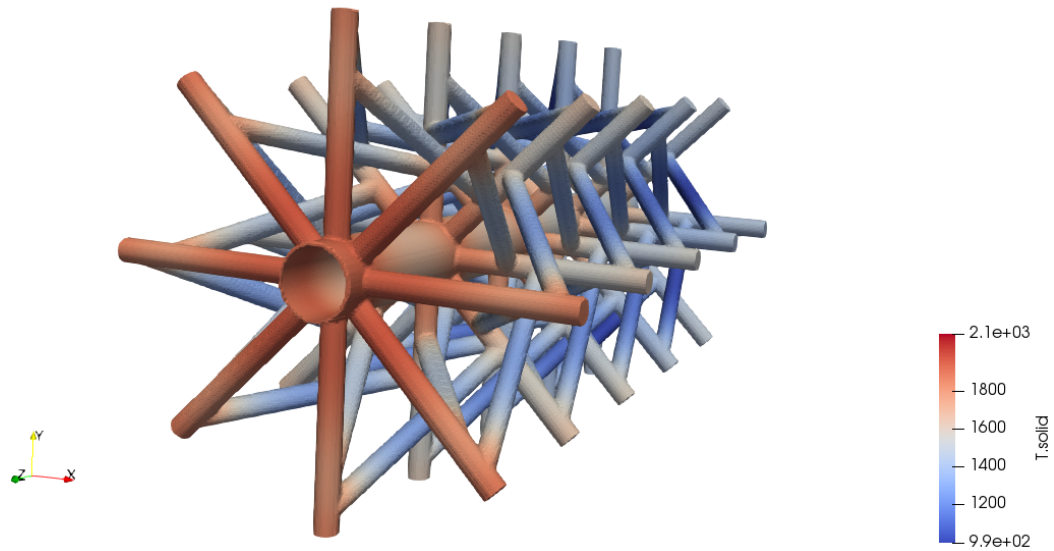
Figure 4.6: *Preliminary POCS structure: temperature distribution after 10 seconds.*

copper cylinder. This assumption is a modeling simplification, which approximate what happens in reality.

4.2.2 Conclusion of preliminary analysis

As can be seen from this preliminary analysis, the fluid dynamics of the model is a good starting point for the real POCS development. The pressure losses inside the channel are only about 6 mbar. Instead, some weaknesses in the conduction of current through the structure is evident. The current density appears well distributed along the struts, but this is based on a modeling assumption. For the case study a more realistic strategy has to be taken into account.

4.3 POCS case study

In the first case study, the pre-catalyst inside a realistic exhaust duct of a V12 engine is analyzed.

The geometry analyzed on the straight pipe shows good fluid dynamic characteristics, for this reason a very similar geometrically designed structure, adapted to the characteristics of a realistic pipe, is recreated. The diameters of the duct and of the struts are the same of the preliminary case while the orientations are varied to follow the shape of the duct; the length of the POCS is increased. Moreover the inner pipe is lengthened towards the outer duct wall in order to be able to create a pole to which apply the positive potential.

For simplicity, only one duct is analyzed, considering its behaviour as characteristic for all the other ducts.

To follow the indications obtained from the previous analysis a fundamental change in the application of the potential difference is made.

The POCS structure has the inlet surface covered by a washcoat layer, so it can be considered a catalyst. In this case the abatement emissions starts to be considered. To simply describe the geometry and its location, the Figure 4.7 is useful.
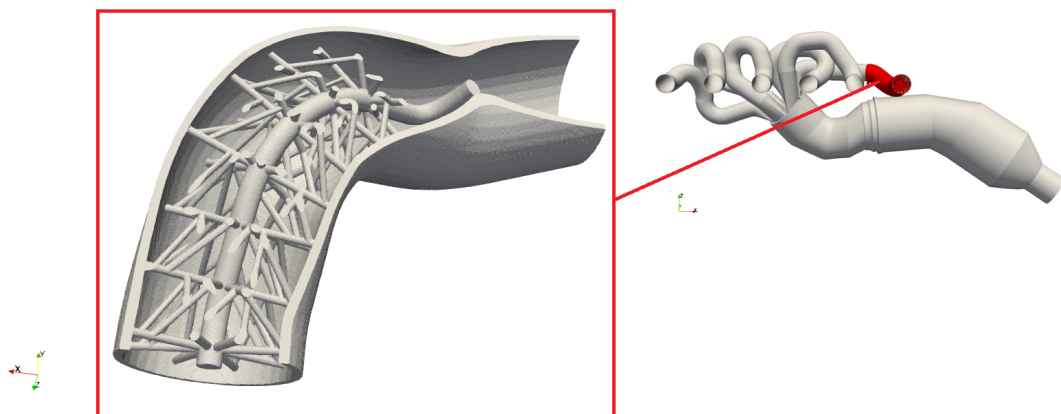
Figure 4.7: *Location of the POCS inside the exhaust ducts and detail of the definitive POCS geometry.*

The section depicted in the red rectangle in Figure 4.7 shows how the structure,

previously designed for a straight duct, has been adapted to the exhaust duct. The geometry presented has a length of about 10 cm, 15 mm longer than before, and includes a series of struts with the same characteristics described above.

4.3.1 Sensitivity Analysis of POCS

Having changed the geometry, a sensitivity analysis is carried out. In this case the sensitivity analysis is performed considering the solver and the condition previously described for the preliminary case. The meshes obtained are the following:

type of mesh	millions of cells	base cell dimensions (x y z) [m]
mesh1	1	(0.0039 0.0019 0.0015)
mesh2	1.27	(0.0031 0.0015 0.0012)
mesh3	2.11	(0.0029 0.0014 0.0011)

Table 4.2: *Properties of different meshes for sensitivity analysis of POCS .*
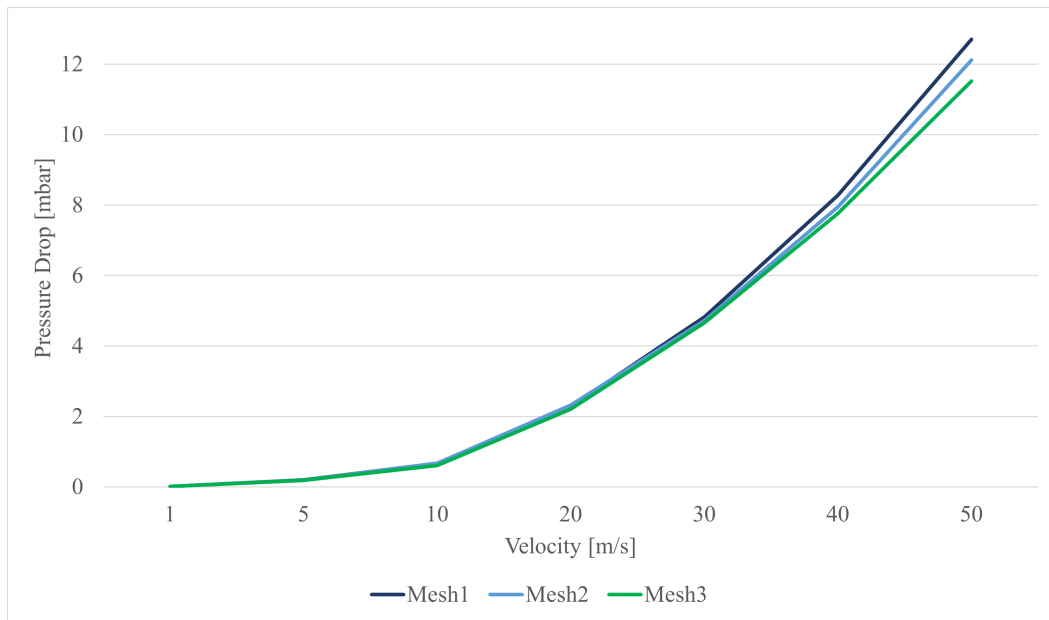
Figure 4.8: *POCS case study: sensitivity analysis.*

The results provide a good reliability of the meshes. As before at low velocity evaluations the data is superimposed, while reaching 50 $\left[\frac{m}{s}\right]$ the curves are slightly

apart. However the variation of the results is in the range of 1 mbar.

The higher pressure drop obtained in this evaluation is about 12 mbar, which is not so far from the values of the straight pipe that are about 6 mbar.

4.3.2 New potential difference application

As mentioned before, it is necessary to think of a new method for conducting current.

In the preliminary analysis the inner pipe conductivity is not considered. In a realistic case the potential is applied on a patch, and then the current flows through the structure thanks to the potential difference. In this case the resistance of the inner pipe has to be taken into account because it directly affects the current flow through the whole structure.

In order to have a correct current distribution inside the POCS, the conductivity of the struts is greatly reduced. To do this, two methods have been devised. The first consists in the use of a structure composed of two materials, steel and silicium carbide, while the second is the introduction of an artificial porosity in the steel. In this work the technological aspects are not analyzed, therefore the hypothesis of a structure having an external and an internal pipe made of steel while all the thin structures composed of silicium carbide is chosen.

For the conductivity (σ) the values considered are about 10^7 $[\frac{S}{m}]$ for the steel region, internal and external pipe, while equal to 100 $[\frac{S}{m}]$ for the struts [15].

As in the pre-analysis, a potential difference is applied between the internal and the external pipe. The inner pipe at the end of the POCS structure is brought towards the outside of the duct, the wall is cut to allow the passage of the pipe. The hole on the external pipe is perfectly filled by insulating material in order to avoid gas leaks and to separate positive and negative potential regions.

Outside of the duct the positive pole patch is defined, as shown in red in Figure 4.9, to which a voltage of 38V is applied.
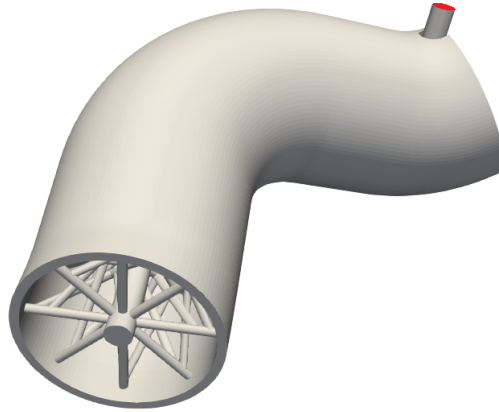
Figure 4.9: *POCS case study: position of positive pole.*

The obtained potential difference distribution on the POCS geometry is shown in Figure 4.10.
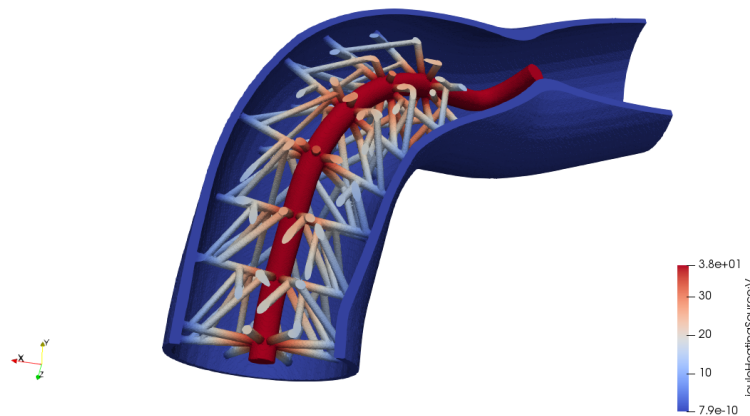
Figure 4.10: *POCS case study: potential difference distribution.*

The materials chosen for this structure make it possible to define a patch for the positive pole, but still maintaining the behaviour of the copper case, in which the inner pipe achieves the maximum potential. In this way the potential is radially distributed inside the POCS.

Moreover, considering the Ohm's law, an increase of voltage produces an increase of current, which means higher heat provided to the system.

4.3.3 Simulation Setup

After verifying the validity of the mesh and studying the method of applying the potential, the analysis on the efficiency of the catalyst begins.

The simulation is aimed at evaluating the abatement of emissions based on some approximations.

In this preliminary case study, in order to simplify the simulation framework, the absence of turbulence is considered a good approximation, as a single duct is considered and the struts further reduce the motion regime by indexing the flow in the channel.

The schemes used for the simulation are the following:

fvSchemes	type	
ddtSchemes $\frac{\partial \Phi}{\partial t}$	default	steadyState
gradSchemes $\nabla \Phi$	default	Gauss linear
divSchemes	default	none
	$div(\phi, U)$	Gauss upwind
	$div(\phi, Y_{i_h})$	Gauss upwind
	$div(\phi_d, p)$	Gauss upwind
	$div(\phi_v, p)$	Gauss upwind
	$div(\phi, K)$	Gauss linear
	$div(\phi, h)$	Gauss upwind
	$div(\phi, e)$	Gauss upwind
	$div(((\rho\nu)d^2(T(\nabla(U))))))$	Gauss linear
laplacianSchemes $\nabla^2 \Phi$	default	Gauss linear uncorrected
interpolationScheme $\Phi\|f$	default	linear
snGradSchemes $\nabla_f{}^\perp \Phi$	default	uncorrected

Table 4.3: *POCS case study: fvSchemes of Fluid region.*

The schemes for the fluid part show no scheme for time discretization, the temporal derivative contributions are set to zero, instead *Gauss linear* scheme (a central difference scheme with 2^{nd}order accuracy) are employed for the gradient and laplacian terms. The interpolation schemes are used to transform cell-centre quantities to face centres, here linear (2nd order method) interpolation is used. The divergence mixes upwind and linear schemes, i.e. first and second order accu-

racy terms. Uncorrected surface-normal gradient scheme is an implicit evaluation based on central-difference scheme without non-orthogonal correction.

Regarding the solid and the washcoat the schemes are:

fvSchemes	type	
ddtSchemes $\frac{\partial \Phi}{\partial t}$	default	Euler
gradSchemes $\nabla \Phi$	default	Gauss linear
divSchemes	default	none
laplacianSchemes $\nabla^2 \Phi$	default	none
	$\nabla^2(\alpha, e)$	Gauss linear uncorrected
	$\nabla^2(\alpha, e.solid)$	Gauss linear uncorrected
	$\nabla^2(jouleHeatingSource : \sigma,$	Gauss linear uncorrected
	$jouleHeatingSource : V)$	
interpolationScheme $\Phi|f$	default	linear
snGradSchemes $\nabla_\perp \Phi$	default	uncorrected

Table 4.4: *POCS case study: fvSchemes of Solid and Washcoat region.*

For solid and washcoat domain the time is discretized by Euler implicit time scheme that is an implicit, first order, transient term. The gradient is defined as in the fluid region while the Laplacian term applies Gauss linear method and here the typical characteristics of the application of the potential are defined.

The equation solvers, tolerances and algorithms are controlled by the fvSolutions. It is important to define the Solutions schemes applied.

The resolution methods present are: preconditioned bi-conjugate gradient PCG, for symmetric matrices, and PBiCG, for asymmetric matrices; smoother, generalized geometric-algebraic multi-grid (GAMG), diagonal.

The diagonal solver determines explicit systems.

The categories listed above need further specifications: for the first it is necessary to indicate how the preconditioning works, the second requires the type of smoother to be adopted, and for the third a series of information to describe the process.

The Solution schemes used are:

fvSolutions	type
ρ	
solver	diagonal
p	
solver	GAMG
smoother	symGaussSeidel
tolerance	$1e-7$
relTol	0.01
U—h—e	
solver	PBiCGStab
preconditioner	DILU
tolerance	$1e-7$
relTol	0.1
PIMPLE	
momentumPredictor	yes
transonic	yes
nOuterCorrectors	150
nCorrectors	1
nNonOrthogonalCorrectors	3
consistent	yes
pMin	0.1
pMax	$2e5$
outerCorrectorResidualControl	
U — p	
tolerance	$5e-3$
relTol	0.1

Table 4.5: *POCS case study: fvSolutions of Fluid region.*

fvSolutions	type
e	
solver	GAMG
smoother	symGaussSeide
tolerance	$1e-6$
relTol	0.1
jouleHeatingSource:V	
solver	PCG
preconditioner	DIC
tolerance	0
relTol	$1e-6$
PIMPLE	
nNonOrthogonalCorrectors	5

Table 4.6: *POCS case study: fvSolutions of Solid region.*

fvSolutions	type
e	
solver	GAMG
smoother	symGaussSeide
tolerance	$1e-6$
relTol	0.1
PIMPLE	
nNonOrthogonalCorrectors	5

Table 4.7: *POCS case study: fvSolutions of Washcoat region.*

As already introduced, the designed structure is covered with a thin layer of active material, called a washcoat, which promote chemical reactions.

Differently from the *fvSchemes*, the *fvSolutions* of solid and washcoat are different due to the definition of the potential characteristics.

Several reactions take place on the catalytic surface, after its activation.

The reactions that mostly describe the washcoat activity in the TWC are summarized in the Table 4.8.

Reations	
oxidation reactions	$CO + \frac{1}{2}O_2 \rightarrow CO_2$
	$H_2 + \frac{1}{2}O_2 \rightarrow H_2O$
	$C_3H_6 + \frac{9}{2}O_2 \rightarrow 3CO_2 + H_2O$
	$C_3H_8 + 5O_2 \rightarrow 3CO_2 + 4H_2O$
reduction reactions	$NO + CO \rightarrow CO_2 + \frac{1}{2}N_2$
	$H_2 + NO \rightarrow H_2O + \frac{1}{2}N_2$
water gas shift reactions	$CO + H_2O \rightarrow CO_2 + H_2$
	$CO_2 + H_2 \rightarrow CO + H_2O$
HC steam reforming	$C_3H_6 + 3H_2O \rightarrow 3CO + 6H_2$
	$C_3H_8 + 3H_2O \rightarrow 3CO + 7H_2$
oxygen storage	$Ce_2O_3 + \frac{1}{2}O_2 \rightarrow 2CeO_2$
	$Ce_2O_3 + NO \rightarrow 2CeO_2 + \frac{1}{2}N_2$
	$2CeO_3 + CO \rightarrow Ce_2O_3 + CO_2$
	$2CeO_3 + H_2 \rightarrow Ce_2O_3 + H_2O$
	$2CeO_3 + \frac{1}{6}C_3H_6 \rightarrow Ce_2O_3 + \frac{1}{2}CO + \frac{1}{2}H_2O$
	$fCe_2O_3 + \frac{1}{2}O_2 \rightarrow 2fCeO_2$
	$2fCeO_3 + CO \rightarrow fCe_2O_3 + CO_2$
	$2fCeO_3 + H_2 \rightarrow fCe_2O_3 + H_2O$
	$2fCeO_3 + \frac{1}{6}C_3H_6 \rightarrow fCe_2O_3 + \frac{1}{2}CO + \frac{1}{2}H_2O$
	$2fCeO_3 + \frac{1}{7}C_3H_8 \rightarrow fCe_2O_3 + \frac{3}{7}CO + \frac{4}{7}H_2O$

Table 4.8: *Chemical reactions.*

These reactions can be used also for the POCS.

4.3.4   Initial and Boundary Conditions

As described above, the 0 directory contains a file for each flow variable which specifies the initial and boundary conditions.

The folder is divided into the different parts of the domain: fluid, solid and wash-coat. For every part the chemical species involved, the temperature, the pressure, and all the data require for the simulation are defined.

 The temperature is imposed at the inlet, with regards to the velocity, it is evident that the fluid cannot pass through the wall so is set noSlip condition at the wall.

Boundary fields	inlet	insulating	positive pole	outlet	interfaces
T	data	zerogradient	zeroGradient	zeroGradient	zeroGradient
P	zeroGradient	zeroGradient	fixedValue	zeroGradient	zeroGradient
U	data	noslip	inletOutlet	noslip	noslip

Table 4.9: *POCS case study: boundary condition.*

Instead, for what concerns the chemical species in the fluid flow, the values considered are those of the air, combined with the data provided after the combustion process in the real engine.

In the Figure 4.11 4.12 4.13 the trend of mass flow, temperature and chemical species concentrations are reported as adimentional values to maintain the confidentiality of the data used for the simulation.
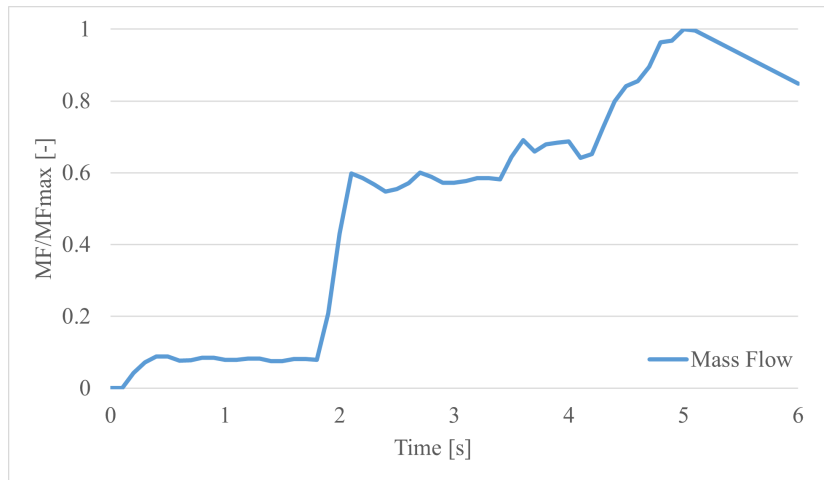
Figure 4.11: *Trend of mass flow at the inlet.*

The mass flow has a peculiar trend. At the beginning it has an almost constant low value but around 2 second it has a fast increase reaching six times the previous value. Then remains approximately constant for 2 seconds before a new rapid increase to the maximum value. After the maximum value, the trend is linearly decreasing up to 6 seconds. The value obtained at 6 seconds is considered to be approximately constant up to 20 seconds.

The temperature trend is different.
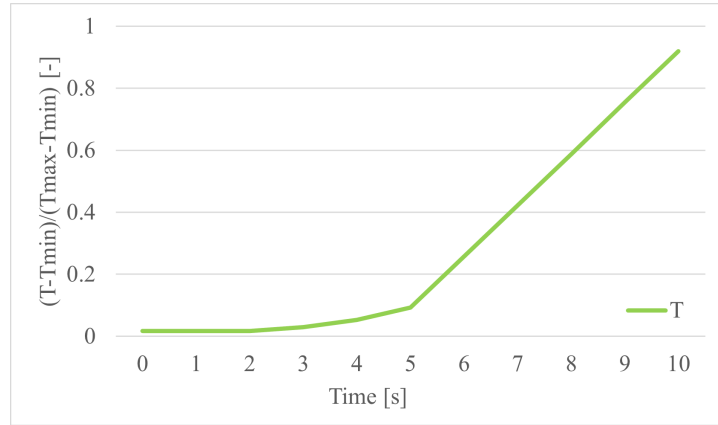
Figure 4.12: *Trend of temperature at the inlet.*

The temperature has a low value for the first 5 seconds. After this starting period the temperature gradually increases achieving the maximum at 10 seconds, then the temperature is considered constant at maximum value till 20s.

The species coming from the engine have a trend strictly linked to the evolution of combustion.
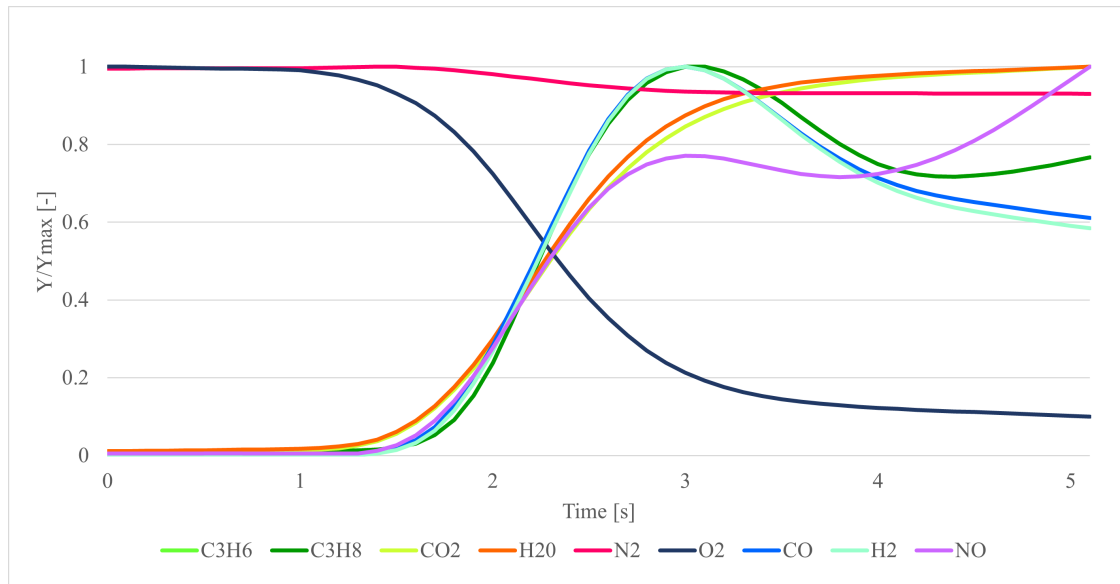
Figure 4.13: *Trend of concentration of chemical species at the inlet.*

The concentration diagram reports the trend of all the species considered. The

trends are very different one to each other. After 5 seconds the concentrations are considered constant at the value reached at the end of this period.

4.4 Data analysis of POCS case study

The discussion of the POCS case study results is focused on the initial period of the engine operation, 0 - 4 seconds, where the inlet gas temperatures remain very low and the introduction of the POCS could be significantly beneficial. Considering the POCS as a catalyst, it is possible to evaluate the abatement of the emission in the POCS region. This analysis allows to obtain the concentration values of pollutants but also the values that describe the flow at the outlet patch. This second result is useful for the following analysis on the exhaust line.

The electrical heating shows a rapid increase of the structure temperature, Figure 4.14 and Figure 4.15, and the consequently increase of fluid temperature, Figure 4.16 and Figure 4.17, starting from the centre of the pipe, where the solid is hotter.
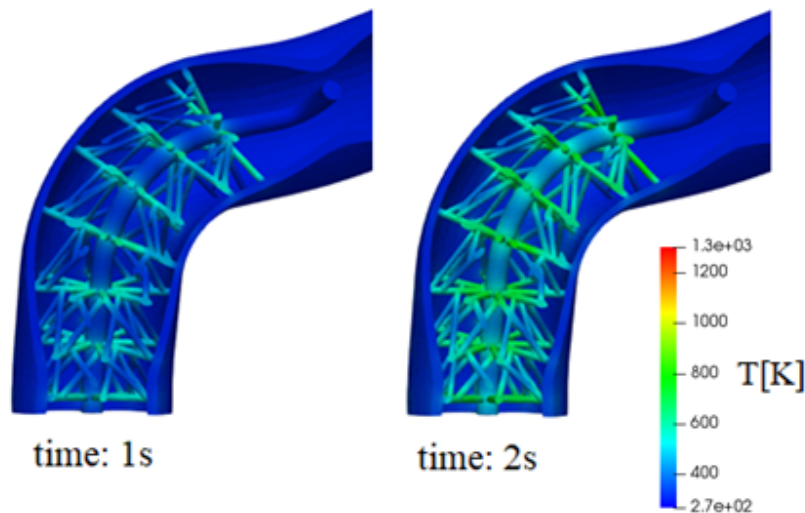
Figure 4.14: *POCS case study: temperature evolution of solid region.*
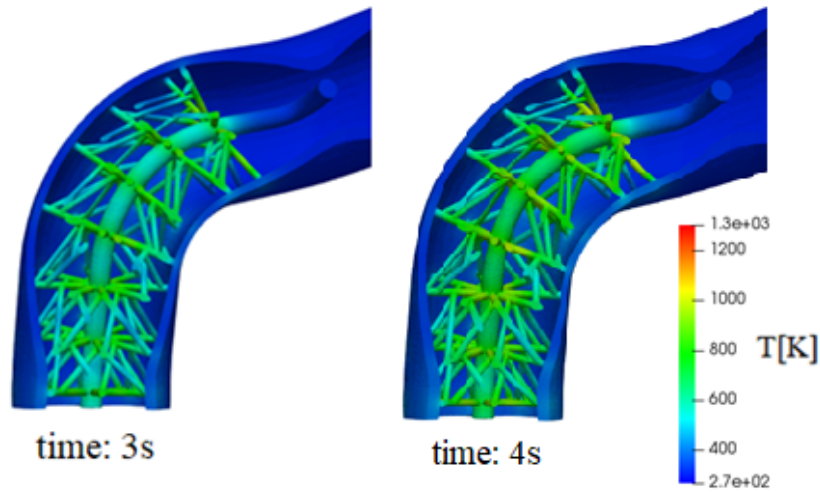
Figure 4.15: *POCS case study: temperature evolution of solid region.*

As displayed in Figure 4.14 and Figure 4.15, the temperature of solid parts of POCS structure increases rapidly. The difference of conductivity inside the POCS creates an optimal temperature distribution along the pipe. The low electrical conductivity of the struts allows to achieve 800K in about 3 seconds, while the central pipe made of stainless steel requires around 4s to achieve the same temperature.
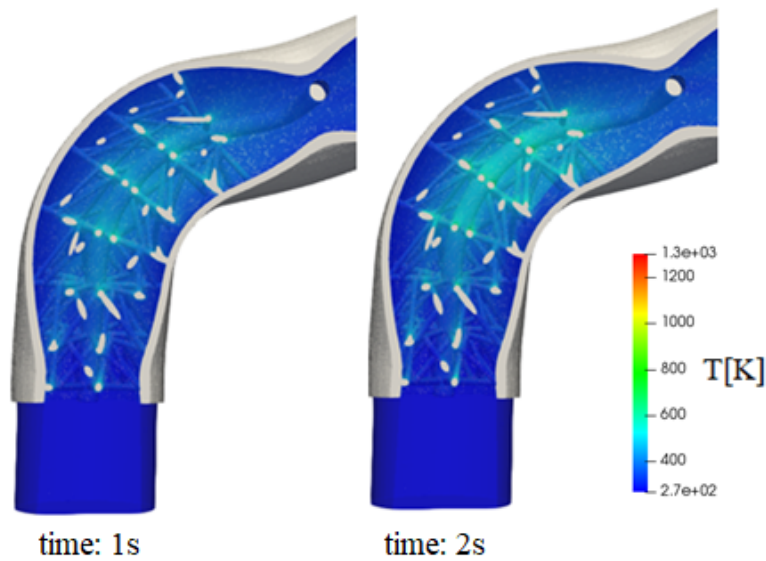
Figure 4.16: *POCS case study: temperature evolution of fluid region.*
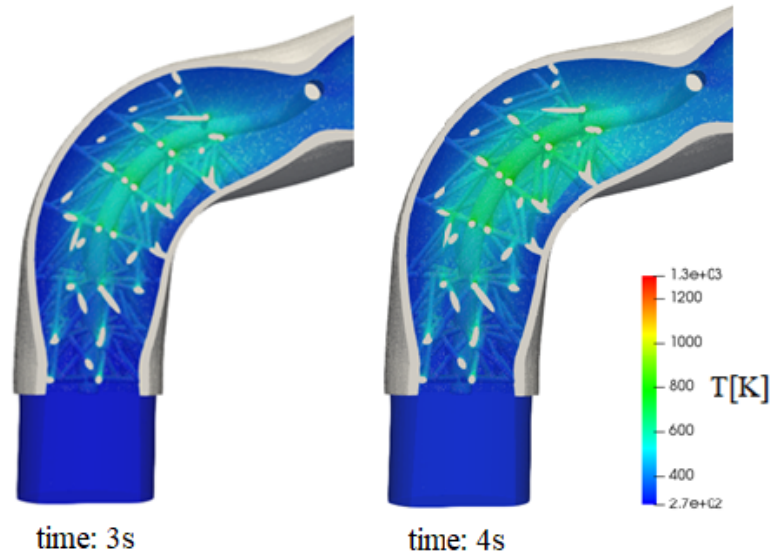
Figure 4.17: *POCS case study: temperature evolution of fluid region.*

As consequence of the increase of solid temperature the fluid heats up. In some parts the catalyst quickly reaches the light-off temperature that leads to a significant abatement of emission even in the first seconds of the simulation. The simulation results are reported in the following diagrams, Figure 4.18, which report the concentrations of the species dimensionless with respect to the maximum concentration of the same species. The diagrams reported in Figure 4.18, show the inlet (red) and outlet (blue) concentration of the main species present in exhaust gases. After 1.5s the curves start to have different value, and the distance between the two curves becomes evident at about 3s.
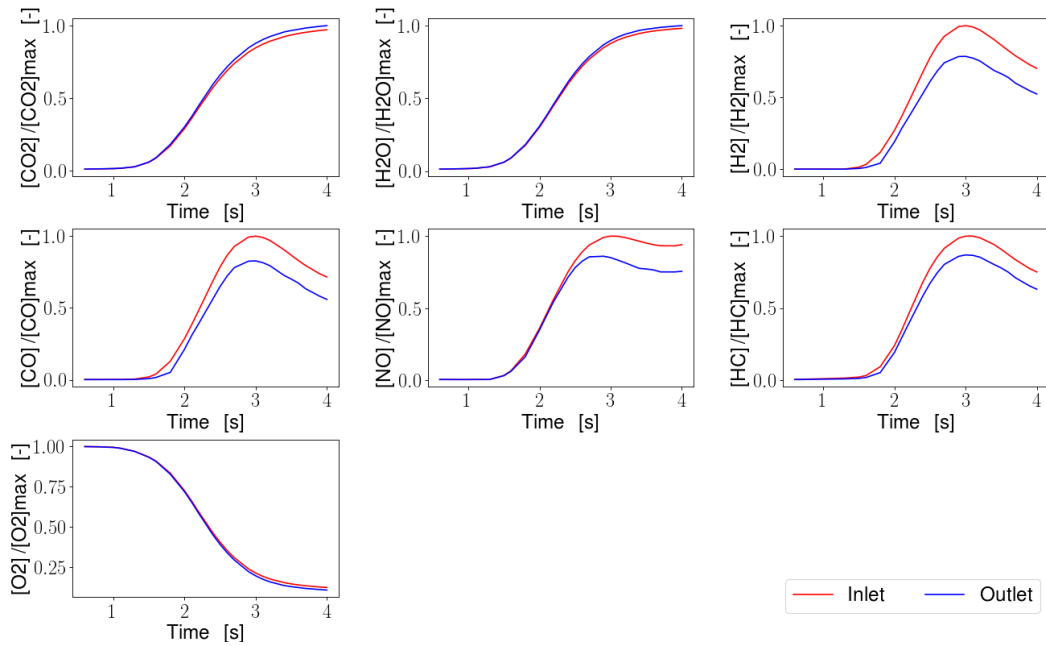
Figure 4.18: *POCS case study: diagrams of abatement for different species as function of time.*

In this evaluation not only the data are to consider but also the abatement distribution inside the channel. For this, the distribution in the duct is shown.
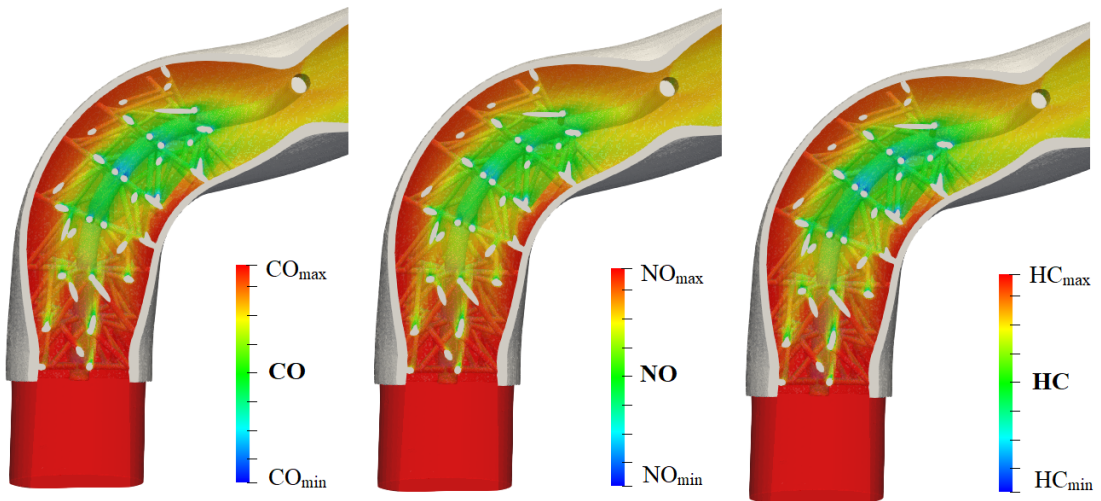
Figure 4.19: *POCS case study: distribution of pollutants after 4s.*

In the Figure 4.19 the abatement distribution of the three main pollutant molecules after 3 seconds of simulation is represented. The link with the temperature distribution, in Figure 4.17, is evident. The lower concentrations of pollutants coincide

with the places where the higher fluid temperatures are.

Another important factor to consider is the mixing ability of the structure. To complete the POCS description the velocity is reported in Figure 4.20.
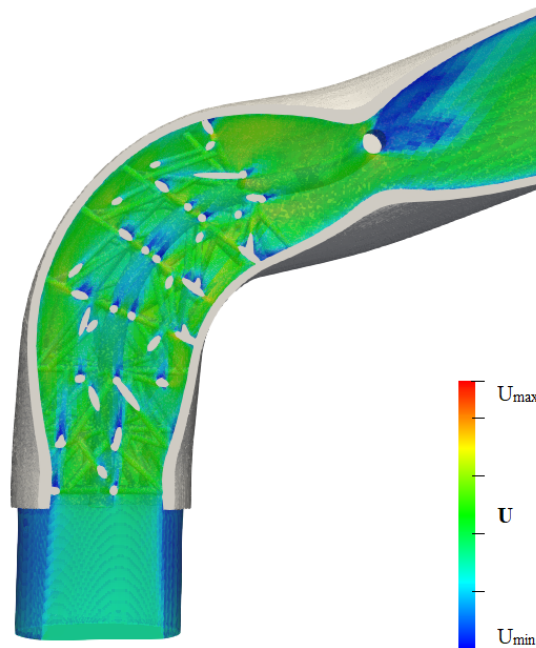
Figure 4.20: *POCS case study: flow velocity at time 2 seconds.*

4.4.1   Conclusion of POCS case study

The preliminary analysis on the POCS structure displayed some critical points on the potential application. The change of exploitation of potential difference is necessary to make the study truthful. The change in conductivity allows a correct distribution of the potential in the structure. In this way the temperature increases very quickly and is homogeneously distributed along the pipe. The high temperature allows the fast activation of the reactions inside the POCS region. In less than 2 seconds the abatement starts, and after 3 seconds a sensible reduction of pollutants is obtained. The data provided by the simulation show that a heat output of approximately 1.7kW is supplied for heating the POCS. For this reason, an intermittent trend of the device is conceivable.

4.5   Exhaust case study

After the analysis carried out on the pre-catalyst, it is analyzed how it affects the entire exhaust duct.

Here is performed an analysis of the system considering two situations:

- The realistic engine exit conditions applied to the inlet faces of the exhaust duct geometry.

- The data obtained from the simulation of the previous case study applied to the inlet patches downstream of the pre-catalyst.

The exhaust pipe is divided in different domains as reported in the Figure 4.21.
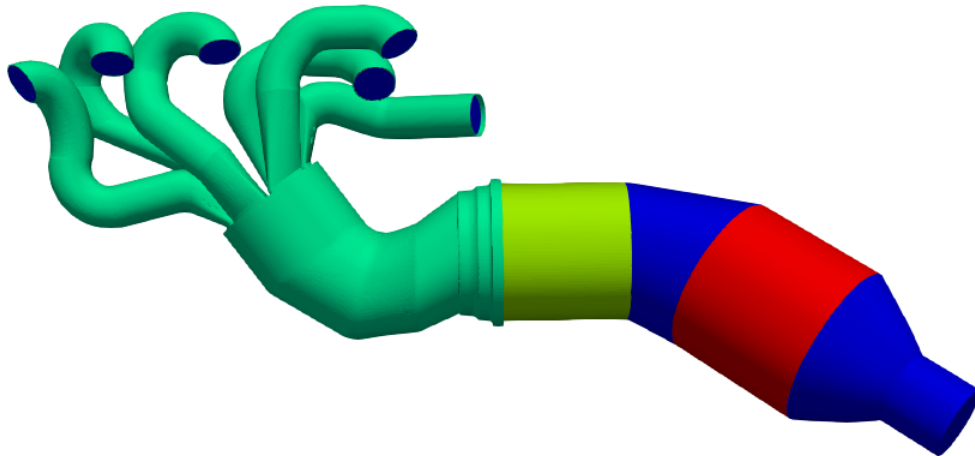
Figure 4.21: *Division of the exhaust pipe domain.*

The exhaust Line is equipped with two catalysts, the green and the red zones in the Figure. For both the cases the inlet patches are considered the hypothetical outlet faces of the POCS.

As evident in Figure 4.21, not only fluid region is considered. The solid domain has an important role in the thermal description, the thermal inertia of the walls shows its influence in particular at the starting of the engine.

4.5.1 Mesh description

The complexity of the geometry, with thin walls, edges and curves required very dense mesh. In particular, the part on the left, in Figure 4.22, in which the ducts are found, required a high level of refinement. Furthermore, three layers are defined to better describe the surface.
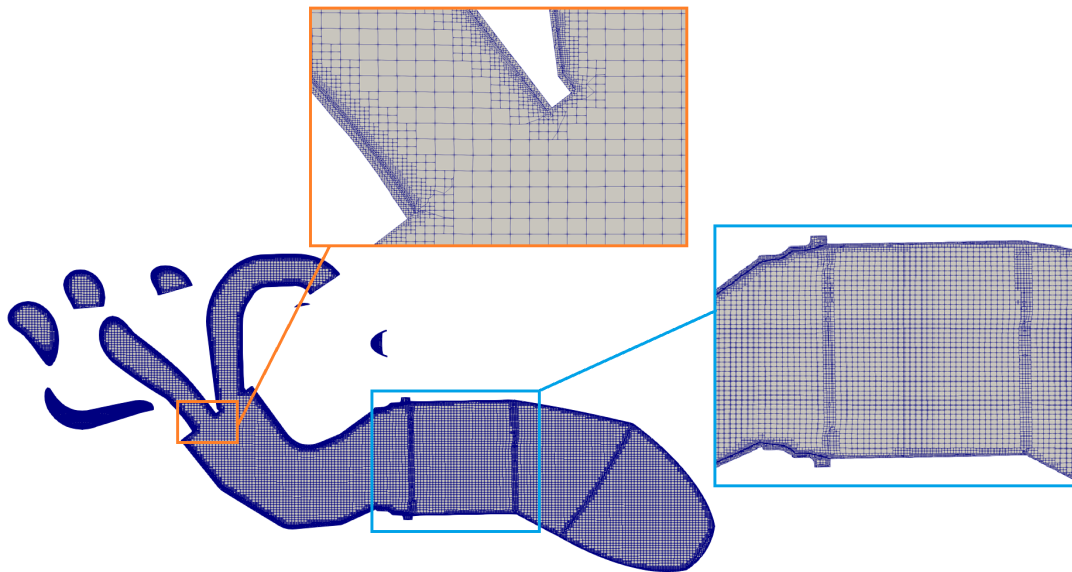
Figure 4.22: *Definition of the multi-region exhaust pipe mesh with details of the critical mesh zones.*

The total number of cells obtained meshing the exhaust system are:

	fluid	solid	CAT1	CAT2
millions of cells	16.8	6.2	0.4	0.57

Table 4.10: *Exhaust line mesh description.*

4.5.2 Simulation Setup

The setup of the two cases appears to be the same. The *Schemes* used are similar to the schemes used in the previous case study, for this reason only the different

parts of the schemes will be reported here.

The substantial differences consist in the introduction of the turbulence model
and the increase of the accuracy referred to speed and energy.

fvSchemes	type	
divSchemes	default	none
	turbolence	Gauss upwind
	$div(\phi, U)$	Gauss linearUpwind grad(U)
	$div(\phi, h)$	Gauss linearUpwind grad(h)
	$div(\phi, k)$	turbolence
	$div(\phi, \omega)$	turbolence
	$div(\phi, \epsilon)$	turbolence

Table 4.11: *Variation in fvSchemes of Fluid region for exhaust line simulation.*

The *linearUpwind* is introduced, which employs *upwind* interpolation weights,
with an explicit correction based on the local cell gradient, always considering the
second order accuracy.

The solid and the catalyst schemes show the adoption of corrected models and
the absence of joule heating souce.

fvSchemes	type	
laplacianSchemes $\nabla^2\Phi$	default	none
	$\nabla^2(\alpha, e)$	Gauss linear corrected
	$\nabla^2(\alpha, e.solid)$	Gauss linear corrected
wallDist	method meshWave	

Table 4.12: *Variation in fvSchemes of Solid region for exhaust line simulation.*

The *mesh-wave* method is applied for calculating the distance to nearest patch for
all cells and boundary.

As for the *Solutions*, they are exactly the same used before omitting the *joule-*

fvSchemes	type	
ddtSchemes $\frac{\partial \Phi}{\partial t}$	default	Euler
gradSchemes $\nabla \Phi$	default	Gauss linear
divSchemes	default	none
laplacianSchemes $\nabla^2 \Phi$	default	none
	$\nabla^2(\alpha, e)$	Gauss linear corrected
	$\nabla^2(\alpha, e.solid)$	Gauss linear corrected
interpolationScheme $\Phi|f$	default	linear
snGradSchemes $\nabla_\perp \Phi$	default	corrected
wallDist	method meshWave	

Table 4.13: *Variation in fvSchemes of catalytic region for exhaust line simulation.*

HeatingSource:V term.

4.5.3 Turbulence Model

Differently from the previous case study, the description of the complete exhaust, with the introduction of mixing zones and wider pipe, requires a turbulent description.

Once the type of flow has been defined, the turbulence model must be specified. In this study the turbulence is characterized by $k - \omega$ SST model, where SST stands for Shear Stress Transport.

The SST formulation switches to a $k - \epsilon$ behaviour in the free-stream, which avoids the $k - \omega$ problem of being sensitive to the inlet free-stream turbulence properties. The $k - \omega$ SST model provides a better prediction of flow separation than most RANS models and also accounts for its good behaviour in adverse pressure gradients. Moreover, this model does not suffer from near wall singularity, and offers the opportunity to directly solve the boundary layer.

The initial values considered for the analyzes are:

Where k is the turbulent kinetic energy and ω is the specific rate of dissipation.

$$
\begin{array}{lll}
k & 0.001 & [\frac{m^2}{s^2}] \\
\omega & 500 & [\frac{1}{s}]
\end{array}
$$

Table 4.14: *Turbulence parameters for exhaust line simulation.*

4.5.4 Initial and Boundary Conditions

Here the domain is composed by: fluid, solid and the two catalyst. The conditions applied are:

Boundary fields	inlet	ducts/exhaust	outlet	interface
T	data	convection	zeroGradient	heattransfer
P	zeroGradient	zeroGradient	fixedValue	zeroGradient
U	data	noslip	inletOutlet	noslip

Table 4.15: *Exhaust line case: boundary conditions.*

The inlet temperature is defined by consistent values, then the other conditions consider the conduction through walls, external convection, and the exchange with the fluid that flows inside the pipe. Instead, the pressure adapts according to the outlet conditions.

The same conditions are defined for speed.

4.6 Data analysis of exhaust systems

The discussion of the results of this case study is focused on the analysis of the time required to reach the first catalyst light off.

As mentioned above, this case study aims to compare the emission abatement data of the two exhaust pipes having the same geometric characteristics but with different inlet conditions.

At first, the inlet conditions applied to the previous case study, the POCS one, are applied to the inlet patches of the six ducts of the exhaust pipe. This provides

the reference values to compare the results of the simulation in which the inlet values are provided by the outlet of POCS simulation.

The analysis of the reference pipe shows the same species concentration at the inlet and outlet of the system for around seven seconds of simulation. Then the inlet and the outlet concentrations start to be different, as shown in the diagrams.

Figure 4.23: *Base line configuration: diagrams of abatement for different species as function of time to evaluate the light-off time. (light-off at 7s)*

To better understand the diagrams reported in Figure 4.23, the spatial representation of the species is useful. In Figure 4.24 the concentration of the main pollutant species at two different time steps are reported. On the left the concentrations after 1 second of simulation, instead, on the right side the concentration after 8 seconds are presented.
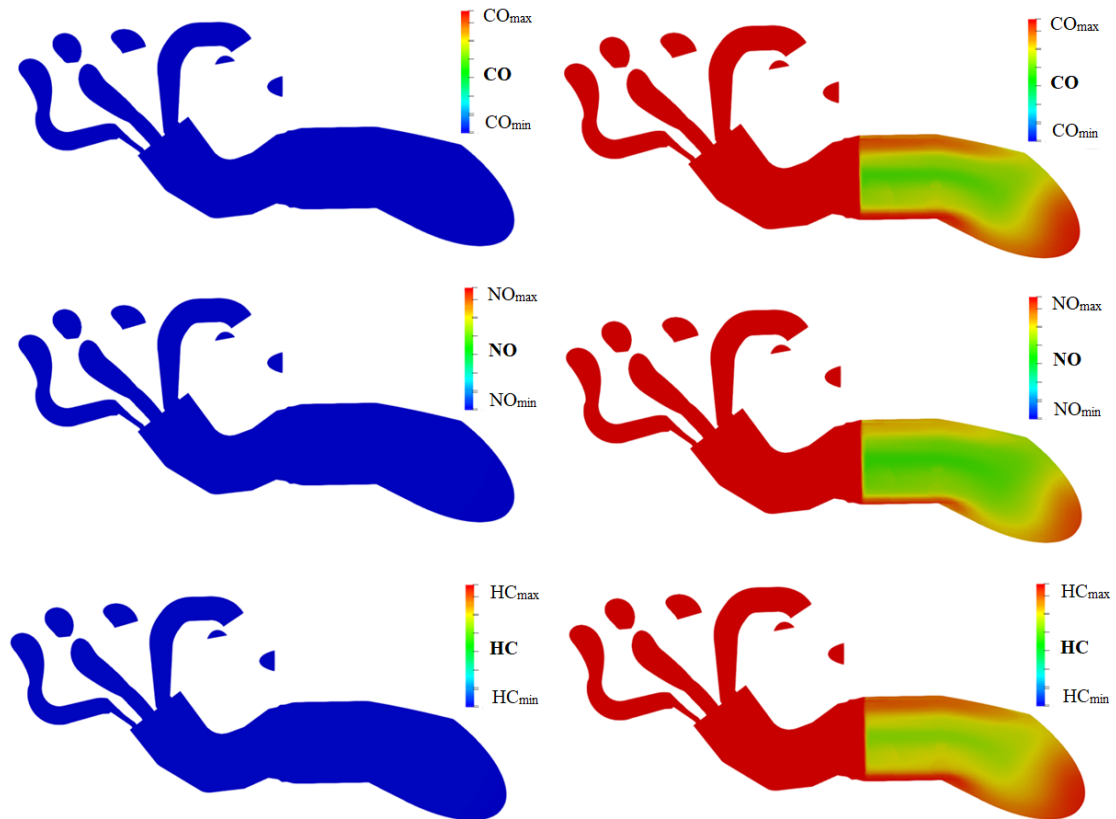
Figure 4.24: *Base line configuration: comparison between concentrations after 1s (left) and after 8s (right).*

On the left side the images show very low emission concentrations due to the species trend imposed at the inlet. As reported in the graph at Figure 4.13, the concentrations increase rapidly after 1.5 seconds. For this reason the images on the right side have very high concentration, red zones, and the presence of the catalyst is evident.

Since the inlet section of the catalyst the pollutants concentrations decrease. It can be seen the influence of low temperature wall, there the conversion rate is lower.

The concentrations profiles are coherent with the temperature values, because in the starting time the temperature is always lower that the activation temperature required for the chemical reactions. When the temperature achieves the activation point, about 600K, the catalytic surface start to convert the pollutant molecules.

In Figure 4.25 the evolution of the average temperature of different sections within the first catalyst is reported.
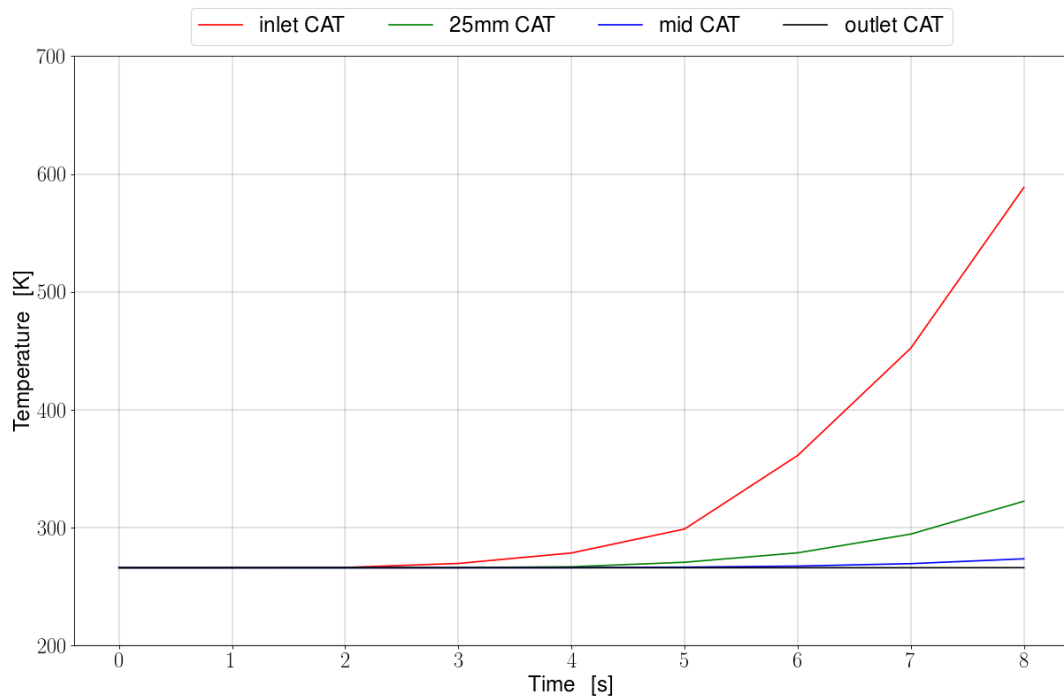
Figure 4.25: *Base line configuration: diagrams of temperature evolution as function of time.*

The second part of the analysis evaluates the POCS influence, so the results of the POCS case study are applied at the inlet patches of the complete exhaust pipe. The presence of an heater changes the abatement trends, as represented in the following diagrams.
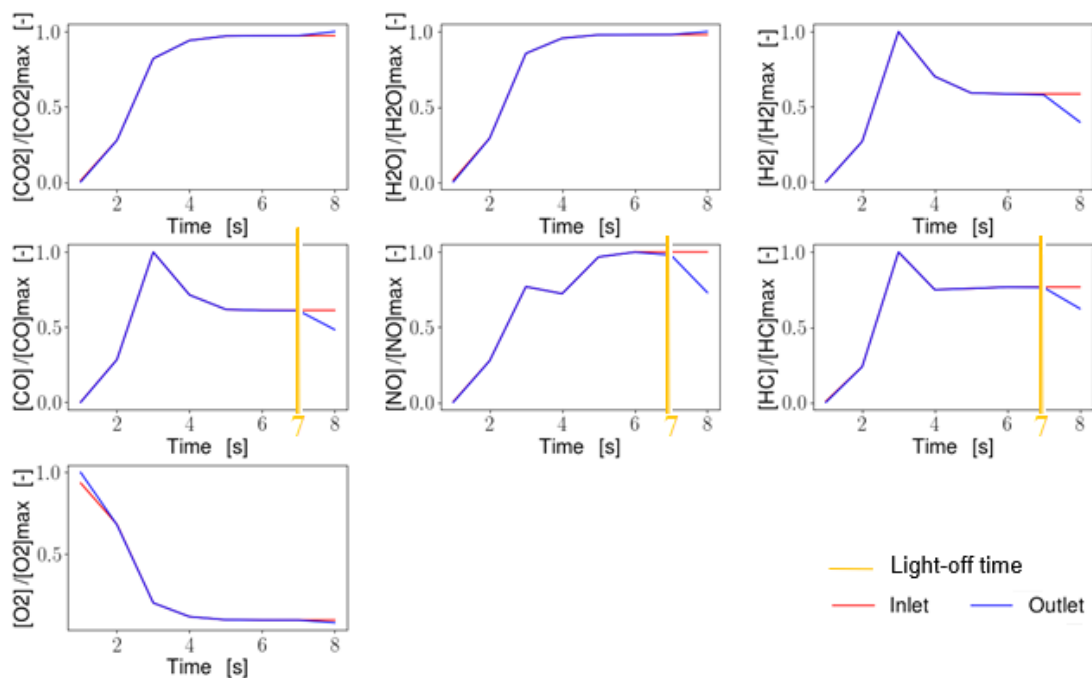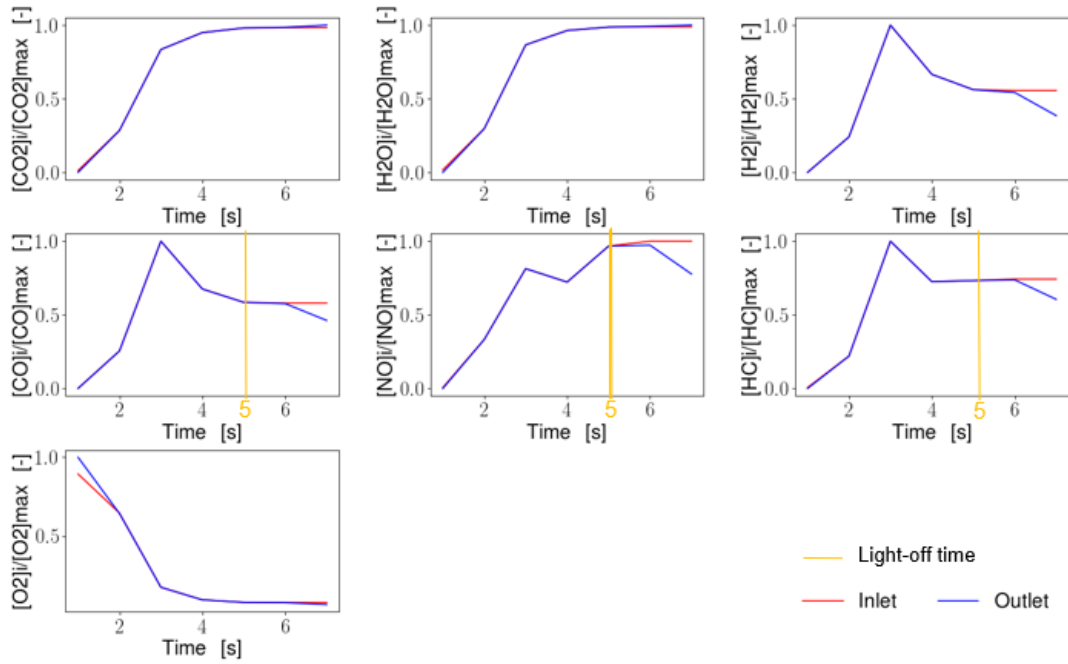

Figure 4.26: *Advanced configuration with introduction of POCS: diagrams of abatement for different species as function of time to evaluate the light-off time. (light-off at 5s)*

The abatement of the molecules starts earlier than in the previous case, after 6 seconds the input quantities are different from those at the output. After 5 seconds some abatements, for example NO_x, are already active. This advance is due to the higher temperature of the flow.

After 5 seconds some points of the first catalyst already register a temperature of 550K, however the average temperature is around 400K. Then, at 7 seconds, the average inlet temperature of the first catalyst reaches 600K. As can be seen in the Figure 4.27.
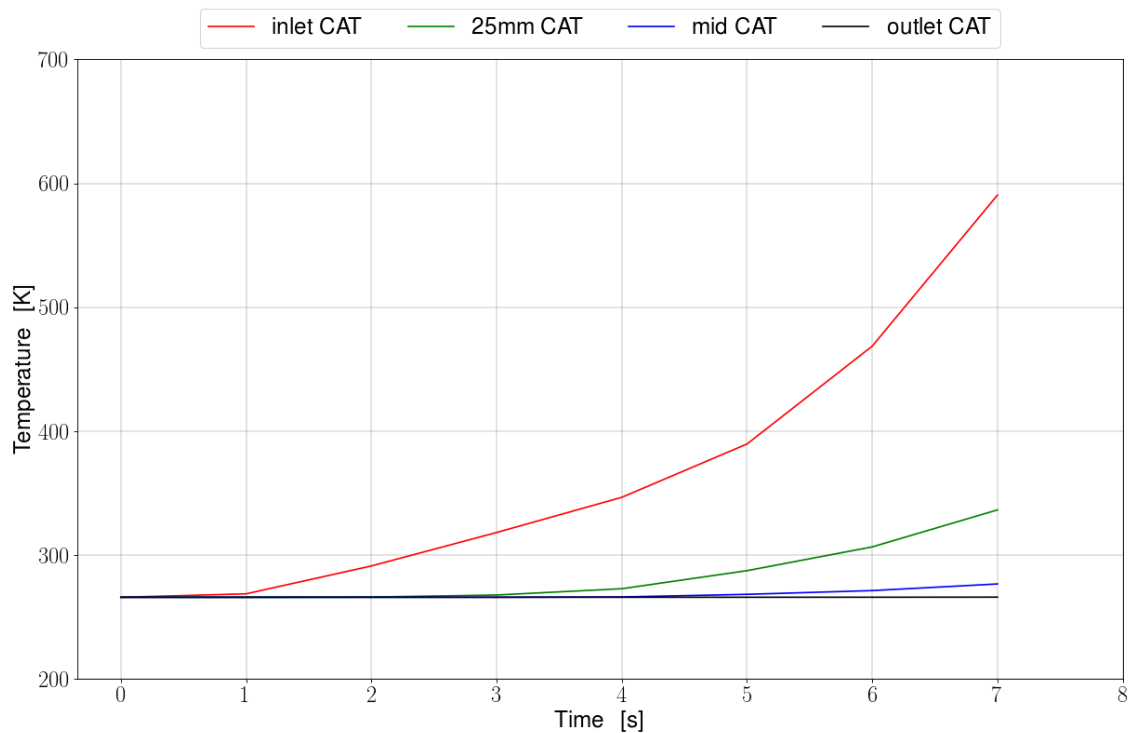
Figure 4.27: *Advanced configuration with introduction of POCS: diagrams of temperature evolution as function of time.*

Here the emission trend is different due to the POCS activity, however for the first 2 seconds the reduction given by the POCS is negligible. As before at the beginning the concentrations of pollutants are low but then the higher flow temperature combined with the change of inlet concentrations show the following spatial concentration. To describe the spatial trend over time, only one species is reported as the trend of pollutants is very similar between polluting species. In Figure 4.28 the CO distribution at 3 different time step is shown.
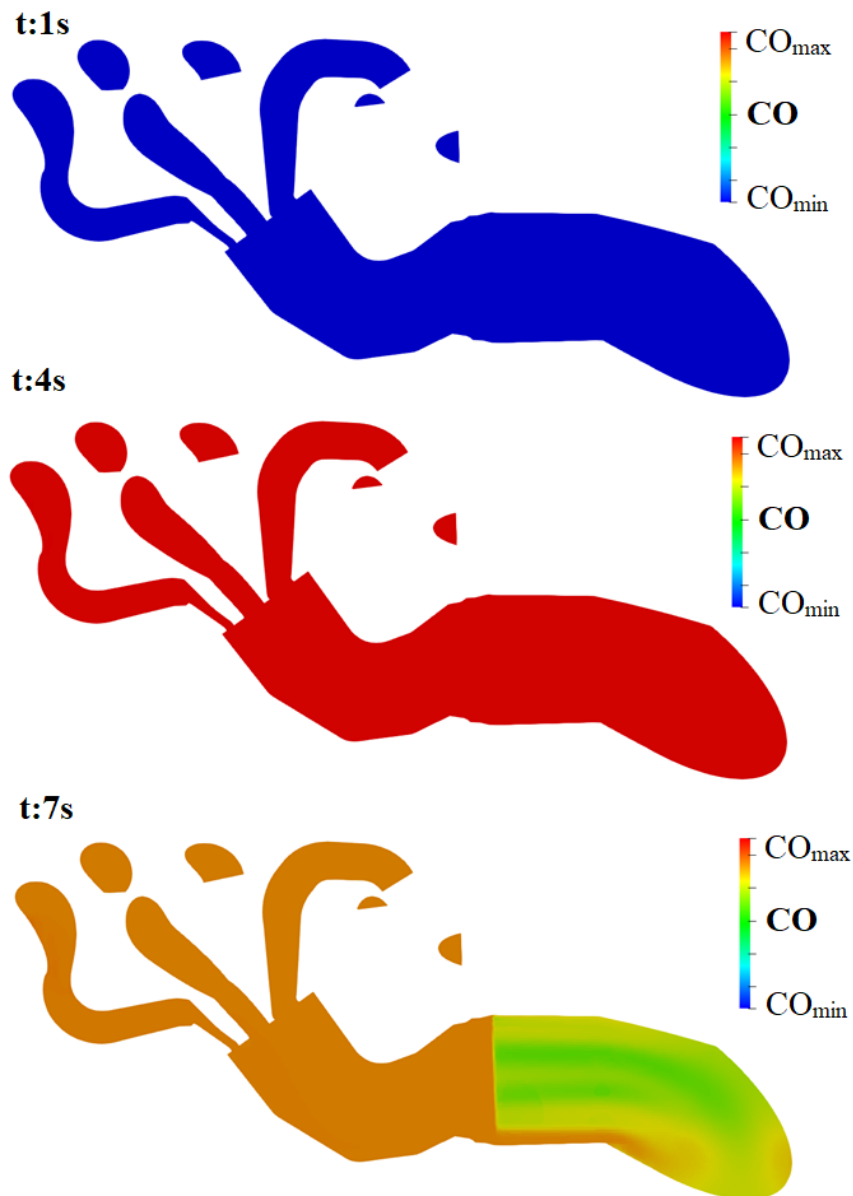
Figure 4.28: *Advanced configuration with introduction of POCS: spatial concentrations of CO over time.*

From this Figure 4.28 the activation of the catalyst is appreciable. The decrease in inlet pollutants at 7s is both the result of a reduction in the inlet pollutant trend and also the effect of the pre-catalyst.

To complete the description, it is possible to compare the abatement of the various pollutants after 7 seconds.
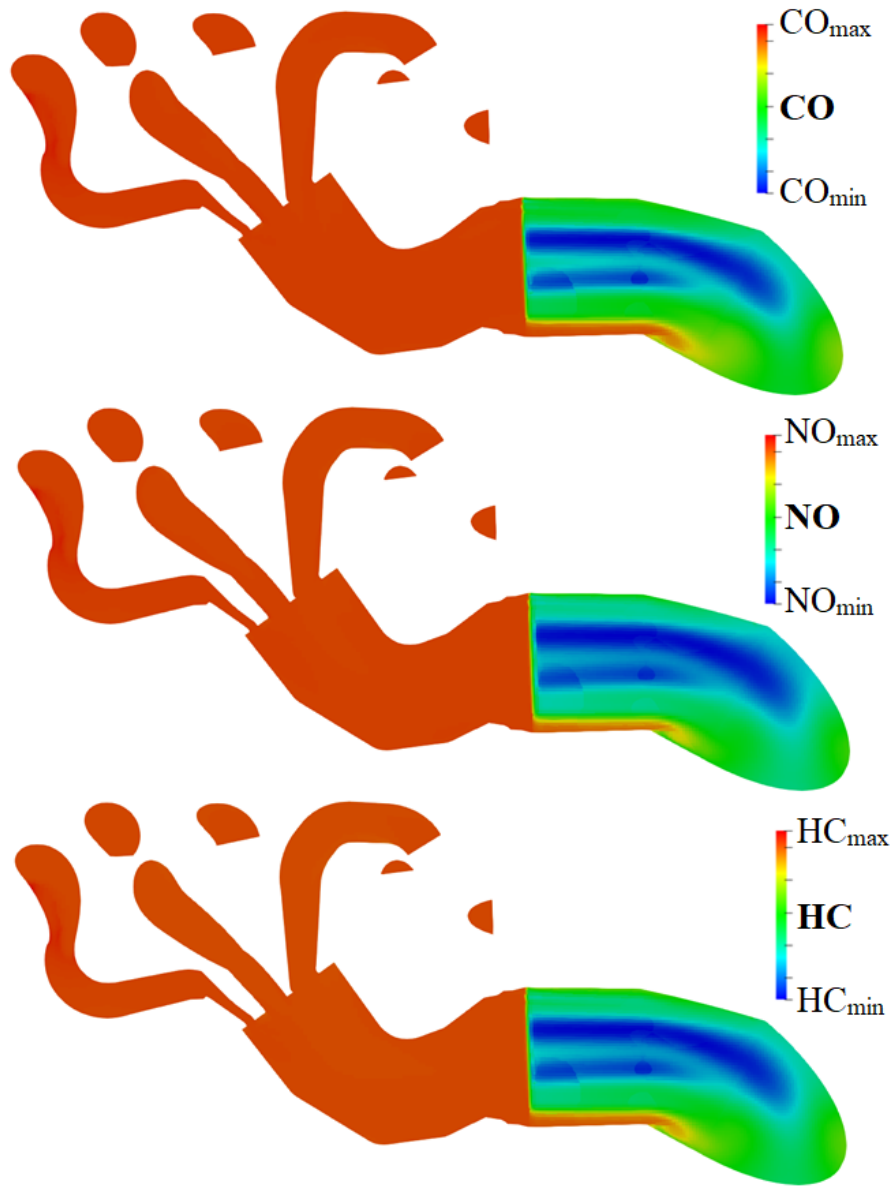
Figure 4.29: *Advanced configuration with introduction of POCS: concentration of pollutants at 7s.*

Finally, after having described the two cases separately, it is useful to compare the results. The gases arrive at the inlet with a different composition but also with different temperature. This is an advantage also for the catalyst conversion. To better understand the two cases, the comparison of the temperature evolution during the time steps is helpful.

In Figure 4.30 the temperature comparison between the base case and the case
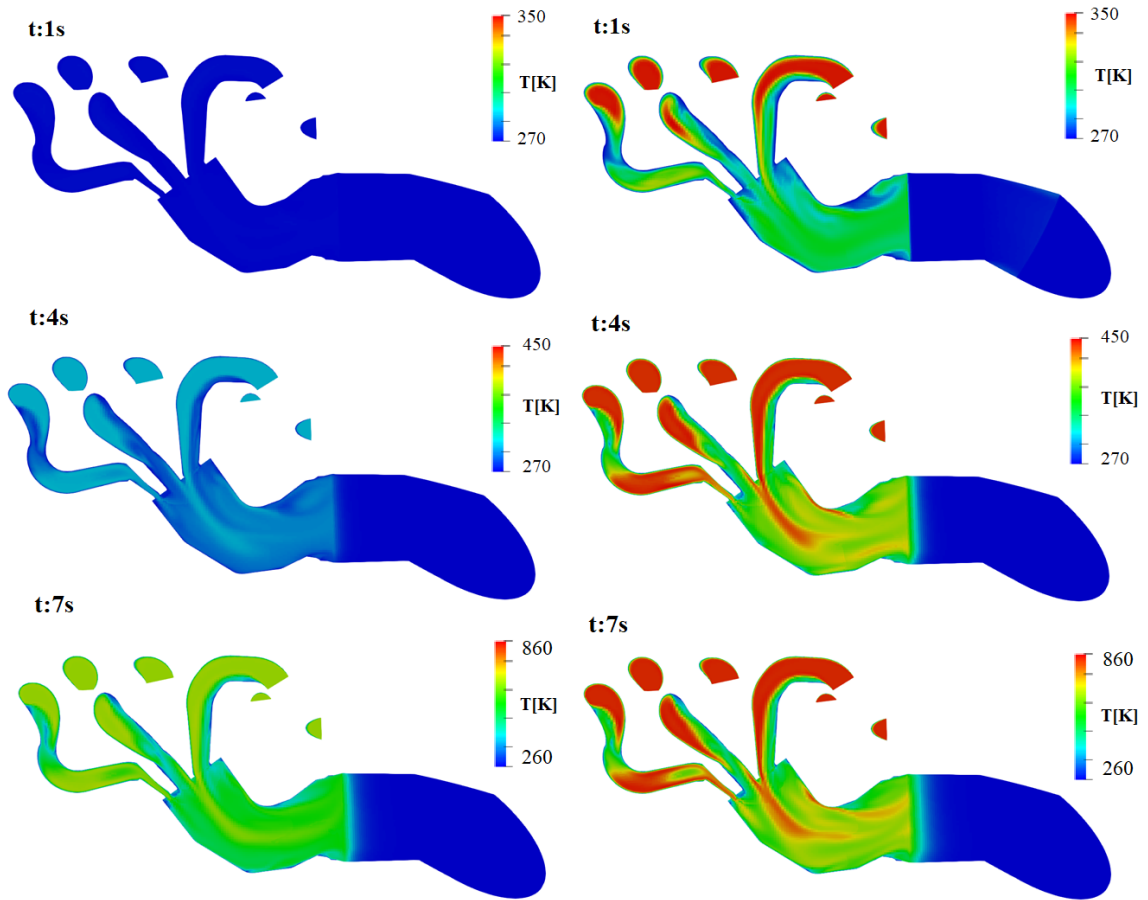
Figure 4.30: *Comparison of the temperature evolution over time between base case (left) and POCS case (right).*

after POCS is reported for a few characteristic seconds. Different temperature scales are used to better describe the temperature evolution along the pipe.

The differences between the left and the right side of the figure is evident. On the left very small variations are present after 4 seconds. The other side, instead, shows an appreciable variation in temperature from the beginning. The first part, immediately after the POCS, has an higher temperature which decreases moving forward in the duct. These thermal losses are due to the exchange of heat with the cold walls. Although these dispersions are present, the flow reaches the first catalyst with a different temperature, as can be seen in the diagram reported in Figure 4.31.

73
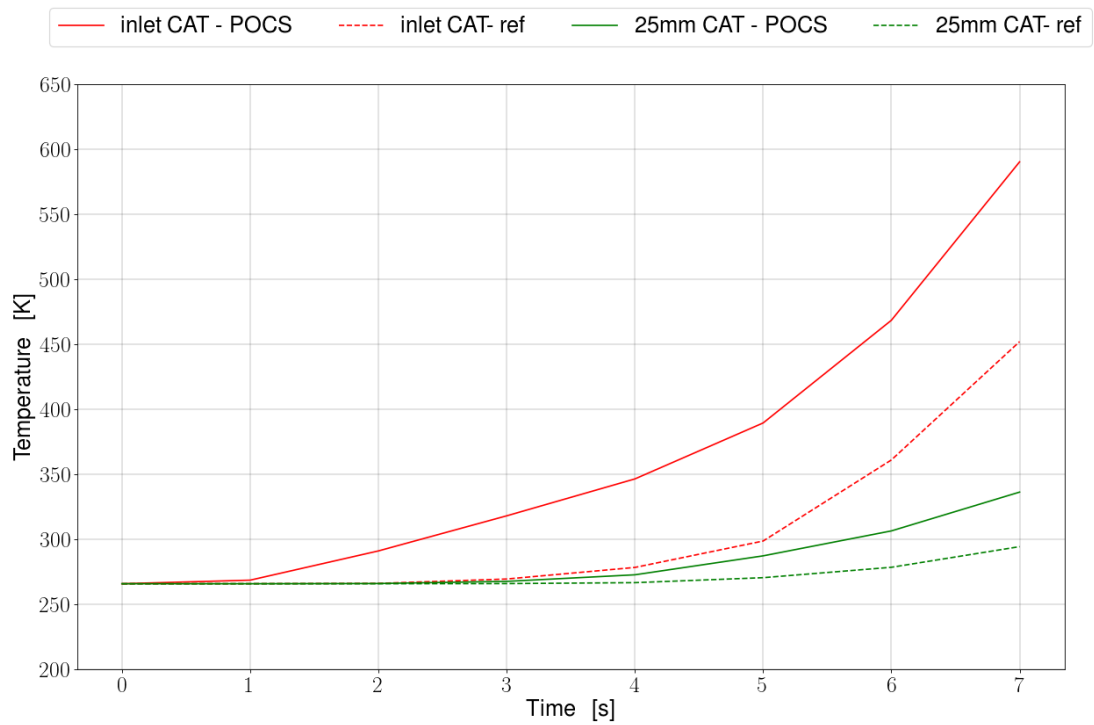
Figure 4.31: *Comparison of the temperature evolution inside the catalyst for the reference case and for the advanced solution with POCS.*
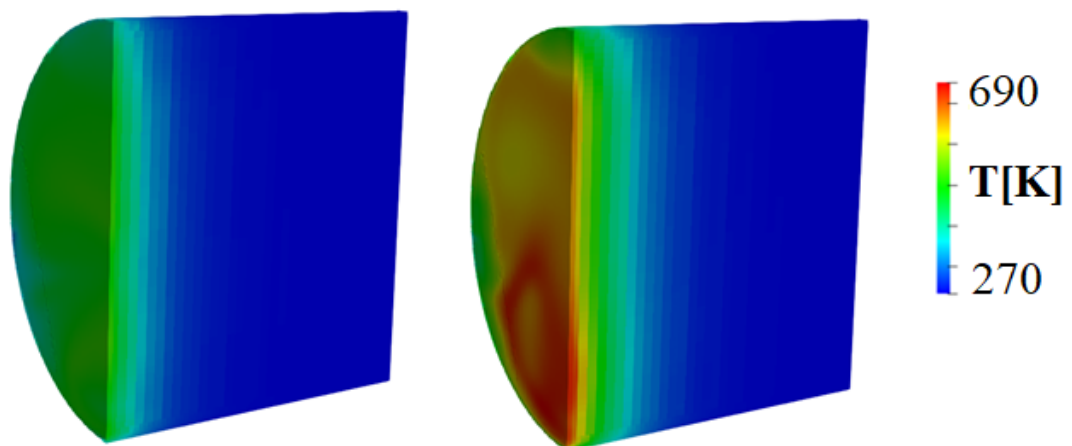
Figure 4.32: *Comparison of the temperature evolution inside the catalyst for the reference case (left) and for the advanced solution with POCS (right).*

To know the differences in the abatement capacity of pollutants in the two cases studied, the cumulative concentrations of the three main species are analyzed. The emissions at the outlet of the reference case are compared with those of the POCS case, at light-off time of the POCS case.
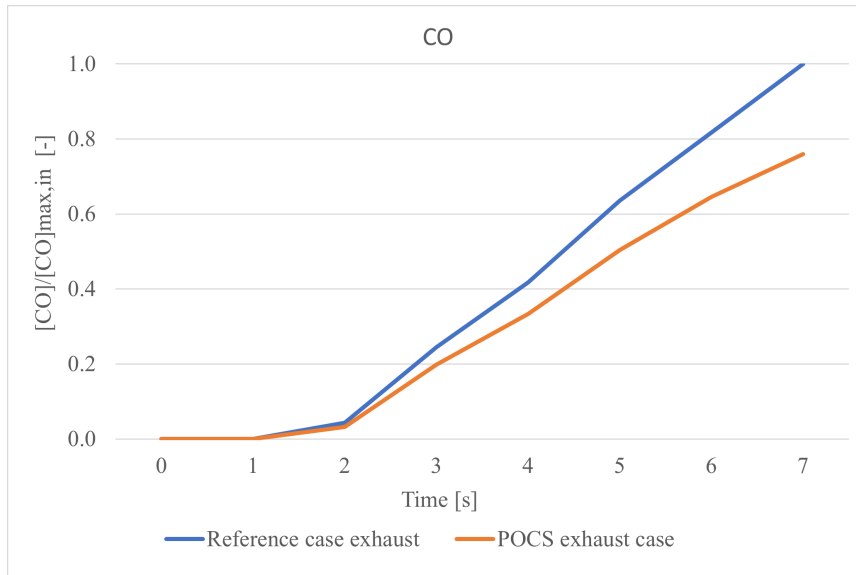
Figure 4.33: *Comparison of cumulative dimensionless concentration of CO.*
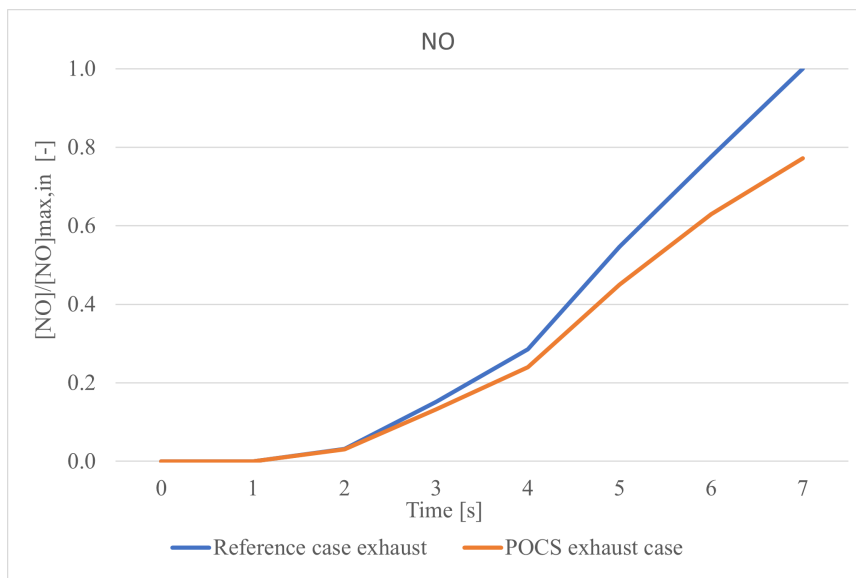
Figure 4.34: *Comparison of cumulative dimensionless concentration of NO.*
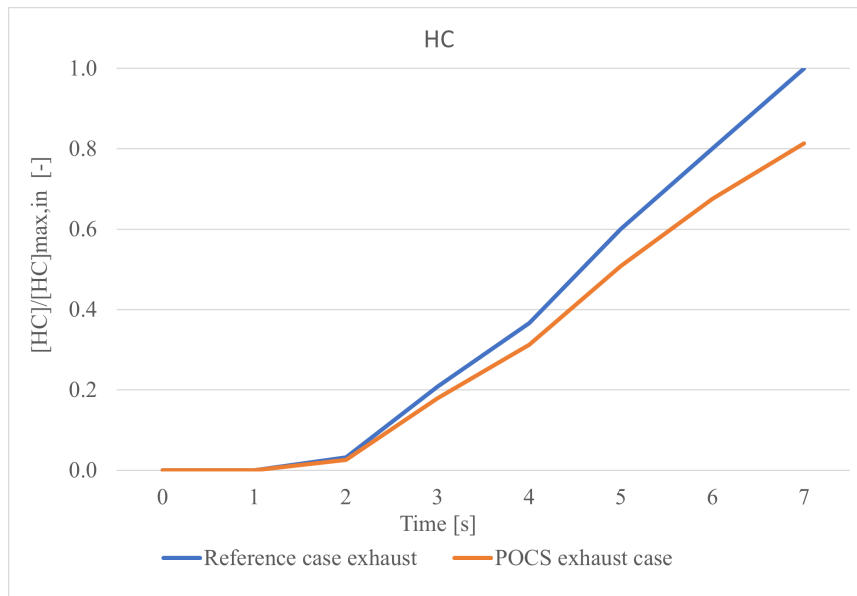
Figure 4.35: *Comparison of cumulative dimensionless concentration of HC.*

As the conversion has not yet begun in the reference case, which begins at about 8 seconds, the reference value coincides with the value of the input pollutants. The deviations shown in the previous figures include the reduction contribution given by the pre-catalyst and the anticipated activation of the catalyst. In all three diagrams a reduction of about 20% between the two cases is shown. Therefore the catalyst still has an abatement efficiency of a few percentage points, since most of the abatement is given by the pre-catalyst.

Another important aspect to consider is the simulation time required. Considering that computational resources are limited, a parallelization of the simulations is applied in order to reduce the time required. To parallelize a problem OpenFOAM uses decomposition of the domain. This process divides the mesh and the fields in a certain number of subdomains and allocates them on separate processors. Therefore the applications are able to run in parallel on individual subdomains, communicating among them by means of a protocol. In this case a manual parallelization is applied in which every individual domain is manually

assigned to one of the ten available processors. In this way the catalyst subdomain and the respective fluid section can be allocated on the same processor. This process allows to obtain the results for 8 seconds of simulation of the aforementioned mesh in about 82 hours.

4.6.1 Conclusion of Exhaust case study

The abatements obtained in the two cases are different. The reference case has a longer period required to heat the catalyst up, during which no reaction occurs. In the second case, lower pollutants are present at the inlet due to the POCS abatement and gases with higher temperatures flow through the exhaust pipe. Along the ducts the temperature is partially lost, due to conduction and convection phenomena with the walls. In any case the reactions inside the main catalyst start in advance of about 2 seconds.

Chapter 5

Impact on overall engine performances

The *gasdyn* code is a 1D thermo-fluid dynamic model for the simulation of the whole engine system, to carry out a fast prediction of IC engine volumetric efficiency, torque, power, fuel consumption, pollutant emissions and tailpipe noise. [19] This code is able to simulate different components from intake to exhaust pipe, thanks to 1D conservation equations with the addition of some approximations to describe the phenomena that the 1D model does not consider. For the numerical solution gasdyn makes use of shock-capturing, 2nd order finite difference numerical methods, with the addition of flux limiting techniques, to achieve accurate and robust results.

The generation and handling of input files for the computer modeling is managed by the pre-processor gasdynPre, which allows the visualization of the engine outline [19].

In this work the analysis is made on a realistic high-performance engine V12, considering only one bank of motor. The setup is made on a prototype engine with a structure similar and for the same application of the engine employed for the other sections of the thesis. The gasdynPre setup considered is the following:
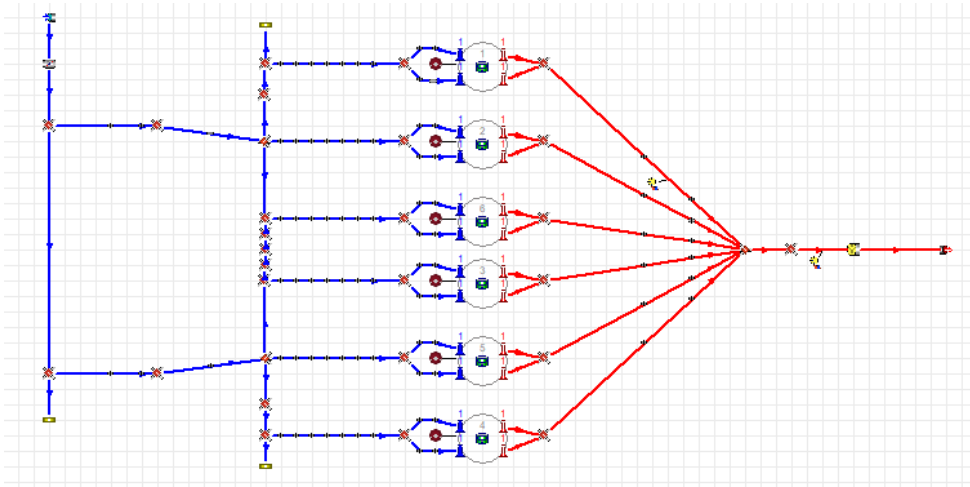
Figure 5.1: *Gasdyn setup of a bank of high-performance engine.*

This type of simulation allows to know the realistic behaviour of the full load engine at different rotational speed in a very short simulation time.

This specific analysis aims to compare a base case with the case in which a POCS is inserted in the exhaust ducts.

The 1D approximation does not permit to assign the adherence condition of the flow to the walls, so the friction is modeled by a source term in momentum conservation equation. The friction factor in a section of channel can be estimated by:

$$f_w = \frac{\Delta p}{\rho} \frac{2d}{l} \frac{1}{U^2} \tag{5.1}$$

Where Δp are the pressure losses, ρ is the density, d is the pipe diameter, l is the length, and U the mean speed.

The friction factor overcomes the limit of 1D simulation, allowing the description of the POCS behaviour inside the exhaust ducts.

The pressure losses in this equation are calculated by the CFD analysis, in the same way of sensitivity analysis described for preliminary mesh analysis. The value considered is referred to 50 $\left[\frac{m}{s}\right]$ of speed, while the diameter and the length are respectively 0.04 [m] and 0.1 [m]. The fiction factor able to represent the POCS structure is around 0.29.

In this way, considering the CFD data for pressure losses, the results are strongly related to the fluid dynamics evaluations. The output files are managed by the post-processor gasdynPost, included in the graphical interface. The data are provided both graphically and numerically and it allows to compare the obtained results from different simulations parameters of different simulations.

This analysis is not carried out to consider the abatement efficiency of the inserted catalyst but simply to verify the influence, due to its presence, on the engine operation, evaluating parameters like efficiency, power and BMEP.

For simplicity the discussion of the results is made evaluating them through diagrams. In the following figures the POCS case, considering a friction factor of 0.29, is reported in red, while the base case in green is reported in green.

Brake Power

The Brake power is the power available at the crankshaft which is different from the power provided by the combustion chambers. The combustion process develops a greater power that is partially lost due to friction or other mechanical losses. The power produced by an engine is expressed in horsepower. When the power developed is measured by means of a dynamometer or similar braking device, it is called brake horsepower.
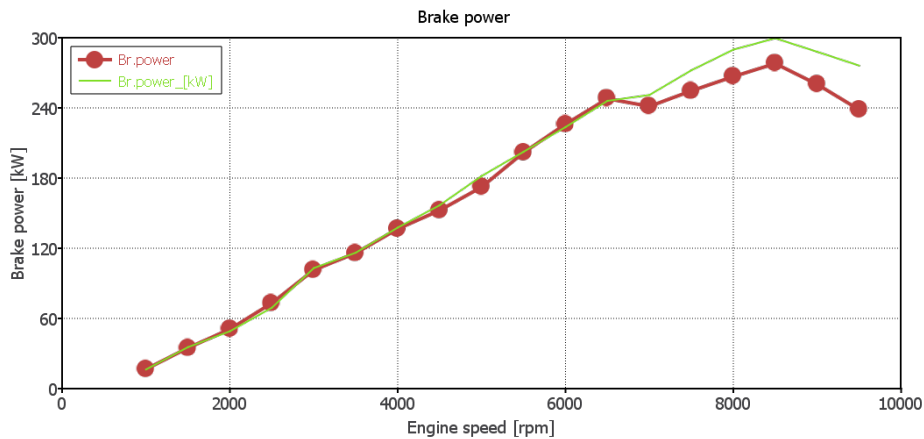
Figure 5.2: *Comparison of Brake Power between between the base configuration and the POCS configuration.*

The first part of the graph shows a perfect superimposition of the behaviours, or only small variations. However at 7000 rpm the power of the base case becomes firmly greater than the POCS case. The result presents a horsepower loss of about 28 Hp, at 8500 rpm.

Total efficiency

When the engine converts fuel into power, the process is rather inefficient and only about a quarter of the potential energy in the fuel is released as power at the flywheel. Inside the engine different efficiencies can be evaluated. Here the total efficiency is considered.
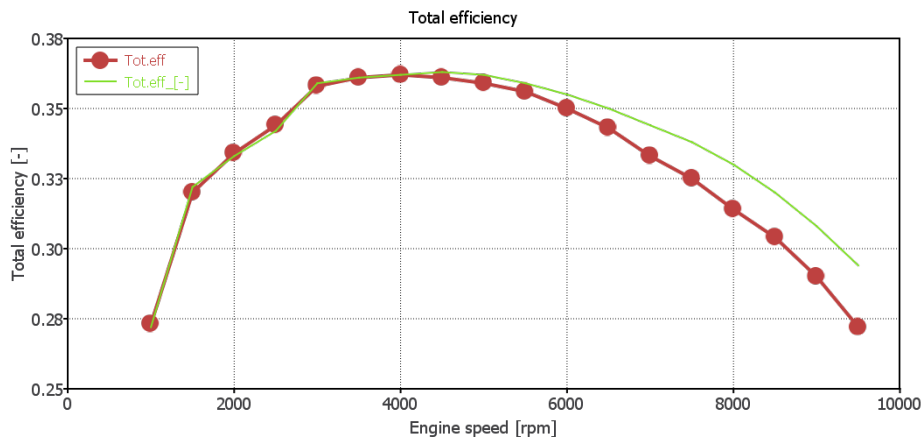
Figure 5.3: *Comparison of total efficiency between the base configuration and the POCS configuration.*

The actual gasoline engine achieves an efficiency of about 38%, and this value varies with engine rotational speed. The pressure losses introduced in the pipe report an efficiency loss of about 2 percentage points.

BMEP - Brake Mean Effective Pressure

The BMEP, i.e. Brake Mean Effective Pressure, is mean effective pressure calculated from measured brake torque. It is a theoretical tool to evaluate the efficiency of a given engine at producing torque from a given displacement. Practically this parameter represents the average pressure forcing the pistons down inside the

engine. This diagram reports a lower torque per litre for the POCS case, in
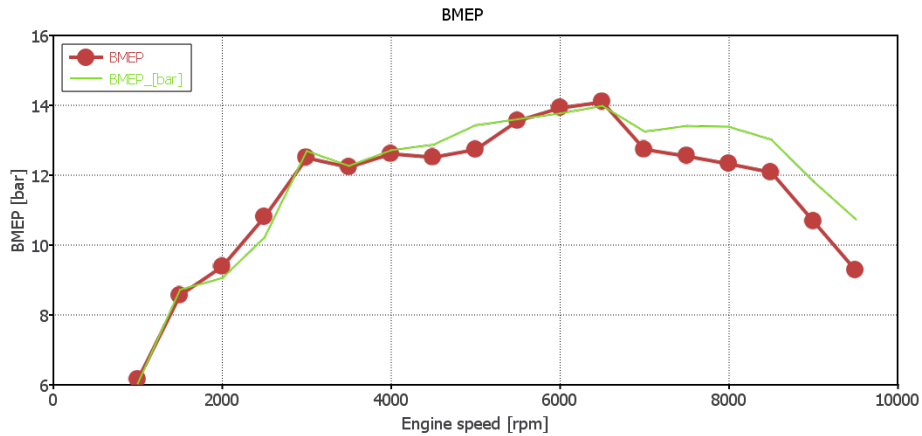
Figure 5.4: *Comparison of BMEP between the base configuration and the POCS configuration.*

particular for speed higher than 6000 rpm, that is coherent with the efficiency reduction. The POCS influence at different rotational engine speed, considering full load conditions, is reported in the graph. At low speed very small difference are present, while increasing the rotational speed the effects are more evident.

5.0.1 Conclusion of the overall impact

At the end the penalties, induced by the POCS presence, at high engine speed are evident. However, the analysis is carried out considering the most critical conditions (full load). Furthermore, the introduction of a component leads to changes in parameters within the system, their optimization could lead to a reduction of the differences shown in this preliminary analysis.

Conclusions and Future Developments

This thesis work focus on the problem of low pollutant conversion efficiencies in ATS at vehicle cold start. The goal of the work is to design a system that can rapidly intervene to promote the early ligh-off of the catalytic reactions in order maximize the abatement efficiency of the ATS.

To do this, an electrically heated pre-catalyst, exploiting the Joule effect, has been designed to be placed inside the exhaust ducts immediately downstream of the engine.

The combination of a heater with a catalytic substrate allows to achieve the optimal reaction temperature in advance, so that the catalytic reactions start in a very low time. In this case after 3 seconds part of the substrate achieves a temperature sufficient to activate the chemical reactions. A reduction of about 20% is thus calculated.

Considering the whole exhaust pipe, the influence of the POCS heating and abatement over the traditional catalysts of ATS has been evaluated.. As shown in the reference case, the reactions in the catalysts present along the pipe are inactive for the first 7 seconds. This lighting period significantly affects the total amount of pollutants emitted.

The simulation, considering the POCS abatement, shows a different scenario. In this case at the inlet hotter gases and lower pollutants concentrations are present. The lower emissions concentration is itself an advantage while the higher temperature of the gases is beneficial to achieve the light-off temperature of the catalyst

in advance. The heat that the POCS provide to the gas flow is partially missing through the walls, so a lower gas temperature is exploitable to warm the catalyst up.

Cities are the areas where there are the greatest problems due to transportation pollutions and where there are longer periods in which the catalyst is cold due to the frequent start and stop. In this context the POCS shows a good development prospective. The data of POCS structure and the consequent data of the exhaust POCS pipe demonstrate a good reduction of emissions in the starting period.

The advantages of this technology are many, first of all the promising abatement results but also the versatility of the system and the flexibility of the geometry.

As regards the geometry, there are many adaptations that can be introduced. The periodicity with which the geometry is repeated makes it easy to lengthen or shorten the structure, but also to make the struts more or less dense, depending on the engine condition. The structure can be also separated as shorter pieces that can be repeated along the duct. This solution could be useful to reach the main catalyst with higher gas temperature.

This system shows a good efficiency on all the pollutants. The combustion of any fuel, from fossil to synthetic, is exploited with air as comburent so the NO_x will be present also after the decarbonization. This POCS system seems to be able to be applied for the design of ATS for future engines running with syntetic fuels.

Another aspect that could be developed is an adaptation strategy of the thermic conditions of the POCS. Preheating the POCS at start-up, as well as being able to turn it on and off as needed would allow to limit losses and make the structure more efficient.

The final step concerns the performances evaluation. The 1D simulation shows a similar trend with a reduction of power at high regimes, around 8000 rpm. Therefore the impact of the preliminary solution is acceptable.

Furthermore, it should be considered the setup used is not optimized for the pres-

ence of the POCS, so there is room for improvement. The optimization of some parameters as well as the use of the turbocharger can lead to a reduction of losses.

Nomenclature

Acronyms

CAD	Computer-Aided Design
CFD	Computational Fluid Dynamics
NEDC	New European Driving Cycle
WLTC	Worldwide Harmonized Light Vehicles Test Procedure
RDE	Real Driving Emissions
PEMS	Portable Emission Measuring Systems
ZLEV	Zero- and Low-Emission Vehicles
ATS	After-Treatment Systems
TWC	Three-Way Catalysts
GPF	Gasoline Particulate Filter
DPF	Diesel Particulate Filters
GDI	Gasoline Direct Injection
POCS	Periodic Open Cell Structures
BMEP	Brake Mean Effective Pressure

Operators

$\sum$	Summation
d	Total derivative
∂	Partial derivative
D	Material derivative
$\vec{\nabla}$	Gradient
$\vec{\nabla}\cdot$	Divergence
$\int$	Integral
$\oint$	Close integral

Abbreviations

t	Time	$[s]$
T	Temperature	$[K]$
ρ	Density	$[kgm^{-3}]$
U	Speed	$[ms^{-1}]$
p	Pressure	$[Pa]$
MM	Molar Mass	$[kgkmol^{-1}]$
R	Universal Gas Constant	$[Jkg^{-1}K^{-1}]$
P	Power	$[W]$
d	Diameter	$[m]$
l	Length	$[m]$
Φ	Generic physical property	$[-]$
m	Mass	$[kg]$
F	Force	$[kg]$
M	Momentum	$[kgms^{-1}]$
S	Surface	$[m^2]$
V	Volume	$[m^3]$
W	Mechanical power	$[W]$
Q	Thermal power	$[W]$
E	Total Internal energy	$[J]$
$\overline{\overline{\sigma}}$	Stress tensor	$[Nm^{-2}]$
$\overline{\overline{\tau}}$	Deviatoric tensor	$[Nm^{-2}]$
λ	Thermal conductivity	$[Wm^{-1}K^{-1}]$
I	Electric current	$[A]$
V	Electric potential	$[V]$
ρ	Electric resistivity	$[\Omega m]$
σ	Electric conductivity	$[Sm^{-1}]$
A	Area	$[m^2]$
I	Electric current	$[\Omega]$

Adimensional Number

Re	Reynolds Number
Pr	Prandtl Number
Sh	Sherwood Number
Sc	Schmidt Number

Subscripts

min	minimum
max	maximum
g	gas phase
w	washcoat
wg	wall gas zone
k	arbitrary specie
el	electrical

Bibliography

[1] European Commission, *Emissions in the automotive sector.* https://ec.europa.eu/growth/sectors/automotive-industry/environmental-protection/emissions-automotive-sector_en

[2] European Commission, *2030 Climate Target Plan.* https://ec.europa.eu/clima/eu-action/european-green-deal/2030-climate-target-plan_en

[3] European Commission, *CO_2 emission performance standards for cars and vans.* https://ec.europa.eu/clima/eu-action/transport-emissions/road-transport-reducing-co2-emissions-vehicles/co2-emission-performance-standards-cars-and-vans_en

[4] European Commission, *Testing of emissions from cars.* https://ec.europa.eu/commission/presscorner/detail/en/MEMO_18_3646

[5] Angelo Onorati, *Internal Combustion Engines - University course materials.* Politecnico di Milano, 2020−2021

[6] S.E. Shcheklein and A.M. Dubinin *Analysis of nitrogen oxide emissions from modernvehicles using hydrogen or other natural andsynthetic fuels in combustion chamber* ELSEVIER, 2019.

[7] Augusto Della Torre, *Modeling of Automotive Propulsion System - University course materials.* Politecnico di Milano, 2019−2020

[8] CFD Direct, The Architects of OpenFOAM, *OpenFOAM User Guide.* https://cfd.direct/openfoam/user-guide/

[9] Open∇FOAM, User Guide, *OpenFOAM User Guide.* https://www.openfoam.com/documentation/user-guide

[10] Internal Combustion Engine Group - Department of Energy - Politecnico di Milano, *LibICEIntakeExhaust Documentation.*

[11] A.Della Torre, F. Lucci, G. Montenegro, A. Onorati, P. Dimopoulos Eggenschwiler,E. Tronconi, G. Groppi, *CFD modeling of catalytic reactions in open-cell foam substrates.* ELSEVIER, 2016.

[12] Matteo Ambrosetti, Gianpiero Groppi, Wilhelm Schwieger, Enrico Tronconi,nHannsjorg Freund, *Packed Periodic Open Cellular Structures - an Option for the Intensification of Non-Adiabatic Catalytic Processes.* ELSEVIER, 2020.

[13] Francesco Lucci, Augusto Della Torre, Gianluca Montenegro, Rolf Kaufmann,Panayotis Dimopoulos Eggenschwiler, *Comparison of geometrical, momentum and mass transfer characteristics of real foams to Kelvin cell lattices for catalyst applications.* ELSEVIER, 2017.

[14] Augusto Della Torre, Gianluca Montenegro, Angelo Onorati, and Tarcisio Cerri - Politecnico di Milano, *CFD Investigation of the Impact of Electrical Heating on the Light-off of a Diesel Oxidation Catalyst.* SAE Technical Papers, 2018.

[15] Yukina Taki, Mettaya Kitiwan, Hirokazu Katsui, and Takashi Goto, *Electrical and thermal properties of offstoichiometric SiC prepared by spark plasma sintering.* Journal of Asian Ceramic Societies, 2018.

[16] Augusto Della Torre, Loris Barillari, Gianluca Montenegro, and Angelo Onorati - Politecnico di Milano, *Numerical Assessment of an After-Treatment System Equipped with a Burner to Speed-Up the Light-Off during Engine Cold Start.* SAE Technical Papers, 2021.

[17] Andrea Vespertini, Augusto Della Torre, Gianluca Montenegro, Angelo Onorati, Enrico Tronconi and Isabella Nova - Politecnico di Milano, *An appraisal of the application of open-cell foams in automotive SCR systems.* National ATI Congress, 2020.

[18] V. Papetti, P. Dimopoulos Eggenschwiler, A. Della Torre, G. Montenegro, A. Onorati, A. Ortona, G. Koltsakis, *Instationary heat and mass transfer phenomena in additive manufactured open cell polyhedral structures for automotive catalysis.* Chemical Engineering Science, 2020.

[19] exothermia, *Theory Guide of Gasdyn.*